BIOSENSING AT AN INDIVIDUALLY ADDRESSABLE ELECTROCHEMICAL ARRAY

by

Wei Sun

A thesis
presented to the University of Waterloo
in fulfillment of the
thesis requirement for the degree of
Doctor of Philosophy
in
Chemistry

Waterloo, Ontario, Canada, 2006

AUTHOR'S DECLARATION FOR ELECTRONIC SUBMISSION OF A THESIS

I hereby declare that I am the sole author of this thesis. This is a true copy of the thesis, including any required final revisions, as accepted by my examiners.

I understand that my thesis may be made electronically available to the public.

Abstract

In this thesis, a novel electrochemical array is reported. The array consists of two planar halves, each having four carbon screen-printed band electrodes (SPEs), orthogonally facing each other and separated by a spacer to yield 16 two-electrode electrochemical cells with 1 mm^2 working electrode areas. The 16 counter electrodes were converted to Ag/AgCl by electrodeposition and anodization. These electrodes were stable for at least 30 days with potentials under the current densities used in our experiments. The 16 working electrodes were modified by Au electrodeposition, and were examined by scanning electron microscopy (SEM) and X-ray photoelectron spectroscopy (XPS).

Immobilization strategies for biomolecules are of paramount importance for successful fabrication of biosensors. This thesis reports a new immobilization method that is based on patterned deposition of alkyl thiosulfates (Bunte salts). Monolayers were formed through electrochemical oxidation of Bunte salts at Au-modified electrodes. Single-component and mixed monolayers were investigated, where the mixed monolayers involved one component with a terminal carboxylic acid functional group to allow immobilization of biomolecules.

Applications of the newly developed immobilization method to an enzyme-based biosensor and an immunosensor were investigated. Glucose and biotin were chosen as model analytes, respectively. Glucose oxidase (GOx) and avidin were covalently immobilized onto the mixed-monolayer-modified electrodes through the carboxylic acid groups. Under the optimized conditions for the fabrication and operation of the

biosensors, the new electrochemical array showed linearity up to 10 mM glucose with a sensitivity of 4.7 nA mM^{-1} and a detection limit of 0.8 mM (S/N=3), and linearity up to 12.8 μM biotin with a detection limit of 0.08 μM (S/N=3).

Acknowledgements

I am very grateful to my supervisor Prof. Susan R. Mikkelsen for giving me the chance to participate in this interesting and challenging research project. Her constant encouragement, support, and invaluable suggestions made this project successful. She has been everything that one could want in a supervisor.

I would like to thank my committee members Prof. Bill Power, Prof. Tadeusz Górecki and Prof. Frances J. Sharom for their support and their guidance. I want to further acknowledge Prof. Tong Leung for providing SEM and XPS testing.

Special thanks go to Andy Mak, Thomas Mann, Agnes Obuchowsk and Melany Wager for sharing experience and valuable suggestions.

This work is dedicated to my parents, my husband and my daughter. I am truly grateful for their love, patience, support and encouragement.

Table of Contents

List of Tables

List of Figures

List of Abbreviations

2D	two-dimensional
AchE	acetylcholinesterase
AFM	atomic force microscopy
APD	anodic pulse deposition
BchE	butyrylcholinesterase
B-LPOD	lactoperoxidase-labeled biotin
B-POD	peroxidase-labeled biotin
CDH	cellobiose dehydrogenase
CV	cyclic voltammetry
DNA	deoxyribonucleic acid
ECAM	electrochemically-assembled monolayers
EDC	N-ethyl-N'-(3-imethylaminopropyl) carbodiimide
EIS	electrochemical impedance spectroscopy
ELISA	enzyme-linked immunosorbent assay
FCA	ferrocenecarboxylic acid
FTIR	Fourier transform infrared spectroscopy
GAA	gold atomic absorption standard solution
GDH	glucose dehydrogenase
GOx	glucose oxidase
HRP	horseradish peroxidase
IR	infrared spectroscopy
NHE	normal hydrogen electrode
PDMS	poly (dimethylsiloxane)
QCM	quartz crystal microbalance
RIA	radio-immunoassay
R.S.D.	relative standard deviation
SAM	self-assembled monolayer
SBP	soybean peroxidase

SCE	saturated calomel electrode
SEM	scanning electron microscopy
SPCE	carbon screen-printed band electrode
SPE	screen-printed electrode
SPR	surface plasmon resonance
STM	scanning tunneling microscopy
THF	tetrahydrofuran
TNT	2,4,6-trinitrotoluene
TYR	tyrosinase
XPS	X-ray photoelectron spectroscopy

Chapter 1: Introduction

1.1 BIOSENSORS

1.1.1 Introduction

Rapid, reliable, low cost, and in some cases, continuous measurement of analytes has been a major goal in analytical sciences. Since biosensors offer many advantages over conventional analytical techniques in terms of simplicity, detection limit, specificity and sensitivity, the development of biosensors for analytical purposes has attracted a great deal of interest in recent years. Biosensors have widespread applications in medical analysis, environmental monitoring and industrial process control.[1-3]

What exactly is a biosensor? "Biosensors are devices, ideally small and portable, that allow the selective quantitation of chemical and biochemical analytes. They consist of two components: the transducer and the chemical recognition element. Chemical recognition is accomplished by exploiting the natural selectivity of biochemical species such as enzymes, antibodies, chemoreceptors, and nucleic acids. In the presence of the analyte, these agents, immobilized at the surface of the transducer, cause a change in a measurable property in the local environment near the transducer surface. The transducer monitors this property, and converts the chemical recognition event into a measurable electronic signal."[4]

The biosensor concept was initiated by Clark and Lyons in 1962 when they coupled the enzyme GOx to a Pt electrode.[5] Since then a variety of biosensors and their associated techniques have been studied and developed. Today there are more than 60

commercial biosensors available for about 120 different analytes.[6] In 1985, the world market for biosensors was $5 million and in 2005 it was a little over $5 billion.[7]

1.1.2 Electrochemical Biosensors

Biosensors are classified and evaluated on the basis of design and functional characteristics such as sensitivity, cost, selectivity, versatility, range, availability, future adaptability and simplicity. On these bases, electrochemical biosensors are favoured over optical sensors mainly because of cost and availability, while piezoelectric and thermal sensors are fairly poorly rated on all characteristics.[8] Amperometric enzyme biosensors form the majority of commercial biosensor devices available today; these biosensors operate at a fixed potential with respect to a reference electrode, while the measured signal is the working electrode current generated by the oxidation or reduction of electroactive species at its surface.

Immobilized antibodies can also be used as highly selective reagents in biosensors. Unlike the enzyme-based biosensors where either the co-substrate or the product of an enzyme reaction is monitored, antibody-based biosensors detect antigen or antibody concentration either by direct changes in the transducer output resulting from the binding event, or by means of indirect competitive and displacement reactions using optical, piezoelectric, or electrochemical techniques. Nevertheless, the majority of the reported antibody-based biosensors (immunosensors) makes use of irreversible binding chemistry; these biosensors are therefore not reusable and thus expensive.

Depending upon the electrochemical property to be measured, electrochemical biosensors can be further divided into conductimetric, potentiometric and amperometric biosensors.

Conductimetric biosensors measure the changes in conductance/impedance of a solution as consequence of the biological component using noble metal electrodes.[9] If the biocatalyst produces ionic products, or consumes ions, and the support solution has low electrical conductivity, this is often a convenient and simple technique. A deoxyribonucleic acid (DNA) biosensor using Faradic impedance spectroscopy based on use of biotinylated oligonucleotide and avidin-HRP (horseradish peroxidase) conjugate has been described.[10]

Potentiometric biosensors measure the potential difference between the working electrode and a reference electrode under conditions of zero current flow.[11] The potential generated is directly proportional to the logarithm of the concentration of an ion in an ideal solution. The basis of this type of biosensor is the Nernst equation, which relates the electrode potential (E) to the concentration of the oxidized and reduced species. For the reaction: $aA + ne^- \Leftrightarrow bB$, the Nernst equation can be described as the following,

$$E = E^0 + \frac{RT}{nF}\ln\left(\frac{[C_A]^a}{[C_B]^b}\right) \qquad (1.1)$$

where E^0 is the standard redox potential, R is the gas constant, T is the absolute temperature, F is the Faraday constant, n is the number of exchanged electrons in the reaction, and C_A, C_B are the concentration of oxidized and reduced species,

respectively. A potentiometric urease-based biosensor for detection of heavy metal ions has been reported recently.[12]

Amperometric biosensors measure the currents resulting from the electrochemical oxidation or reduction of an electroactive species under a constant potential applied to working electrodes. The most important of these is the glucose biosensor, which has been successfully commercialized for blood glucose monitoring in diabetics.[13] Other examples of enzyme-based amperometric biosensors include the phenol sensors, which utilize cellobiose dehydrogenase (CDH) or glucose dehydrogenase (GDH);[14] the lactate biosensor, which is based on lactate oxidase immobilized to a conducting copolymer through glutaraldehyde;[15] and the alcohol biosensor, which is based on peroxidase and alcohol oxidase.[16] Most of the electrochemical immunosensors are based on enzyme-linked immunosorbent assay (ELISA) principles, with sensor-immobilized antibodies or antigens where the enzyme label such as peroxidase, alkaline phosphatase or GOx, is indicated amperometrically by measuring the produced iodine, p-aminophenol or hydrogen peroxide, respectively.[17-19]

1.2 SCREEN-PRINTING TECHNOLOGY

1.2.1 Introduction

The technique of screen-printing (thick-film) is now well-established as a reliable method for the fabrication of electrochemical sensors and biosensors for biomedical, industrial and environmental applications.[20] The potential of this method for the production of commercial devices is exemplified by the personal glucose biosensor

used widely by diabetics.[13] Screen-printing technology was adapted from the microelectronic industry for the production of electrodes, and has advantages of design flexibility, process automation, good reproducibility, a wide choice of materials, and low cost. It has thus been sought as an alternative method for mass production of biosensors.

SPEs are extremely versatile and have been reported as transducers in biosensors for a wide variety of applications.[21] They have been used in enzyme-based biosensors for the detection of lactate,[22] uric acid,[23] urea and creatinine,[24] cholesterol,[25] and in immunosensors for progesterone,[26] ochratoxin[27] and aflatoxin M1 in milk.[28] Research is not limited to these compounds, however, and biosensors for DNA,[29] pesticides,[30] trace metals,[12] herbicides,[31] as well as microorganisms[32] have been reported. Not only do SPEs have the ability to determine a large variety of analytes, but they also possess low detection levels and good operational stability. The lowest SPE detection limit encountered to date has been the subfemtomolar detection of alkaline phosphatase.[33]

1.2.2 Materials

The basic steps in the screen-printing process involve screen-printing of suitable inks onto planar substrate materials by forcing them through a patterned stencil or mask followed by a proper thermal curing. The most common substrates are alumina ceramics and various plastic-based materials. The use of ceramics allows for the high curing temperatures that are needed for gold- and platinum-based inks. Plastic substrates are used for printing silver- or carbon-based inks, as the curing temperatures required are lower. Other possible substrates are nitrocellulose and fibreglass.

A wide range of inks with different physical and chemical properties (e.g. viscosity, conductivity, thermal resistance, and water resistance) can be used to meet diversified requirements in biosensor fabrication. Commercial carbon- and metal-based (gold or platinum) ink formulations are commonly used for printing the working electrodes, whereas silver-based inks are used for obtaining the reference electrodes. The compositions of commercial ink formulations differ substantially, and the exact ink formulations are regarded by the manufacturers as proprietary information. Therefore it is imperative to gain knowledge into how these differences affect electrochemical properties (e.g. electron transfer kinetics, background current, voltammetric peak height, and impedance). Carbon-based inks are particularly attractive for the construction of biosensors due to the simple construction procedures required, the low background current they exhibit, the wide operating potential window, the ability for surface regeneration, and the low cost.[34] Several studies have been carried out to assess the electrochemical behaviour and electroanalytical performance of different inks with different redox-active compounds.

Wang et al.[35] studied four different commercial carbon-based ink formulations (Gwent, Ercon, Acheson and Dupont) using four benchmark redox systems (ferrocyanide, catechol, acetaminophen and ascorbic acid). Results from this study showed there were substantial differences in the electrochemical behaviours of the inks toward different compounds. For example, cyclic voltammetry (CV) of catechol led to peak separations of 146 mV, 317 mV, 346 mV, and 445 mV for Gwent, Ercon, Acheson and Dupont inks, respectively.[35] For comparison, a glassy carbon electrode used for CV of the same solution gave a peak separation of 70 mV. Similarly, wide-

ranging results were seen for other redox systems tested. In addition to the different electrochemical reactivities of these redox systems, electroanalytical performance also varied depending on the electrochemical technique employed (e.g., pulse voltammetry, amperometry and anodic stripping voltammetry).[35]

Dock and Ruzgas[36] evaluated eight screen-printed carbon electrodes (SPCEs) and found a strong correlation between the reversibility of the ferri/ferrocyanide redox couple and the sensitivity for catechol at the same electrodes modified with the enzyme, CDH. As in the previous study, differences in the electrochemical behaviour of the inks were very evident. Peak separations ranged from 53 mV for a homemade carbon-based ink to 316 mV for an ink produced by BVT Technologies. In another interesting study, carbon-based inks from Asahi, Jujo and Gwent all showed similar cathodic and anodic peak shapes and peak separation values for hexaammineruthenium (III) and hexachloroiridate (IV).[37] However, only the Gwent ink exhibited recognizable voltammetric redox peaks for other redox couples (ferricyanide, dopamine, and hydroquinone).[37]

These studies demonstrate that electrochemical properties of SPCEs are dependent on ink formulations and this behaviour is similar to that of other carbon materials. The most notable comparison is carbon paste (composed of graphite mixed with mineral oil) which is limited by the amount of carbon exposed at the electrode surface, and it has been shown that electron-transfer rates strongly correlate with the carbon loading.[38] Choosing different commercial carbon-based ink formulations may prove beneficial in improving the electron transfer reactivity of redox-active

compounds. However, the selection and use of a particular product is not a simple task as the required composition may not be commercially available.

1.2.3 Printing Patterns

Various electrode patterns can be utilized, including two- or three-electrode systems, as well as electrochemical arrays.[39] These electrodes are robust, easy to mass produce, inexpensive, and yield reproducible results.[40, 41]

Up to now, most of the screen-printed biosensors are used for single parameter measurements associated with electrochemical detection.[30, 42-46] Screen-printed multi-channel arrays have the potential for monitoring several different compounds simultaneously. Screen-printing technology enables easy production of very flexible configurations of electrode-array devices that can be converted into biosensor arrays by modifying individual electrodes with different biological components. The multi-dimensional response from the array is analyzed and interpreted using modern statistical techniques popularly known as chemometrics. The designs of such sensors are still the object of discussion as well. Different arrangements, i.e. linear or circular, maintain different dispersion of the analyte zone. Recently, a unique amperometric multi-enzyme biosensor, assembled on a screen-printed array for the detection of pesticides (organophosphates and carbamates) and phenols, has been reported (Figure 1.1).[39] The array consists of one printed Ag/AgCl reference electrode surrounded by eight radially distributed printed working electrodes of either carbon or platinum. The array is based on the combination of enzymes: acetylcholinesterase (AchE), butyrylcholinesterase (BchE), tyrosinase (TYR), GOx, soybean peroxidase (SBP), HRP

and CDH. The relative standard deviation (R.S.D.) was below 7% for different enzyme substrates, and one assay was completed within less than 10 min. The detection limits for pesticides and phenols were in the nanomolar and micromolar ranges, respectively.

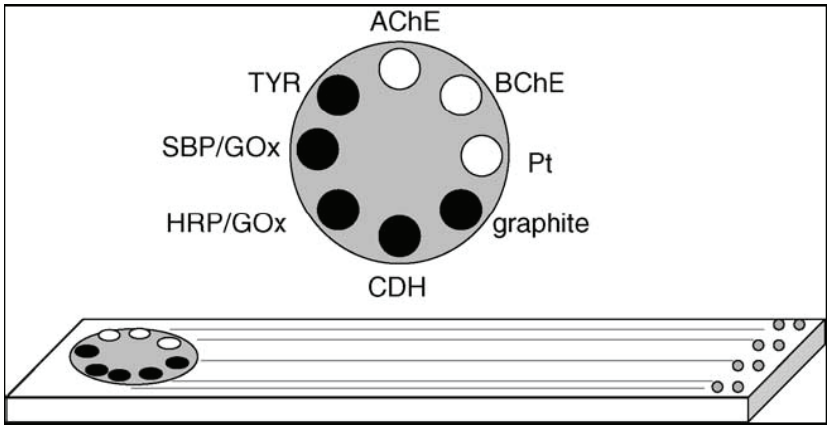

Figure 1.1 The construction of the eight-electrode screen-printed array and the illustration of the final distribution of enzymes on the working electrodes.[39]

More recently, thin film technology, based on silicon, has made advances in electrochemical analysis. Thin film technology offers better spatial resolution but it is associated with higher equipment cost and low flexibility for chemical modifications. In contrast, thick film technology (screen-printing) offers striking advantages when smaller batches of low cost, robust chemical and biosensors have to be made with modest resolution (ca. 100-500 μm).[20, 47-49] Therefore, the choice between thin film photolithography and thick film screen-printing for sensor fabrication is determined by cost. Thin film technology allows for sensor arrays of individually addressable electrodes with reduced dimensions, to probe small volumes and simultaneously

monitor several analytes.[50] However, chemical cross-talk is of concern when developing microarrays. Chemical cross-talk in electrochemical sensor arrays occurs when diffusion layers of individual electrodes consuming analyte overlap due to their close proximity.[50, 51] A microarray (Figure 1.2) consisting of 10 individually addressable electrodes in a 130 μm radius was produced to study the interaction of adjacent electrodes. It was shown that chemical cross-talk occurred at electrodes separated by less than 100 μm.[51]

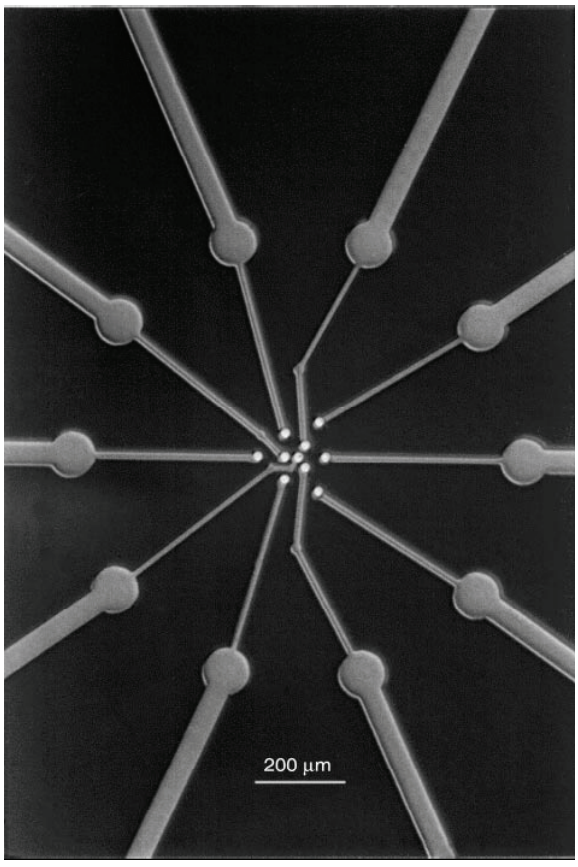

Figure 1.2 Microphotograph of the microsensor array. Bright dots indicated the platinum electrode surfaces.[51]

Researchers developing lab-on-a-chip devices have a great interest in the miniaturization of electrodes. The ability to obtain quantitative information based on redox activity coupled with the sample preparation, liquid handling and manipulation capability offers increased power for these devices. Consequently, SPEs have been applied to microscale voltammetric analysis on microfluidic chips for the detection of 2,4,6-trinitrotoluene (TNT), catechol, hydrazine and nickel.[52]

In summary, screen-printing technology has shown its great utility to biosensor researchers. With the technology, biosensor design can be more flexible: disposable or reusable, single or multiple purposes, rectangular or circular sensing surface, mediated or direct electrode process. SPEs are readily modified and offer inexpensive one-time use. Gold and platinum modification will allow us to evaluate further possibilities with these devices.

1.2.4 Gold Electrodeposition on SPCEs

The use of different metals like gold, platinum and silver has been suggested for the manufacture of highly active electrodes for many electrochemical applications.[52-54] Gold has been largely employed in methodologies and techniques for investigation of molecular ion recognition, catalysis, electron transfer and studies of surface phenomena that require stable and reproducible surfaces, such as surface plasmon resonance (SPR),[55] scanning tunneling microscopy (STM),[56] quartz crystal microbalance(QCM),[57] voltammetry,[58] amperometry,[59] electrochemical impedance spectroscopy[56] and molecular self-assembly.[53] During the past several years, considerable attention has been focused on self-assembled monolayers (SAMs) prepared on gold surfaces by

spontaneous chemisorption of alkanethiols and disulfides, because of their stability, well-ordered structure, ease of preparation and flexibility in design of the tail group.[60-62] These well-defined organic films provide the possibility of immobilization of biomolecules. Gold surfaces modified with thiol-based compounds have a broad range of applications including enzyme biosensors,[63] biosensors in DNA chips,[64] detection arrays for airborne contaminants,[65] and immunoassays for a biomarker (prostate-specific antigen).[66]

Screen-printed gold electrodes have already been employed for heavy metals detection[67] and in immunosensors,[68, 69] microbial biosensors,[70] and DNA biosensors.[71] However, they are not practical due to high ink costs (20-25 US $/g). In addition, gold-based inks have a polyester base and do not produce pure gold surfaces. Therefore, differing electrochemical behaviour may be expected compared to pure gold electrodes.

Currently, gold nanoparticle-based materials have attracted much attention because of their unique mechanical, electronic, and catalytic properties.[72-75] Nanoparticles can play an important role in immobilization of biomolecules due to their large specific surface area, excellent biocompatibility and good conductivity. Biosensors based on the immobilization of proteins on gold nanoparticles have been developed for the determination of hydrogen peroxide, nitrite, glucose, phenol and DNA.[76-80] Only metallic nanostructures with uniformly functionalized surfaces could be used to immobilize biomolecules. Without functionalization the native metal surfaces are prone to nonspecific protein adsorption and degradation (oxidation and decomposition).[81] Several procedures have been proposed and applied to the immobilization of metal nanoparticles, such as electrolysis deposition and monolayer

assistance embedding.[82-85] However, it is still a challenge to control the shape, size, and density of nanoparticles, which are important parameters for the purpose of immobilizing biomolecules.

Electroplating is a common technique employed for the development of gold electrodes. Tetrachloroauric acid has been used to electroplate on a glassy carbon electrode by applying a constant potential of -0.10 V vs. Ag/AgCl for 5 min in 0.2 M potassium chloride to yield gold modified surfaces.[86, 87] Gold atomic absorption standard solution (GAA solution) has also been employed. The solution is ready to use, but is typically diluted. Dilution from 1005 to 50 mg/L (in 0.25 wt % HCl) has yielded functional gold electrodes for decentralized testing of trace lead. SPEs were gold modified by holding the carbon electrodes at -0.40 V for 20 min, followed by a second step to +0.70 V for 5 min.[88, 89]

Once the carbon SPEs are modified by gold plating, they should behave as gold electrodes, and be readily further modified to produce SAMs.

1.3 PATTERNING MONOLAYERS BY ELECTRODEPOSITION OF BUNTE SALTS

1.3.1 Introduction

High selectivity provided by biomolecules (antibodies, enzymes, nucleic acids) or biological systems (receptors, whole cells) is exploited in biosensors. Most commonly, the biomolecules are immobilized on, or in close proximity to, the surface of the

transducer. As a consequence, immobilization strategies for biomolecules are of paramount importance for successful fabrication of biosensors.

Many physical and chemical methods[90] for immobilizing biomolecules, like physical adsorption, chemical binding, entrapment, and encapsulation, have been developed. Some problems still exist, such as conformational change affecting the functional activity, adsorption with random orientation, detachment of the biological components and fragility of the membrane resulting in less sensitivity and short longevity. Thus, there is an ever-increasing demand for better assembly techniques for immobilization of biomolecules.

SAMs, especially functionalized SAMs, which provide a common platform for immobilizing biomolecules, has received particular attention in recent years.[91, 92] Among the various SAM systems that have been studied, SAMs prepared on noble metal surfaces, especially on gold, by spontaneous chemisorption of alkanethiols has shown the greatest promise because of their advantages over other methods.[60-62] One of the valuable benefits of the system is that it provides the potential to control the properties of the electrode/solution interface on a molecular scale. The system has been used for both immunosensors[93-95] and enzyme biosensors[96-100] by employing reactive SAMs to immobilize biomolecules.

Alkanethiols employed in self-assembly comprise three significant parts: the surface-active head group (sulfur), which binds strongly to the metal substrate (gold, platinum or silver), the alkyl chain, giving stability to the assembly by van der Waals interaction, and the ω-functionality, which is the decisive part in terms of coupling of

biomolecules to the alkanethiol monolayer. An ideal pure monolayer is depicted in Figure 1.3. The alkane chains are all in the trans-conformation, tilted slightly from normal to the metal surface by ~20-30°, resulting in the formation of a densely packed, highly ordered monolayer. Through the proper selection of the terminal functional group, specific surface/solution interactions (chemical covalent, electrostatic, or hydrophobic) can be exploited to immobilize molecules at the interface. Functional groups such as $-NH_2$, -OH and -COOH have been widely used. Sawaguchi et al.[101] and Kajiya et al.[96] have reported immobilizing enzymes through step-by-step reactions from gold electrodes modified with NH_2-terminated thiols. In this system, the thiol monolayer was used as an anchor layer, and enzyme molecules were attached on the layer using glutaraldehyde as a linking agent. Willner et al.[102] have described the covalent attachment of enzyme molecules by the use of COOH-terminated thiol monolayers as the anchor layers. In an amperometric sensor COOH-terminated SAM ($HS(CH_2)_nCOOH$ with n=15 or 11) is used to immobilize cytochrome c via

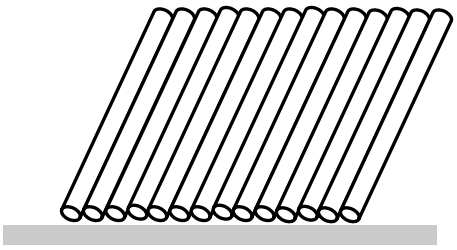

Figure 1.3 Depiction of a pure alkanethiol mononolayer.

carbodiimide activation.[103] A glucose biosensor has been prepared by cross-linking GOx to a SAM from ω-hydroxyl alkanethiol by glutaric dialdehyde.[99] As the densely packed monolayers block electrode surfaces, most applications of SAMs for the fabrication of enzyme electrodes utilize short chain alkanethiols where the resultant disordered SAM allows electrochemistry to occur at the metal below.[63, 104]

Immobilization of biomolecules using alkanethiols requires functionality at the terminal end of the molecule, to allow a bond to be formed between the biomolecule and the monolayer. Grazing incidence infrared spectroscopy shows that ω-substituted alkanethiols also are densely packed, highly oriented and ordered. As long as the endgroup ($-NH_2$ or -OH) is relatively small (< 5 Å), the orientation of the monolayer is not influenced.[105] However, more bulky groups (COOH, ferrocene) decrease the density of packing and ordering. Overabundance of surface functionalities, steric hindrance, and less ordered monolayers can lead to denaturation and reduced activity of biomolecules.[106, 107] One approach to overcome the problems is to dilute the functional groups in the monolayer by forming a so-called mixed monolayer.[108, 109] Mixed monolayers possess various advantages over a one-component monolayer. The combination of various functional groups, for example, allows the control of the degree and distribution of hydrophilicity and charge on the monolayer surface. Using alkanethiols of various chain lengths adds even more versatility: long alkanethiolates, which may be specifically functionalized, protrude from a basis of short alkanethiolates in the SAM. The shorter alkanethiolates may stabilize the monolayer and function as a spacer between the functionalities. The functionalities can act as specific binding sites for biomolecules. An ideal mixed monolayer is shown in Figure 1.4. The SAM consists

of a homogeneous mixture of the components, which is important for immobilizing biomolecules.

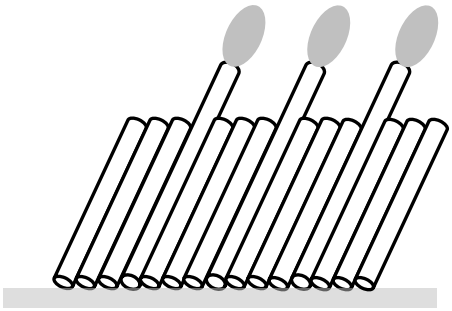

Figure 1.4 Depiction of an ideal monolayer with two components. Functional groups (shaded) are exposed to a solution or gaseous phase.

Homogenous mixed SAMs offer the possibility to 'dilute' ω-substituted alkanethiols with shorter non-substituted thiols in order to have anchor groups available for immobilization procedures in which steric hindrance is possibly reduced. Figure 1.5 shows the importance of the absence of steric hindrance in binding a biomolecule (streptavidin) to the surface of a biotin-terminated monolayer. Furthermore, by varying the composition of a mixed SAM, the density of attachment points, and hence the surface loading of recognition molecules, can be controlled.

At present, it is still difficult to prepare and characterize mixed SAMs with controlled chemical, structural, and biological properties. Coadsorption of two or more thiols from solution onto a surface is the method most often used for the preparation of mixed SAMs. However, many complex factors arise when attempting to pattern

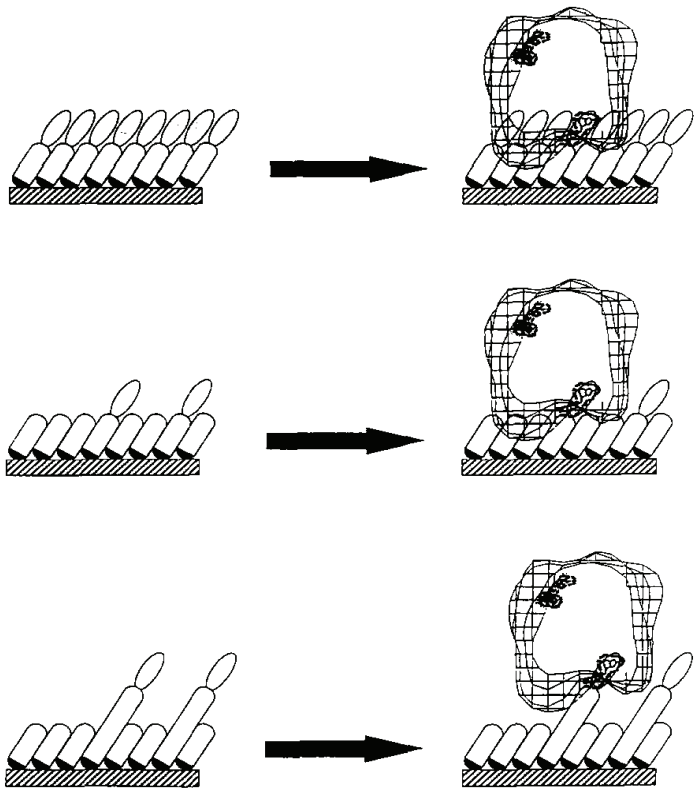

Figure 1.5 Schematic representation of a SAM of thiols and the binding of streptavidin to them. (Top) A pure monolayer. Binding of streptadidin is severely sterically hindered. (Centre) A monolayer of a mixture of thiols with the same length of the alkane moiety. There still is steric hindrance. (Bottom) Addition of a spacer allows binding without steric hindrance.[110]

molecules on a surface by simple solution-phase coadsorption. It is important to note that the relative fractional surface coverage of the molecules will not necessarily be the same as that of the coadsorption solution, an observation supported by contact angle, scanning probe microscopy and electrochemical studies.[111-115] Factors that affect the competition for the surface include the relative solvation of the adsorbates by the solution, the sticking probability of each molecule, and the degree of interaction

between the molecules once they are adsorbed. Differing self-assembling components are often separated into domains (islands) once organized (Figure 1.6).

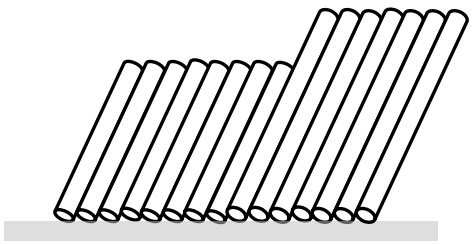

Figure 1.6 Depiction of a phase-separated SAM.

Numerous two-component SAM systems prepared from coadsorption of thiols have been investigated. Such systems include SAMs with short- and long-chain alkanethiols,[113, 116, 117] molecules that differ both in chain length and functional groups (i.e., 3-mercaptopropanol and n-tetradecanethiol[118]), molecules of similar length but with differing terminal groups (i.e., n-hexadecanethiol and its ω-methyl ester analog,[119] n-undecanethiol and 11-mercaptoundecanoic acid[120]) and molecules of similar length but with differing, buried functional groups (i.e., 3-mercapto-N-nonylpropionamide and n-decanethiol[115, 121]). However, only adsorbates with similar molecular composition will not phase-segregate into discrete single-component domains (islands) (n-decanethiol and n-dodecanethiol[122]). Thiols employed in mixed monolayers for the purpose of coupling biomolecues are usually different in chain length (in order to avoid steric hindrance) and functional groups. Therefore, coadsorption of thiols is not a

general method that allows the formation of homogenous SAMs with adsorbates of different molecular composition.

Bunte salts provide a potential alternative to the use of alkanethiols for forming SAMs.[123-126] Bunte salts have the general formula $RSSO_3M$, where R is either an aliphatic or aromatic group and M a monovalent cation. These compounds possess several properties that are advantageous over corresponding thiols. First, the presence of an ionic headgroup greatly improves their solubility in aqueous solution relative to those of the corresponding alkanethiols. Therefore, SAMs can be formed from Bunte salts in aqueous solution, instead of organic solvents such as ethanol, hexane and acetonitrile which have been applied to the thiol-based SAMs. Consideration of waste disposal issues in chemical processing suggests water as the best solvent, rather than organic solvents. Furthermore, a major advantage in using Bunte salts is their ease of synthesis compared to that of the corresponding thiols. Bunte salts can be conveniently obtained by the reaction of sodium thiosulfate with alkenes having terminal electron-withdrawing groups such as –Cl or –Br (Equation 1.2).[127]

$$RX + Na_2S_2O_3 \rightarrow R - S_2O_3Na + NaX \qquad (1.2)$$

where RX is alkyl halide and R is either an aliphatic or aromatic group.

Bunte salts can form SAMs on metal surfaces either by chemisorption[123, 125] or by electrochemical methods.[124, 126] The following sections will give more details about SAMs formed by using these two techniques.

1.3.2 Chemisorption of Bunte Salts

Bunte salts can form SAMs by the conventional chemisorption method. Bunte salts adsorb on metal surfaces in a manner similar to that reported for disulfides.[123, 128] After diffusion of Bunte salts to the metal surface, the S-SO_3 bond is cleaved, yielding an adsorbed thiolated species and a weakly bound sulfite species that can desorb from the surface or be displaced by the adsorption of alkyl thiosulfates.[123-125, 129-131] At high coverage, the adsorption of sulfite ions would result in molecule-sized defects that are not likely to be completely filled by the bulky thiosulfate molecules. Therefore, SAMs formed from chemisorption of Bunte salts are usually less ordered compared to those formed from the corresponding thiols.

Two-dimensional (2D) SAMs formed on flat gold and platinum surfaces from Bunte salts have been investigated.[123, 131] Sodium *S*-dodecylthiosulfate ($C_{12}SSO_3Na$), potassium *S*- (2,5-dihydroxyphenyl) thiosulfate ($QSSO_3K$), and dipotassium *S*, *S'*- (3,6-dihydroxy-1, 2-phenylene) bisthiosulfate ($Q(SSO_3K)_2$ can form SAMs on gold through simple chemisorption.[123] XPS shows that the resulting Au-S bond is indistinguishable from that formed from chemisorption of corresponding alkanethiols. However, the rate of adsorption of Bunte salts is slower and the maximum coverage of SAMs formed from Bunte salts is smaller than that achieved with corresponding thiols. Similar results were obtained on platinum surfaces.[131] The differences in the adsorption rates and surface coverage between Bunte salts and thiols are attributed to the bulky thiosulfate headgroup. The mechanism of SAM formation from Bunte salts is described in Figure 1.7.[123] The S-SO_3 bond is cleaved upon adsorption of the Bunte salt on the gold surface

to yield adsorbed thiolated and sulfite species. Weakly bound sulfite can desorb or be displaced by another thiolated species. The formation of a SAM from Bunte salts can be tentatively presented as a successive dissociative chemisorption of thiosulfate molecules and desorption of the sulfite moieties.

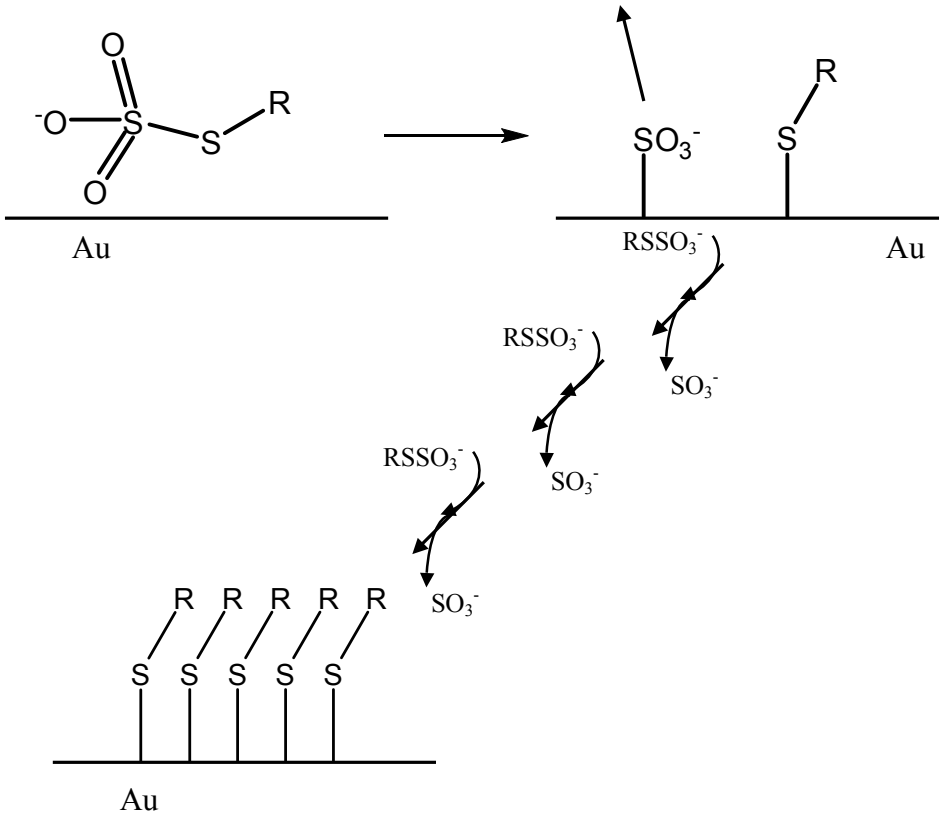

Figure 1.7 Chemisorption of Bunte salts on gold and the formation of a self-assembled monolayer.[123]

Chemisorption of Bunte salts has recently found applications in nanotechnology. The method produced important breakthroughs in terms of its stability to organize

nanoclusters at precisely controlled length scales using suitable bi-functional molecules with different terminal functional groups. The synthesis of monolayer-protected gold and silver nanoparticles has been reported.[129, 130] Functionalized gold clusters are synthesized by means of *S*-dodecylthiosulfate.[129] The results from NMR spectroscopy, XPS and Fourier transform infrared (FTIR) spectroscopy show that the resulting monolayer-protected clusters are indistinguishable in composition, monolayer architecture, and Au-S bonding from those prepared from the corresponding thiol.

Bunte salts have also been used to form monolayers on other metal surfaces. Jennings et al.[125] used thiosulfates to form monolayers on copper in aqueous and organic solvents, to provide a molecule-thick barrier against corrosion and oxidation. Results from infrared (IR) spectroscopy indicates that SAMs formed from Bunte salts on copper contain molecular-scale defects, lower adsorbate density, and more disordered alkyl chains than SAMs formed from alkanethiols, which is in agreement with results obtained using gold substrates.[123] Electrochemical impedance spectroscopy (EIS) reveals that SAMs formed from organic solvents are less ordered than those formed from aqueous solution on copper.

In summary, in terms of monolayer quality, SAMs formed from chemisorption of Bunte salts are not advantageous over SAMs formed from the corresponding thiols.

1.3.3 Electrochemically-Assembled Monolayers (ECAMs) of Bunte Salts

SAMs formed by electrochemical techniques are not new. Advances have been made using the electrochemical oxidation of Bunte salts on gold electrodes to control the formation of SAMs,[132-134] and reductive desorption of monolayers from modified

electrodes has been demonstrated.[135, 136] The electrochemical oxidation of Bunte salts is known to produce disulfides.[137] This method has recently been employed to form SAMs on gold.[124, 126] The key advantage of this electrochemical technique over the conventional chemisorption of alkanethiols is that SAMs can be selectively formed only on electrodes with potentials high enough to oxidize the Bunte salts.[124] The selectivity of the technique offers the potential to fabricate microelectrode arrays with differentiated surface chemistry, a goal of great importance in the fabrication of sophisticated sensor arrays. Other attractive features of this electrosynthesis of SAMs include: a) the control it provides over the degree of coverage; b) the short time needed to form SAMs; c) the ability to form SAMs easily on gold that is not freshly evaporated; d) the ease of preparation of Bunte salts.

Hydroquinone-thiosulfate and naphthoquinone-thiosulfate have been deposited from aqueous solutions on gold electrodes by means of anodic oxidation.[126] The monolayers are complete in about 40 s. This is significantly faster than the rate at which a thiol monolayer adsorbs spontaneously. The mechanism of ECAMs has been investigated: the electrochemical oxidation of thiosulfates produces a thioradical as the primary product, which dimerizes spontaneously to the disulfide and adsorbs onto the electrode (Equation 1.3-1.5). Self-adsorption of Bunte salts is hindered in aqueous solution with KCl as the supporting electrolyte.[126] The mechanism of the KCl effect is not discussed in this work.

$$H_2QSSO_3^- \rightarrow H_2QS^* + SO_3 + e^- \qquad (1.3)$$

$$H_2QS^* \Leftrightarrow QS^* + 2e^- + 2H^+ \qquad (1.4)$$

$$2QS^{*} \rightarrow QSSQ \qquad (1.5)$$

$$QSSQ + 4e^{-} + 4H^{+} \Leftrightarrow H_2QSSQH_2 \qquad (1.6)$$

Ferguson et al.[124] showed that C_{16}-thiosulfate would selectively deposit on gold electrodes with potentials high enough to oxidize the thiosulfate by the application of anodic pulses (anodic pulse deposition (APD)) from a tetrahydrofuran (THF) solution. Maximum coverage is achieved in less than 20 min, which is much shorter than the time required for thiol chemisorption. In addition, the extent of coverage can be controlled by adjusting the pulse number. XPS spectra of monolayers formed by the electrochemical oxidation of a Bunte salt and the chemisorption of the corresponding thiol were indistinguishable. These authors also mentioned that SAMs can also form from aqueous solutions by the reduction of Bunte salts, a process known to produce thiols.[127] No details about the reduction of Bunte salts were discussed in this study.

In summary, ECAM of Bunte salts provides an opportunity to modify electrode surfaces to specific requirements. The approach is advantageous over chemisorption of thiols in terms of selectivity, preparation procedure, formation speed and the coverage control it provides. Among these advantages, the most promising is that it provides the possibility of depositing films selectively on structures of arbitrary shape or unapproachable location, such as within a fluidic microchannel. The monolayer is not removed locally but is rather deposited locally where anodic pulses produce the disulfide. Thus, contamination of different monolayers that are spatially close to each other is prevented.

1.4 OBJECTIVES

The first objective of this project was to design and fabricate an individually addressable electrochemical array based on screen-printing technology. The SPCEs were then converted into either Ag/AgCl reference electrodes or gold electrodes by electrodeposition. The array of two-electrode cells has then been electrochemically characterized.

The second objective of this project was to investigate single-component monolayers and two-component mixed monolayers formed electrochemically from Bunte salts, and to apply the results to the fabrication of enzyme-based biosensors and immunosensors.

Chapter 2: Fabrication and Characterization of an Individually Addressable Electrochemical Array

2.1 INTRODUCTION

2.1.1 Introduction

The area of biosensors is driven towards development of small, hand held and battery-operated instruments suited for on-site decentralized biomedical and industrial analysis, or environmental monitoring.[20] An electrochemical instrument would be ideal for this purpose, because electrochemical instrumentation has the potential to be compact, inexpensive, rugged, and versatile.[138] Compared to single electrodes, sensor arrays have the advantage of testing multiple analytes simultaneously. This is one of the reasons why research on electrochemical arrays has become of recent interest. The resulting responses from the array can be analyzed and interpreted using modern statistical techniques popularly known as chemometrics, hence leading to greatly improved chemical information. Application examples can be found in food,[139-141] environmental[39, 142] or clinical analytical chemistry,[143, 144] where arrays offer advantages such as fast and simple measurements directly on-site without any sample pretreatment.

A trend in the development of array biosensors is the movement towards miniaturized systems. Several advantages are obtained by microarray systems such as increased mass transport due to radial diffusion (resulting in a faster response at the transducer), reduced double-layer capacitance due to smaller electrode areas (the signal

to noise ratio is increased), and reduced ohmic drop.[50, 145] Despite the positive properties attributable to microarray systems, there are situations where macroarrays can be more favorable. Generally, macro systems are more robust towards contamination (dust particles, pollutants in the matrix and impure enzymes) and chemical cross-talk between the sensors.[146] The directed immobilization of functional biomolecules on individual microscopic regions is still a challenge.[50] Thus, a macroarray system can be a better choice if the purpose is to create biosensor arrays, especially at the initial stages of their development.

Screen-printing technology enables easy production of very flexible configurations of electrode-array devices that can be converted into biosensor arrays by modifying individual electrodes in the array with different biological components. These arrays can be disposable because they can be mass-produced at low cost. However, up to now, most of the SPE-based biosensors are used for single parameter measurements associated with electrochemical detection.[30, 42-46] Recently, multi-enzyme biosensor arrays based on screen-printing technology have been developed.[39, 141, 142]

The procedure of screen-printing is shown in Figure 2.1. The main parts of the printer include a printing table with various screens, which may be fabricated of stainless steel mesh, nylon, or polyester, stretched taut on a supporting framework. The electrode pattern is photographically formed onto the mesh using a filler emulsion which blocks all screen areas except the actual pattern to be produced. Screen mesh sizes are chosen according to the ink specifications provided by the suppliers. The screen is positioned above the desired substrate, allowing an approximate gap of about

0.5 mm. Once the screen has been positioned, the ink is applied to the screen surface, and scraped along the screen by a squeegee. The pressure under which the squeegee operates allows the highly viscous inks to be forced through the screen openings and deposited onto the substrates.

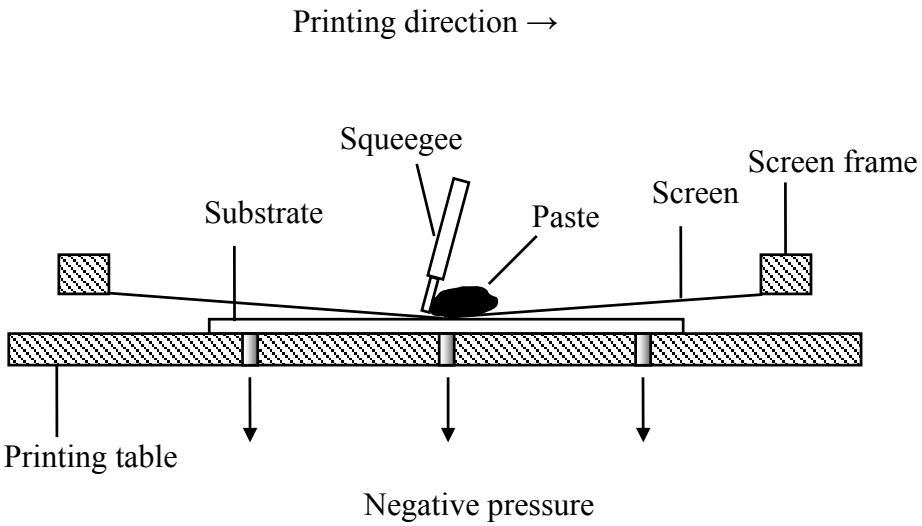

Figure 2.1 Screen-printing process. Negative pressure is generated by an air compressor.

The design of the sensor array plays a very important role in the quality of the analytical information, especially when used for *in vivo* measurements in clinical analysis.[147] The sensor array may be a three-electrode (working, auxiliary, and reference electrodes) or a two-electrode configuration (working and counter electrodes). Electrode arrays have been fabricated in a number of geometries. The simplest geometry from the standpoint of fabrication is random. Although difficult to

characterize geometrically, random arrays are fairly simple to construct from readily available materials.[148-150] Figure 2.2 shows an electrode array prepared by sealing thousands of carbon wires randomly into epoxy resin.[151] Arrays of electrodes based on disks have also been fabricated.[39, 152]

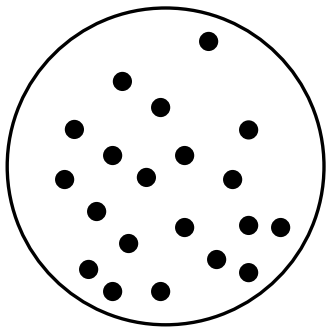

Figure 2.2 Depiction of an electrode array prepared by sealing carbon wires randomly into epoxy.

In recent years, a variety of carbon-based inks have been investigated as electrode materials. Such inks are composed of graphite particles, a polymeric binder (for these particles) and other additives for the promotion of dispersion, printing and adhesion. Electrodes made with carbon-based inks show relatively low background current, a wide operating potential window, convenient modification, renewability and low cost.[34] Electrochemical performance of a series of SPCEs has been investigated for sensors.[36] Commercially available carbon-based ink was chosen in this work to produce electrodes.

Electrochemical sensors need a reference or counter electrode to define an accurate electrochemical potential in the electrolyte solution, and the behavior of these

reference or counter electrodes is of critical importance for the reliable response of the electrochemical cell. Ag/AgCl electrodes are of special interest for the development of biosensors. Although many reports of various electrochemical sensors have appeared, only a few have dealt with the fabrication of planar reference electrodes. Desmond et al.[153] have developed a micropseudoreference electrode by combining silicon and screen-printing technology. In this work, a Ag/AgCl film was screen-printed onto a platinum layer deposited on an oxidized silicon substrate. The resulting Ag/AgCl pseudoreference electrode was manually modified by casting a resin containing powdered KCl and some additives required for polymerization. Another disposable reference electrode was developed using double matrix membrane technology.[154] In this work, a conducting Ag/AgCl film was screen-printed on heat-sealing paper, covered with filter paper and laminated together with the second sheet of the heat-sealing film. A micro-machined liquid-junction Ag/AgCl electrode, reported by Suzuki et al.,[155] is based on thin films of silver deposited on glass wafers using photolithography. The AgCl layer was formed chemically using $FeCl_3$ as an oxidant. In a recent report, a Ag/AgCl reference electrode was fabricated by screen-printing technology using a silver-silver chloride-based paste and a UV-cured protective paste. The electrodes obtained exhibit long operation and storage lifetimes and their potentials are not influenced by common components of real samples, such as chlorides as well as other halide anions, alkaline and heavy metal cations, complexing ligands and redox agents.[156]

For many biosensors, carbon-based materials are the most suitable; but for an array of electrodes modified with different biological components, gold electrodes are

of interest as they are readily modified by chemisorption of thiols.[60-62] Gold surfaces modified with thiols to produce SAMs have been employed in enzyme biosensors,[96-100] immunosensors,[93-95] and DNA chips.[64] Although gold-based inks are commercially available, and gold SPEs have been reported in many applications,[67-71, 157] they are not cost-effective (20-25 US $/g). Therefore, gold electrodeposition has been used in the current work to modify SPCEs. Modification of the gold surface has allowed the evaluation of further possibilities with the array.

Well-known problems with electrode arrays are electrical and chemical cross-talk.[51, 158] Electrical cross-talk can arise when independent electrode pairs are operated in the same solution, particularly when the potential difference between the reference and working electrodes is different. Further, because the individual sensing elements consume analyte in amperometric sensors, there is the possibility that the diffusion layers for adjacent sensing elements will overlap if they are in close proximity. This phenomenon is termed "chemical cross-talk". The effect of interaction of adjacent electrode elements has been examined by Wilson et al.,[51] and results have shown that the sensing elements must be separated by about 100 μm in order to avoid interference from adjacent sensors.

In this chapter, the design, fabrication and characterization of a disposable electrochemical array based on screen-printing are reported. The array, shown in Figure 2.3, consists of two halves, each having four printed carbon band electrodes, to yield an array of 4 × 4 individually addressable working electrodes with areas of 1 mm^2. A poly (dimethylsiloxane) (PDMS) sheet is employed as a spacer to construct microfluidic channels between the two halves. Bonding pads allow for external electronic

connections. The array contains 16 two-electrode cells, and the design offers the possibility to obtain a multi-parametric biosensor. SPCEs on one half were converted to Ag/AgCl electrodes using electrodeposition and anodization procedures and used as counter electrodes, and the SPCEs on the other half were electrodeposited with gold. The performance of the Ag/AgCl electrodes was investigated with ferrocenecarboxylic acid (FCA) using CV, and the surface features of the Au-deposited electrodes were investigated by SEM and XPS. The resulting array was then electrochemically characterized, using potassium ferricyanide, for reproducibility and chemical cross-talk.

2.1.2 Preceding Work

SPCE-based electrochemical arrays with different geometric arrangements have been studied in this research group. The method for the activation of SPCEs has been adapted from Thomas Mann's work.[159] The electrodeposition method for gold has been adapted from the M.Sc. research of Gabriele Hager.[160]

2.2 EXPERIMENTAL SECTION

2.2.1 Materials and Instrumentation

Potassium ferricyanide, FCA, potassium nitrate, silver nitrate, hydrogen tetrachloroaurate (III) hydrate (99.999%) and silver wire were purchased from Aldrich. Tris[hydroxylmethyl]aminomethane (Trizma base), tris[hydroxymethyl]aminomethane hydrochloride (Trizma hydrochloride) and ethylenediamine dihydrochloride were obtained from Sigma. BDH supplied potassium chloride, potassium cyanide, hydrochloric acid, sodium chloride and ammonia solution.

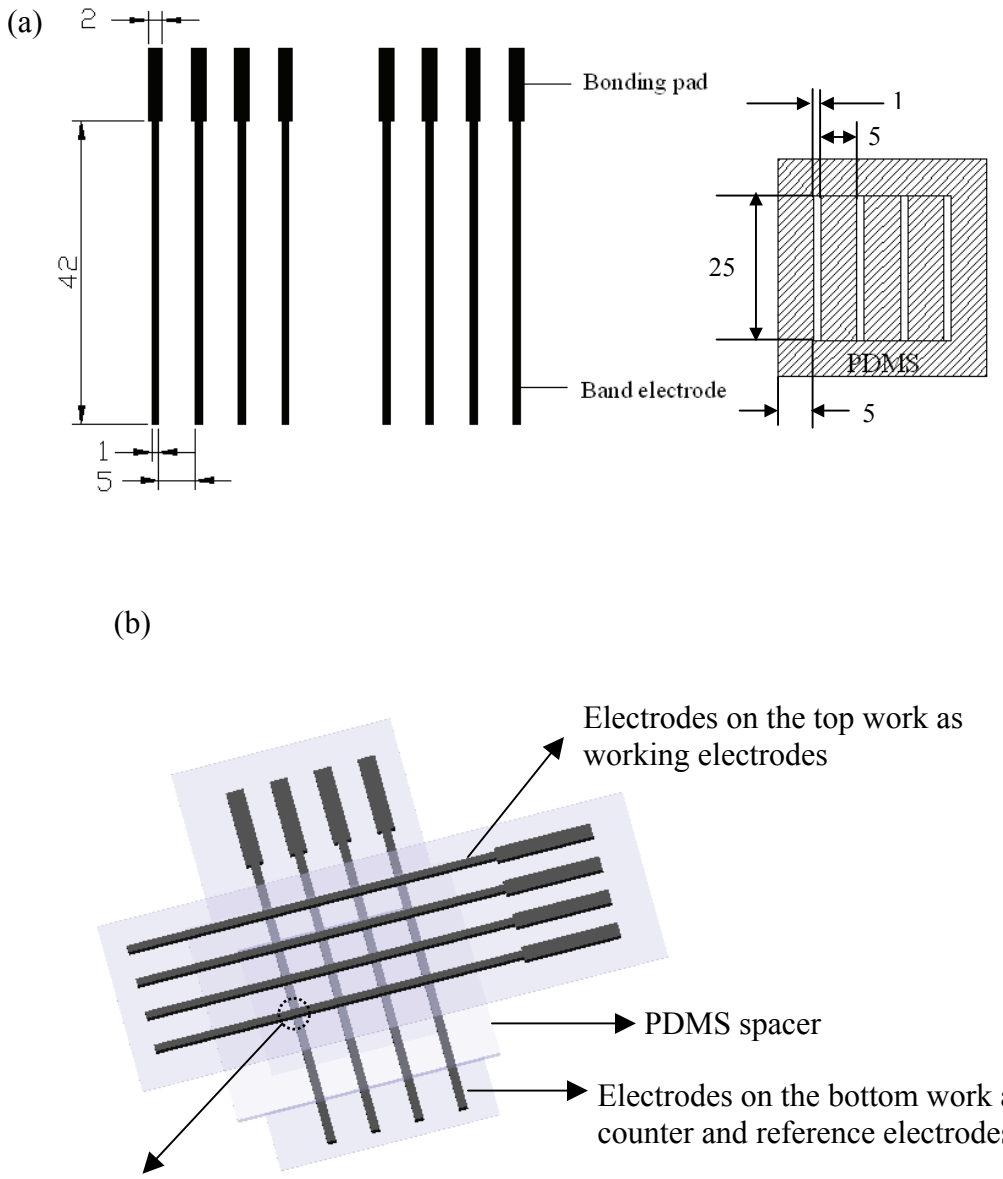

Figure 2.3 Schematic diagrams of (a) two halves of the screen-printed electrochemical array, and a PDMS spacer. Dimensions in mm; (b) the electrochemical array: the two halves are clamped face-to-face, with electrode bands at right angles. A PDMS spacer is used to construct microfluidic channels between the two halves. The thickness of the PDMS is 1 mm.

All reagents were of analytical-reagent grade. All solutions were prepared in water purified by a Milli-Q water purification system; its resistivity was > 18 MΩcm.

Electrochemical arrays were prepared using a DEK Model 248 semi-automatic screen printer (DEK Inc., Flemington, NJ) equipped with a vacuum tooling plate (DEK) to allow printing onto flexible substrate materials. Screens were designed with AutoCAD, manufactured by Hybrid Integrated Services (Mississauga, Ont.). Touch-Key E82-03 graphite conductive ink was purchased from Coates Screen. Polyester D (250 μm) sheets were obtained from Cadillac Plastic.

PDMS prepolymer (base) and curing agent (Sylgard® 184) were purchased from Dow Corning.

An EG & G Potentiostat/Galvanostat and a CHI650A Potentiostat were employed. Bioanalytical Systems supplied Ag/AgCl (3 M NaCl) reference electrodes and glassy carbon electrodes (3 mm diameter).

A scanning electron microscope (LEO FESEM 1530) was used to examine the surface morphology of the SPCEs and gold-modified SPCEs.

XPS analysis was performed using a multi-technique ultra-high vacuum Imaging XPS Microprobe system (Thermo VG Scientific ESCALab 250) equipped with a hemispherical analyser (of 150 mm mean radius) and amonochromatic AlKa (1486.60 eV) X-ray source.

A Branson 1200 ultrasonic bath was employed for cleaning the SPCEs.

2.2.2 Methods

2.2.2.1 Screen-Printed Sensor Array

The electrochemical array design used in this work is shown in Figure 2.3. Polyester sheets (approximately 35 cm × 35 cm) as screen-printing substrates were first cleaned with ethanol and pretreated at 83 °C for 1 h in a convection oven. This procedure cleaned the substrate sheets of any particulate matter, as well as preventing shrinkage or warping later in the process. The graphite conducting ink was then applied to the screen surface and printed onto the polyester surface. The screen-printed electrodes were cured immediately for 15 min at 93 °C.

The PDMS used in the experiments is supplied in two components, a base and a curing agent. A 10:1 (w/w) mixture of PDMS base and curing agent was stirred thoroughly and then poured onto a mold (Figure 2.4), which is made of Teflon® and has the dimensional features of the array, and cured for 4 h at 60 °C. The liquid PDMS pre-polymer conforms to the shape of the mold and replicates the features of the mold with high fidelity. The thickness of the PDMS spacer is 1 mm. The low surface free energy and elasticity of PDMS allow its release from Teflon® molds without damaging the mold or itself. PDMS can seal to itself or to other surfaces reversibly and without distortion of the channels, because it is elastic. A reversible seal provided by simple van der Waals contact is watertight but cannot withstand pressures greater than ~ 5 psi.[161]

The assembly of the electrochemical array is shown in Figure 2.3(b). The arrays were then sandwiched between two glass plates using clips, to provide mechanical

stability. The PDMS spacer created the microfluidic channels between the two halves of the electrochemical array.

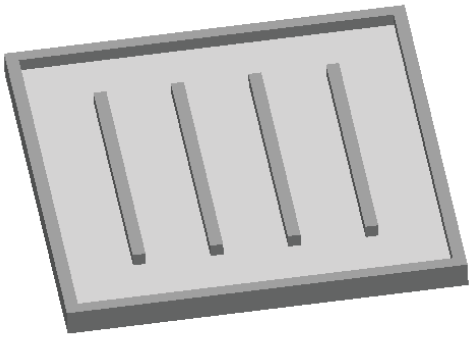

Figure 2.4 The mold for construction of the PDMS spacer.

2.2.2.2 Ag/AgCl Reference Electrodes

SPCEs were pretreated by sonicating in ethanol for 2 min, rinsed with water, and wiped vigorously with a Kimwipe before plating. Two steps were involved in the fabrication of the Ag/AgCl reference electrodes. First, silver was electrodeposited. The plating procedure is adapted from Scharifker et al.[162] The plating solution contains 0.1 M $AgNO_3$, 1.0 M KNO_3 and 1.0 M NH_4OH. The potential was stepped from -0.4 V (1s) to -0.3 V (1s) for 200 cycles. Complete reflective silver coverage can be obtained with this method. Second, the AgCl layer was formed electrochemically in a 0.1 M KCl solution, by stepping the potential from 0.4 V (1s) to 0.3 V (1s) for 20 cycles. In both steps, silver wires were employed as auxiliary and reference electrodes. The performance of the Ag/AgCl reference electrodes was investigated in 0.1 mM FCA in

0.1 M Tris buffer (pH 7.0) using CV. These experiments used a two-electrode system: a glassy carbon electrode (3 mm diameter) was used as the working electrode, and the Ag/AgCl electrode under investigation was used as the counter electrode.

2.2.2.3 Gold-Modified SPCEs

The gold plating solution was prepared from two separate solutions. Solution 1 was prepared by combining 0.533 g $HAuCl_4$, 4.853 g KNO_3 and 0.558 g KCN in 100 mL water and was reduced in volume to about 50 mL by boiling. Solution 2 was prepared by dissolving 6.81 g $NH_2(CH_2)_2NH_2 \cdot 2HCl$ in 80 mL water, followed by pH adjustment to 1.00 using concentrated HCl. Solutions 1 and 2 were combined and diluted to 200 mL. The gold concentration in the final plating solution was 7.86×10^{-3} M.

The gold plating solution was de-aerated with pure nitrogen gas for about 30 min before use. The pretreatment of SPCEs was the same as that used for silver plating. SPCEs were activated by an electrochemical method: the potential was stepped to -2.0 V for 60 s and +1.0 V for 60 s. Gold plating was achieved by stepping the potential 900 times from -1.1 V (1s) to +0.8 V (0.1s) and back again. Nitrogen over the electrochemical cell was used to maintain the de-aerated environment within the cell and to create agitation in the solution during the plating process. In the activation and plating steps, a commercial Ag/ AgCl electrode (3 M NaCl) and a Pt wire were used as the reference and auxiliary electrodes, respectively.

This method provided a visually complete, reflective gold surface. The surface properties of the gold-modified SPCEs were investigated with XPS and SEM.

2.2.2.4 Electrochemical Behavior of the Array

Electrode-to-electrode variability in area and surface properties in the screen-printed array is expected to contribute to imprecision in the final assays. Because of this, the reproducibility of the electrodes on the same array and different arrays was investigated by CV, using 1.0 mM potassium ferricyanide in 0.1 M KCl. Cyclic voltammograms from each individually addressable working electrode were recorded while applying a potential scan from +0.45 to -0.10 V at a scan rate of 20 mV/s. In these experiments, gold-modified SPCEs were used as the working electrodes, and home-made Ag/AgCl electrodes served as counter electrodes in two-electrode cells.

2.2.2.5 Chemical Cross-Talk

Two EG & G Potentiostats/Galvanostats were used for the investigation of chemical cross-talk. The entire electrochemical array was set in a Faraday cage that was earth grounded.

2.3 RESULTS AND DISCUSSION

2.3.1 Ag/AgCl Reference Electrodes

The performance of the home-made Ag/AgCl reference electrodes was investigated in 0.1 mM FCA by CV at a scan rate of 50 mV/s. Six electrodes were tested and Figure 2.5 shows typical voltammograms using house-made Ag/AgCl as a counter electrode, and a glassy carbon electrode (Bioanalytical Systems, West Lafayette, IN, USA) as a working electrode.

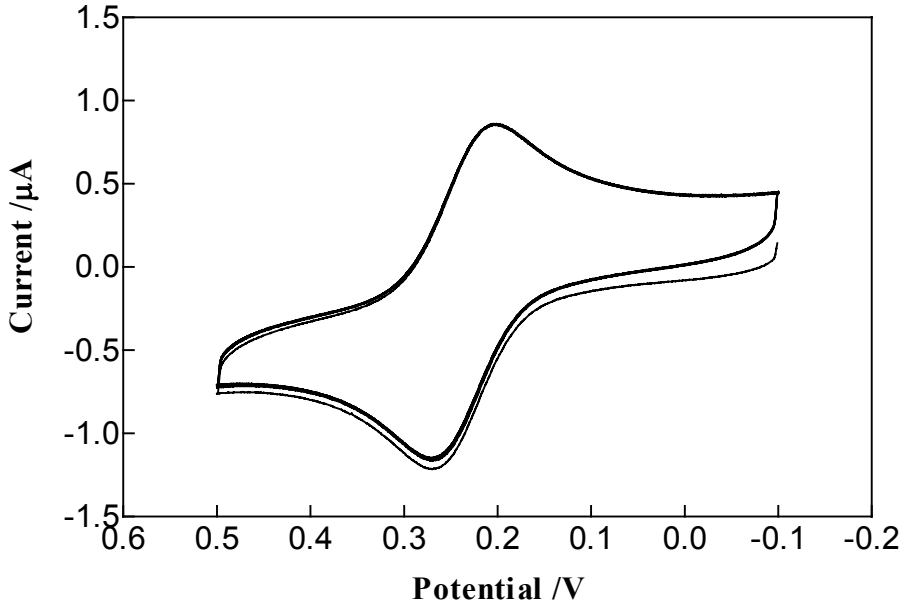

Figure 2.5 Cyclic voltammograms of 0.1 mM FCA in 0.1 M Tris buffer (pH 7.0), scan rate 50 mV/s, 10 cycles.

The potential of the home-made Ag/AgCl reference electrodes can be determined from the positions of the anodic and cathodic peaks for FCA in Figure 2.5, since a literature value is available for the formal potential ($E^{0'}$) of this species under identical conditions (+0.289 V vs. SCE[163]):

$$E^{0'} = \frac{E_{p,a} + E_{p,c}}{2} \qquad (2.1)$$

where $E_{p,a}$ is the anodic and $E_{p,c}$ is the cathodic peak potential. Over ten cycles, $E^{0'}$ was found to be +0.238 V (± 1.3%) vs. the home-made Ag/AgCl reference electrode. Since the potential of the saturated calomel electrode (SCE) reference electrode is +0.241 V vs. normal hydrogen electrode (NHE),[164] the potential of the home-made Ag/AgCl reference electrode is +0.292 V vs. NHE.

This value can be compared with the value calculated from the Nernst equation, with $E^{0}_{Ag/AgCl} = +0.222V$ vs. NHE[164] and $[Cl^-]$=0.09 M:

$$E_{Ag/AgCl} = E^{0}_{Ag/AgCl} - 0.0592 \log[Cl^-] \qquad (2.2)$$

From Equation 2.2, the theoretical value for the potential of the home-made Ag/AgCl reference electrode is +0.284 V vs. NHE, which is very close to the value from the experiments (+0.292 V). Therefore, the behavior of home-made Ag/AgCl reference electrodes can be predicted by the Nernst equation. Moreover, the home-made Ag/AgCl as a reference electrode provides a constant, stable potential.

The storage stability of home-made Ag/AgCl electrodes was also investigated with the same method described above. $E^{0'}_{Fc(vs.Ag/AgCl)}$ was chosen to evaluate the stability of Ag/AgCl electrodes after they were stored dry at room temperature. Table 2.1 summarizes the results.

As seen in Table 2.1, home-made Ag/AgCl electrodes show good storage stability for at least 30 days.

Table 2.1 Storage stability of home-made Ag/AgCl reference electrodes.

Storage time (days)	1	2	3	15	30
$E^{0'}_{Fc(vs.Ag/AgCl)}$ (mV)*	238 ± 3	237 ± 1	237 ± 2	238 ± 2	239 ± 3

* 0.1 mM FCA in 0.1 M Tris buffer (pH 7.0), scan rate 50 mV/s. (n=6)

2.3.2 Surface Properties of Gold-Modified SPCEs

The surface topography of the electrodeposited gold layer is expected to play a key role in further modification of the electrodes. SEM images of a SPCE and a gold-modified SPCE are shown in Figure 2.6. The scans were performed in imaging mode and at a magnification of 1000×. The image of the unmodified SPCE reveals the granular particles (Figure 2.6(a)), and the image of the gold-modified SPCE (Figure 2.6(b)) indicates that gold coverage is almost complete, with some carbon particles exposed at the surface of the electrode. Based on the CV results obtained, these areas do not contribute to voltammetric signals (Figure 2.7).

Data from XPS confirm the above results that gold coverage on the surface of SPCE is almost complete (Figure 2.8). Other than gold and carbon, zinc was also found on the surface of the electrode. Zinc exists as an impurity (0.2 ppm) in hydrogen tetrachloroaurate (III) hydrate. Zinc cations were reduced at the negative potential used during the gold-plating process.

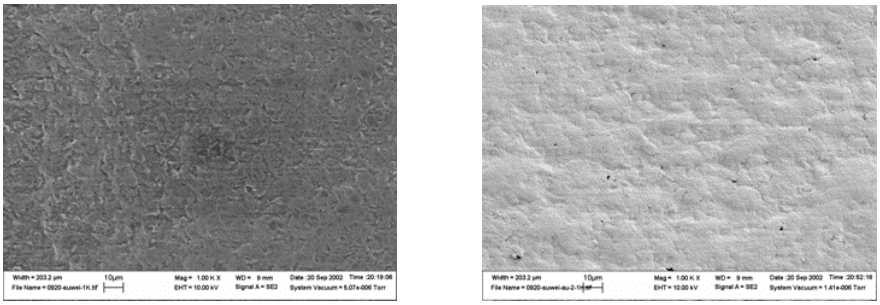

(a) (b)

Figure 2.6 SEM images of a (a) SPCE and (b) gold-modified SPCE, taken at 1000× magnification.

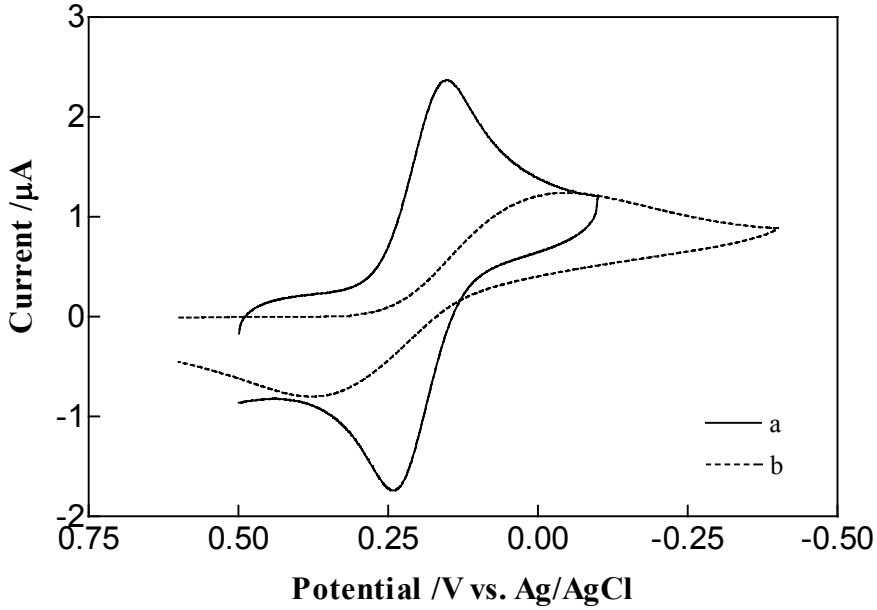

Figure 2.7 Cyclic voltammograms for a gold-modified SPCE (a) and SPCE (b) using 1.0 mM $K_3Fe(CN)_6$ in 0.1 M KCl, employing commercial Ag/AgCl and Pt wire as reference electrode and auxiliary electrode, respectively. Geometric areas of the working electrodes are 1 mm^2, scan rate 50 mV/s.

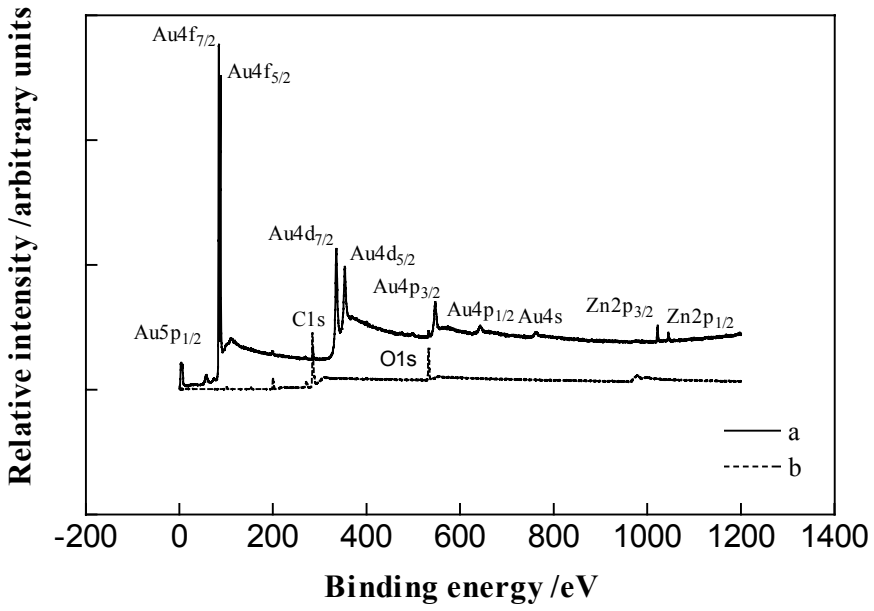

Figure 2.8 X-ray photoelectron spectrum for a gold-modified SPCE (a); and a SPCE (b).

2.3.3 Reproducibility of the Array

The electrochemical reproducibility of the working electrode elements of the array was tested with a simple, well-known electroactive species, $K_3Fe(CN)_6$, using CV. The cyclic voltammetric experiments were conducted in a 1.0 mM $K_3Fe(CN)_6$ solution with 0.1 M KCl as supporting electrolyte and a potential scan rate of 20 mV/s. Cyclic voltammograms were recorded at each electrode and Figure 2.9 shows a typical voltammogram. Both peak potentials and peak currents were recorded on the 16 electrodes of 3 different arrays to evaluate reproducibility. Table 2.2 summarizes the results obtained. In these experiments, gold-modified SPCEs were used as working electrodes, and home-made Ag/AgCl electrodes worked as counter electrodes.

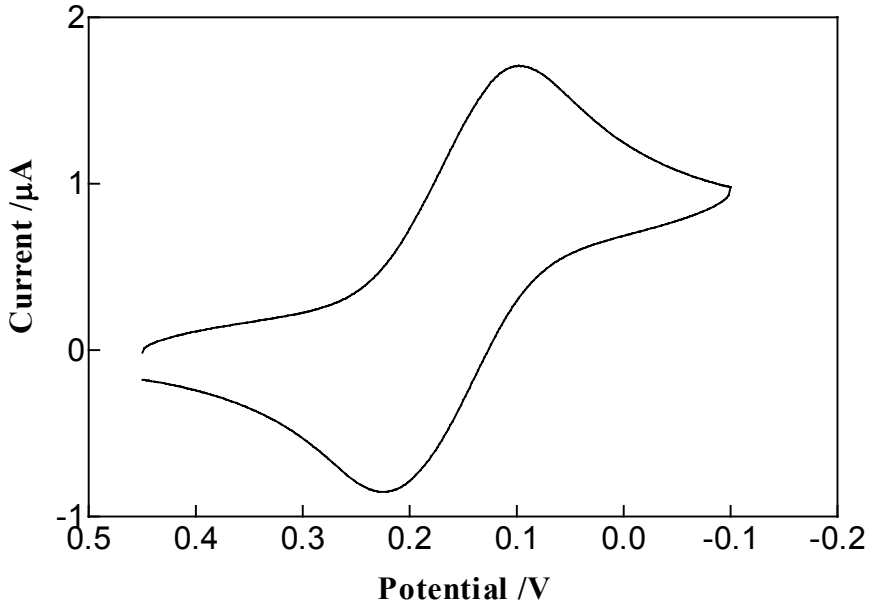

Figure 2.9 Cyclic voltammogram using 1.0 mM $K_3Fe(CN)_6$ (in 0.1 M KCl) from one of the individually addressable working electrodes, scan rate 20 mV/s.

As can be seen in Table 2.2, very low variation in peak currents and potentials was found within a particular array. For example, R.S.D. values were 7.4%, 4.5%, 8.9% and 7.4% for reduction potential, oxidation potential, reduction current, and oxidation current, respectively in array (2). Therefore, the 16 electrodes composing a particular array can be considered as almost identical and used interchangeably for further applications.

Moreover, the array-to-array variations of the electrochemical characteristics were very good.

Table 2.2 Peak potentials and peak currents for different electrodes on a given array and different arrays. *

Electrode-to-electrode	Reduction potential (V)	Reduction current (μA)	Oxidation potential (V)	Oxidation current (μA)
On the same array (1)	0.103 ± 0.005	1.23 ± 0.07	0.215 ± 0.006	1.19 ± 0.06
(2)	0.108 ± 0.008	1.35 ± 0.12	0.223 ± 0.010	1.22 ± 0.09
(3)	0.101 ± 0.007	1.19 ± 0.10	0.209 ± 0.007	1.08 ± 0.08

*1.0 mM $K_3Fe(CN)_6$ in 0.1 M KCl. Potential scan from +0.45 to -0.10 V; scan rate 20 mV/s.

2.3.4 Chemical Cross-Talk

The chemical cross-talk between adjacent sensing elements on the array were evaluated using 1.0 mM $K_3Fe(CN)_6$. Figure 2.10 shows a typical cyclic voltammogram from an individually addressable electrode. In case (a) CV was done only on one electrode (for example, electrode1) so that there was no interference from adjacent electrodes due to chemical cross-talk. In case (b) CV was done on two adjacent electrodes (for example, electrode 1 and electrode 2) simultaneously, and signals from electrode 1 recorded under this condition was used to compare with that obtained in case (a). If chemical cross-talk exists between adjacent electrodes, the responses from electrodes are smaller than those obtained from electrodes without chemical-talk. As seen in Figure 2.10, no significant difference was observed between these two cases. From this we concluded that the diffusion layers of the adjacent array electrodes did not overlap on this time scale and the 16 individual electrode signals can be regarded as 16 independent current signals at short time scales.[165, 166]

2.4 CONCLUSIONS

An individually addressable electrochemical array was designed and fabricated based on screen-printing. PDMS worked as a spacer and created microfluidic channels in the array. The Ag/AgCl reference electrodes converted from SPCEs by electroplating and anodization procedures showed good storage stability. Gold modification of the SPCEs was achieved with hydrogen tetrachloroaurate (III) solution. The results from SEM and XPS indicated that coverage was almost complete, even though there were defects on

the surface. The reproducibility of the array consisting of home-made Ag/AgCl reference electrodes and gold-modified working electrodes was evaluated by CV, and R.S.D. values were found to be below 9.0% for electrode-to-electrode variability on the same array and different arrays. Simultaneous multichannel measurements are feasible since no chemical cross-talk was observed between adjacent sensing elements on the array.

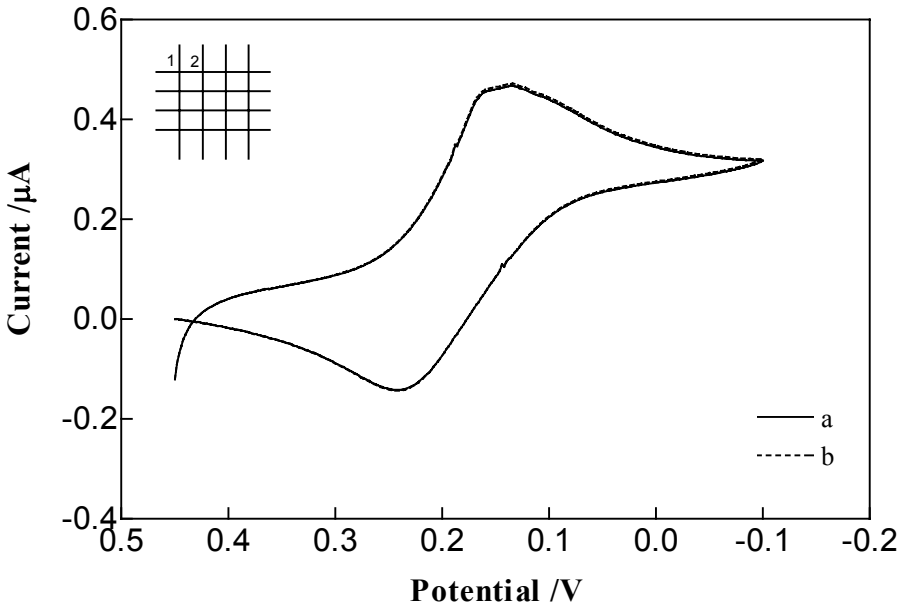

Figure 2.10 Cyclic voltammograms in 1.0 mM $K_3Fe(CN)_6$ (in 0.1 M KCl) for electrode 1 when CV was conducted (a) only on electrode 1 and (b) on electrode 1 and the adjacent electrode (electrode 2) simultaneously. Scan rate 2 mV/s. Inset is the array.

Chapter 3: Patterned Electrodeposition of Bunte Salts

3.1 INTRODUCTION

The immobilization of biomolecules onto the surfaces of electrically-conducting materials is an active area of research useful for a range of applications including the construction of electrochemical biosensors. A general methodology that is currently being utilized for this purpose is the self-assembly of molecules on specific surfaces such as the chemisorption of thiols on gold. SAMs prepared with thiols are stable and easily prepared with virtually any desired functionality.

The terminal functional group of a monolayer is critical for the purpose of immobilizing biomolecules. The evidence to date suggests that, as expected, the functional groups are present at the distal end of the thiol molecules,[111, 167, 168] which is a prerequisite for immobilizing biomolecules. However, bulky functional groups (COOH, ferrocene) may disturb the structure of the monolayer.

Binary mixed monolayers have been studied for the purpose of immobilizing biomolecules. Overabundance of surface functional groups, steric hindrance, and the concomitant less ordered monolayers, which lead to denaturation and reduced activity of biomolecules, can be avoided by controlling the surface composition and distribution of the adsorbates. In a binary matrix, long chain components bearing functional groups (e.g., -COOH) provide binding sites for biomolecules and act as a framework, preventing a probe molecule from penetrating through the monolayer; short chain components act as a template that induces defects within the framework that permit the penetration of redox probes.

Much work has been published on functionalized, alkanethiol-based mixed SAMs prepared by coadsorption of two or more different thiols from solution. Many complex factors can affect the assembly process of mixed monolayers, such as solvation of the adsorbates in the solution, the adhesion probability of each molecule, and the degree of interaction between the molecules once they are adsorbed. Mixed SAMs composed of short- and long-chain alkanethiols,[113, 116, 117] molecules that differ both in chain length and functional groups,[118] molecules of similar length but with differing terminal groups[119, 120] and molecules of similar length but with differing, buried functional groups,[115, 121] have been investigated. However, the assembling components are often separated into islands if they are chemically dissimilar.

Bunte salts provide a potential alternative to the use of alkanethiols for forming SAMs.[123-126] The chemical[169] or electrochemical oxidation[137] of Bunte salts is known to produce disulfides. Bunte salts can form monolayers on metal surfaces either by chemisorption[123, 125] or by electrochemical methods.[124, 126] These compounds are more soluble in aqueous solution than the corresponding thiols and are easily synthesized. They can be conveniently obtained by the reaction of sodium thiolsulfate with terminal alkenes having electron-withdrawing groups.[127] Compared to SAMs prepared by chemisorption of the corresponding thiols, SAMs formed from chemisorption of Bunte salts have molecular-scale defects, lower adsorbate density and more disordered alkyl chains compared to thiol-based SAMs.[123]

Some previous studies of electrochemical-assembly of Bunte salts have been done.[124, 126] Nann et al.[126] reported that hydroquinone-thiosulfate and naphthoquinone-thiosulfate can be deposited from aqueous solutions on gold electrodes by means of

anodic oxidation. The monolayer was complete in about 40 s. This is much shorter than the time required for thiol chemisorption. Ferguson et al.[124] showed that C_{16}-thiosulfate can be selectively electrodeposited on gold electrodes in THF/0.1 M Bu_4NBF_4. Monolayers produced in this way are very similar to those prepared using the conventional adsorption of thiols or disulfides, as indicated by several methods of characterization including contact angle measurements, ellipsometry, and high-resolution XPS. In particular, the XPS results for monolayers produced by both methods were indistinguishable. An earlier study of hexylthiosulfate and benzylthiosulfate at gold electrodes was carried out in two aqueous electrolytes: 0.5 M H_2SO_4 and 1 M $NaHCO_3$.[137] The most recent research studied different Bunte salts ($CH_3(CH_2)_nS_2O_3Na$, n=7,9,11,13,15) dissolved in THF/0.1 M Bu_4NBF_4.[170] The proposed mechanism of electrochemical-assembly of Bunte salts is summarized in Figure 3.1.[124, 137, 170] Electrochemical oxidation of Bunte salts leads to the formation of an alkylsulfide radical by release of SO_3;[137] this radical can then combine directly with the gold surface, or couple to form a disulfide. Either of these pathways would be expected to lead to the formation of monolayers, as disulfides oxidatively add to gold surfaces readily.[171] Finally, SO_3 would be expected to react with any water in the solvent to form sulfate ions.

Several advantages of the electrochemical method over conventional chemisorption exist: monolayers can be completed in a short time; monolayers can be selectively formed only on electrodes with potentials high enough to oxidize Bunte salts; and the coverage of monolayers can be controlled by adjusting the time for oxidation.[124, 170] The selectivity of this method offers the potential to fabricate

microelectrode arrays with differentiated surface chemistry, a goal of great importance in the fabrication of sophisticated sensor arrays.

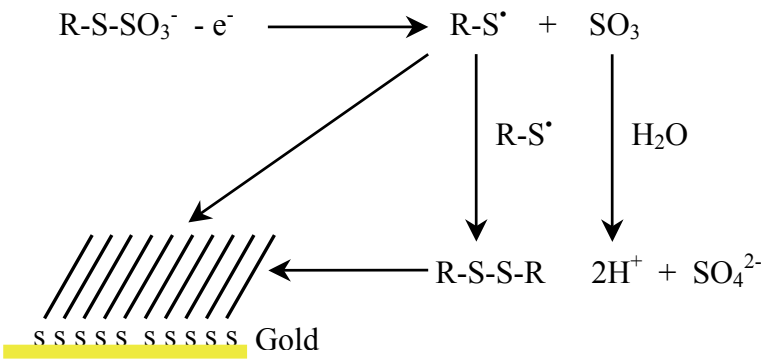

Figure 3.1 Mechanism for monolayer formation by electrochemical oxidation of Bunte salts at a gold electrode.[124, 137, 170]

The monolayers can be characterized by a variety of methods including physical measurements like contact angle and wettability, ellipsometry, XPS, IR, QCM, STM, atomic force microscopy (AFM), fluorescence spectroscopy, and SPR. Electrochemical techniques like CV and impedance measurements are especially useful for monitoring monolayer quality for biosensors. For example, although a monolayer can completely cover a metal surface, some 'pinhole' defects are always present and these allow direct contact of redox active molecules with the electrode surface.

In this chapter, experiments with single- and binary-component monolayers, formed electrochemically from Bunte salts, are reported. The binary mixed monolayers were designed to contain short- and long-chain components, where the long-chain

component bears a functional group (-COOH) that can act as a binding site for biomolecules. The short-chain component allows electrochemistry to occur at the electrode surface below. The factors that affect the assembly of the monolayers, such as solvent, electrochemical technique employed, and concentration of Bunte salts were studied. The resulting single- and binary-component monolayers were electrochemically characterized, and their stabilities were also investigated.

3.2 EXPERIMENTAL SECTION

3.2.1 Materials and Instrumentation

1-Chlorobutane (99.5%), 1-chlorohexane (99%), 1-chlorooctane (99%), 1-chlorodecane (98%), 11-bromoundecanoic acid (99%), potassium thiosulfate pentahydrate (99.5%), and ethyl alcohol were obtained from Aldrich. Chloroform was obtained from Sigma. Nitric acid was purchased from Fisher Scientific.

Commercially available Revlon nail enamel (Clear 76), purchased at a local pharmacy, and white vinyl gloss (C99-5103-1G), supplied by Screentec, were employed for defining SPCE areas.

RE 111 Rotavapor was used to evaporate solvent for synthesis of Bunte salts.

Elemental analyses were performed by M-H-W Laboratories (Phoenix, U.S.A).

An EG & G Potentiostat/Galvanostat and a CHI650A Potentiostat were employed. Bioanalytical Systems supplied Ag/AgCl (3 M NaCl) reference electrodes.

All electrochemistry experiments were performed in a conventional three-electrode configuration, with a platinum wire as the auxiliary electrode, and Ag/AgCl

(3 M NaCl) as the reference electrode. The working electrode was a bare or monolayer-modified gold-covered SPCE (geometric area 1.0 mm^2).

3.2.2 Methods

3.2.2.1 Preparation of Bunte Salts, $CH_3(CH_2)_n S_2O_3Na$ (n=3,5,7) and $HOOC(CH_2)_{10}S_2O_3Na$

Bunte salts were prepared following a literature procedure.[127, 129, 172-176] The reactions used 1-chlorobutane, 1-chlorohexane, 1-chlorooctane, 1-chlorodecane, and 11-bromoundecanoic acid. For synthesis of $CH_3(CH_2)_nS_2O_3Na$ (n=3,5,7), alkyl halides (0.01 mol) dissolved in ethanol (total volume 15 mL) was added to a solution of sodium thiosulfate (0.01 mol) in 15 mL water, and the mixture was refluxed under argon for 4.5 h. After cooling, the solvent was removed using a Rotavapor, and the crude product was collected and recrystallized from hot ethanol. For synthesis of $HOOC(CH_2)_{10}S_2O_3Na$, 11-bromoundecanoic acid (0.01 mol) dissolved in 15 mL ethanol was added to a sodium thiosulfate (0.01 mol) in 15 mL water, and the mixture was refluxed under argon until it became homogeneous (30 min). After cooling, the solvent was removed using a Rotavapor, and unreacted 11-bromoundecanoic acid was extracted from $CHCl_3$. The crude product was recrystallized from hot ethanol. Table 3.1 summarizes the elemental analysis results for these compounds.

3.2.2.2 Preparation of Gold Substrate

Gold-modified SPCEs (prepared by the method described in Section 2.2.2.3) were used

Table 3.1 Bunte salts used in this work.

$$R - X + Na_2S_2O_3 \rightarrow R - S_2O_3Na + NaX$$

Starting materials	Bunte salts			Elemental analysis*					
	Abbreviation	Formula	Yield, %	C, %		H, %		S, %	
				(theory)	(found)	(theory)	found)	(theory)	(found)
$CH_3(CH_2)_3Cl$	C4	$CH_3(CH_2)_3S_2O_3Na$	55	24.99	25.00	4.72	4.84	33.36	33.18
$CH_3(CH_2)_5Cl$	C6	$CH_3(CH_2)_5S_2O_3Na$	52	32.71	32.51	5.95	6.04	29.11	28.87
$CH_3(CH_2)_7Cl$	C8	$CH_3(CH_2)_7S_2O_3Na$	50	38.69	38.56	6.90	7.06	25.82	25.66
$HOOC(CH_2)_{10}Br$	C10-COOH	$HOOC(CH_2)_{10}S_2O_3Na$	85	41.24	41.51	6.61	6.65	20.02	20.07

* All elemental analysis results are within ±0.3% of the respective theoretical values.

as the substrates for the formation of monolayers. The electrode areas were 1 mm × 1 mm and defined using either clear nail polish or white vinyl gloss ink (depending on the assembly solvent). Before the assembly process, the electrode was cleaned in aqua regia solution containing 14% HCl and 9% HNO_3 for 10 s, rinsed with water, and blown dry with nitrogen.

3.2.2.3 Electrochemical-Assembly of Bunte Salts

Solutions of Bunte salts (total concentration 2.0 mM) were deaerated with nitrogen for 20 min before use in order to prevent etching which has been reported for gold surface exposed to thiosulfate solutions containing an oxidizing species.[177] Potential pulses and CV were employed to form monolayers. After the electrochemical deposition step, electrodes were rinsed with the corresponding solvent and water. Monolayer formation was examined by CV at a scan rate of 100 mV/s in 1.0 mM $K_3Fe(CN)_6$ with 0.1 M KCl. Complete monolayer formation is expected to result in blocked surfaces displaying no Faradic signals with ferricyanide.

3.2.2.4 Electrochemical Characterization of Monolayers

The electrochemical responses of $K_3Fe(CN)_6$ and FCA at electrodes modified with binary monolayers were investigated using CV.

Measurement of capacitance is another valuable method that can be used to assess the quality of molecular packing in monolayers. CV in 0.1 M KCl was performed to determine the capacitance values of gold-modified SPCEs before and after monolayer formation. The potential was scanned at 100 mV/s between -0.1 and

+0.3 V. The double-layer capacitance of the monolayer-covered electrodes can then be calculated using the following equation: [178, 179]

$$C_{dl} = i_c \cdot \upsilon^{-1} \cdot A^{-1} \qquad (3.1)$$

where C_{dl} is the double-layer capacitance, i_c is the charging current, υ is the scan rate, and A is the electrode surface area. The difference between the charging currents measured at a given potential on the anodic and cathodic segments of the voltammograms is equal to twice the charging current. The values reported in this work were measured at +0.1 V. The electroactive areas of the gold-covered SPCEs were determined prior to monolayer formation in 1.0 mM ferricyanide with 0.1 M KCl using chronoamperometry.[180] Briefly, experiments were performed by stepping from +0.5 to -0. 1 V for 15 s. Data were plotted as $i \cdot t^{1/2}$ vs. t, and the $t = 0$ intercept was determined by extrapolation of the linear regression line. The electrochemical surface areas (A) were calculated using the Cottrell equation as:

$$A = \frac{i \cdot t^{1/2} \pi^{1/2}}{FCD^{1/2}} \qquad (3.2)$$

where i is the current, t is the time, F is the Faraday constant, C is the concentration and D the diffusion coefficient. The diffusion coefficient for $K_3Fe(CN)_6$ employed for all data calculations was 7.6×10^{-6} cm^2 s^{-1}.[181]

The electrochemical stabilities of the monolayer-modified electrodes were investigated as a function of electrode potential in 0.1 M H_2SO_4. The storage stabilities of monolayers were also examined under different conditions.

3.2.2.5 Control Experiments

For the synthesis of C10-COOH, it is really hard to totally remove starting materials $HOOC(CH_2)_{10}Br$ and NaBr, so they are present as impurities. The existence of Br^- was detected by silver nitrate ($[Br^-]<3.0\%$). The influence of these impurities on the formation of monolayers was investigated by CV using $Fe(CN)_6^{3-}$ and capacitance determined by CV in 0.1 M KCl.

3.3 RESULTS AND DISCUSSION

3.3.1 Oxidation of Bunte Salts

Initial studies of the electrochemistry of the Bunte salts were carried out using CV in 0.2 M phosphate buffer (pH 6.0). Although acid hydrolysis can occur in aqueous solution, leading to the respective mercaptans, the reaction needs a few hours to occur under reflux conditions. Experiments in this work have been carried out at shorter times (less than 1 h) as well as at room temperature. Figure 3.2 shows typical cyclic voltammograms recorded at a gold-modified SPCE in 0.2 M phosphate buffer (pH 6.0) in the absence and presence of C4. The inset magnifies the data in the range of potentials from +0.3 to +1.2 V.

Similar results were obtained with the other Bunte salts shown in Table 3.1.

The oxidation wave between +0.9 to +1.0 V in Figure 3.2 represents the formation of gold oxide on the electrode surface.[182] When the scan direction is reversed, there is a cathodic peak at about 0.5 V representing the reduction of gold oxide. The decrease in peak currents for waves characteristic of gold oxide generation and

reduction during sweeping of the electrode potential was observed in the presence of C4 (Figure 3.2). The suppression of gold oxide generation and reduction resulted from blocking of the free gold surface, arising from the formation of monolayers.

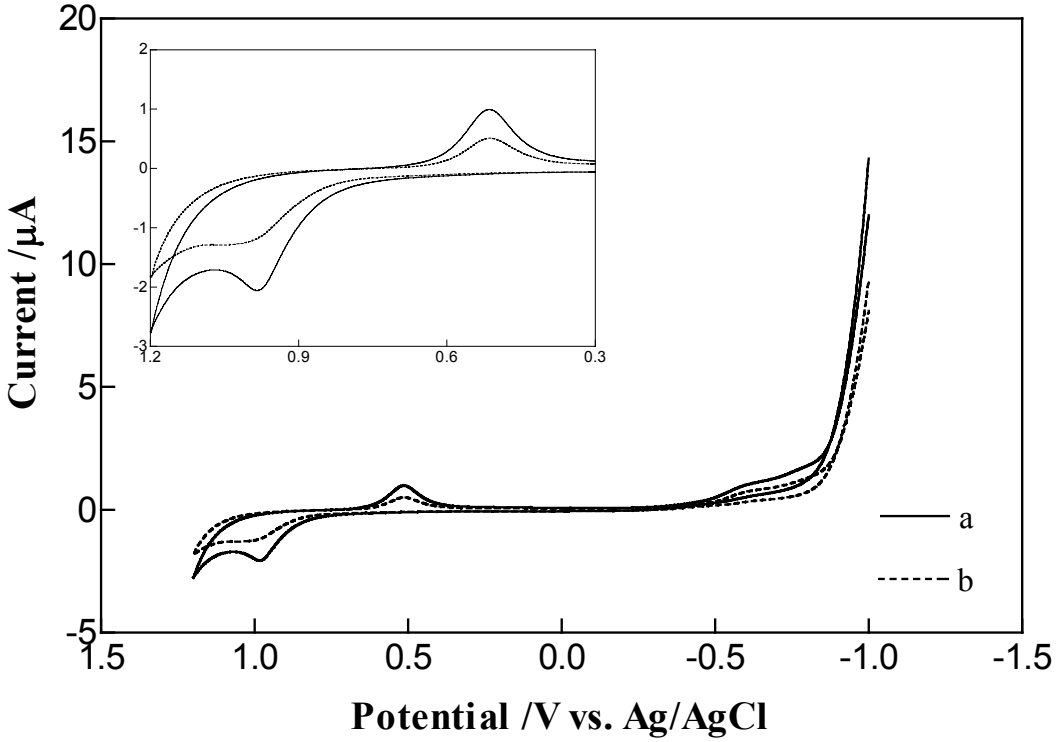

Figure 3.2 Cyclic voltammograms of 0.2 M phosphate buffer (pH 6.0) (a), and 0.2 M phosphate buffer (pH 6.0) with 2.0 mM C4 (b). Scan rate 10 mV/s. Inset shows data in the range of potentials from +0.3 to +1.2 V.

3.3.2 Electrochemical-Assembly of Bunte Salts

3.3.2.1 Potential Pulse and CV

Two electrochemical techniques were investigated to assess the formation of

monolayers from Bunte salts. The first technique involved potential pulses: the potential was stepped from a resting value of -0.2 V vs. Ag/AgCl to a particular positive value in the range producing anodic current in the cyclic voltammogram (Figure 3.2, +0.3 to +1.2 V). The gold electrode was held at this positive potential for 0.2 s and then stepped back to the -0.2 V resting potential for 4 s. This method is similar to the pulse method reported by Ferguson et al.[124, 170] In their work, gold electrodes (prepared by thermal evaporation of gold on glass slides) were immersed into THF solution containing Bunte salts, and the potential was stepped from -0.9 V to a particular positive value vs. Ag/AgCl in the range producing an anodic current.[124, 170]

To optimize the procedure for gold-modified SPCEs, this process was repeated 3 times using a separate sample for each potential from +0.3 to +1.2 V in 0.1 V increments. The current-time trace obtained from C4 over first 50 cycles is shown in Figure 3.3. Initially large current magnitudes can be seen to decay to smaller values over this time period, suggesting that the reaction is occurring at a steadily diminishing electrode area.

The growth of monolayers was also followed systematically, as a function of the pulse numbers to a given potential. The ability of a monolayer to block electron transfer between the gold surface and an electron donor or acceptor in solution is a useful measure of its completeness.[178] Therefore, the degree of completeness of each resulting monolayer was monitored using CV in 1.0 mM $K_3Fe(CN)_6$ with 0.1 M KCl. As the degree of monolayer integrity increases, the current for electron transfer will be largely decreased. $Fe(CN)_6^{3-}$ was selected as an electrochemical probe because it is a

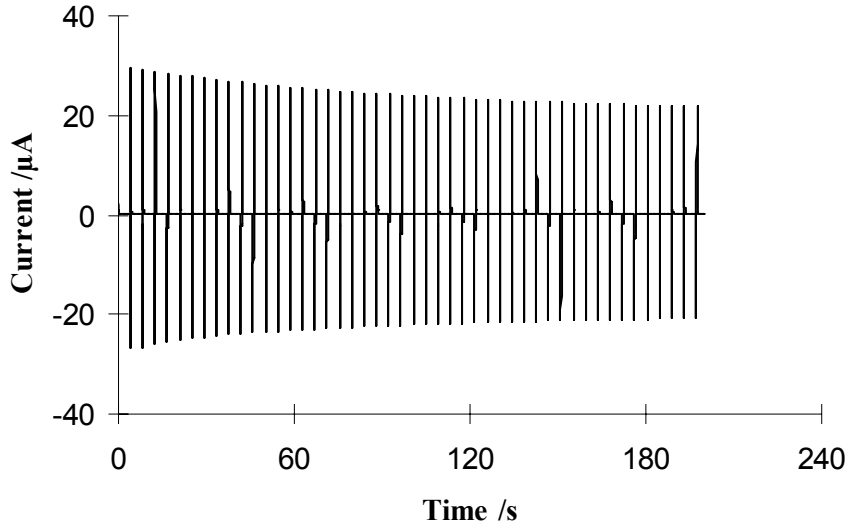

Figure 3.3 Current-time curve of 0.2 M phosphate buffer (pH 6.0) containing 2.0 mM C4 during the first 50 pulse cycles by pulsing between -0.2 V (4s) and +0.8 V (0.1s) vs. Ag/AgCl.

well-characterized one-electron outer-sphere redox couple with fast heterogeneous electron-transfer kinetics at gold.[183-185] Figure 3.4(a) shows a cyclic voltammogram of a bare gold-modified SPCE. Figure 3.4(b)-(d) shows the cyclic voltammograms recorded on C4-covered electrodes generated with from 50, 100, and 250 pulses at +0.8 V vs. Ag/AgCl. At the bare gold SPCE, the shape of the cyclic voltammogram was indicative of a diffusion-limited redox process (Figure 3.4(a)). The voltammograms for monolayer-covered electrodes were markedly different: the reduction of $K_3Fe(CN)_6$ was inhibited by all monolayers to some extent. The initially very large voltammetric peaks disappeared after first 50 pulses, and complete blockage of the electrode surface is evident after 250 cycles. Thus, the complete monolayer can be obtained in less than 20 min with this method. Completeness of the monolayer is defined as the absence of

measurable Faradic currents for the ferri/ferrocyanide redox couple, as shown in Figure 3.4(d), which is indistinguishable from that obtained from the same electrode in the background solution of 0.1 M KCl (data not shown).

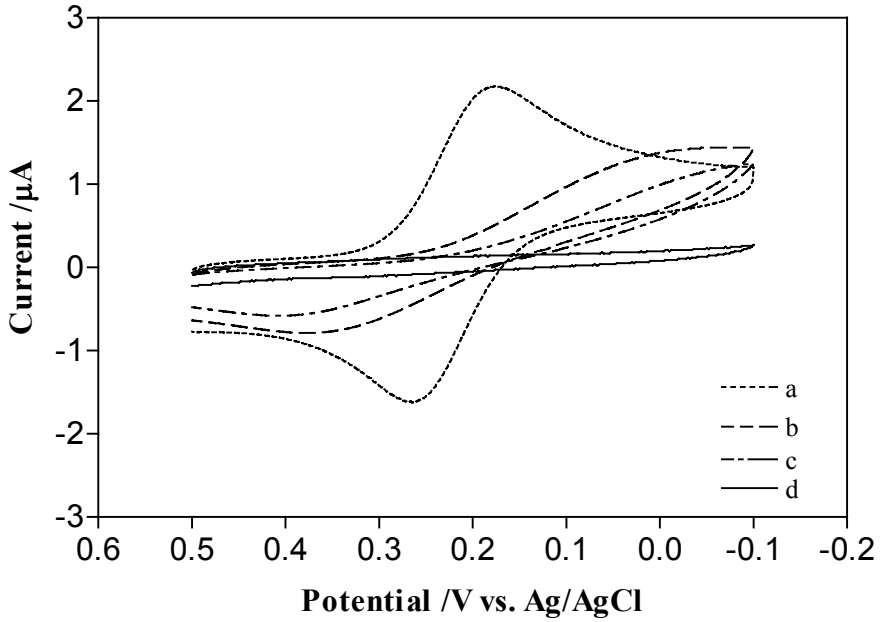

Figure 3.4 Cyclic voltammograms of 1.0 mM $K_3Fe(CN)_6$ in 0.1 M KCl recorded on a gold modified SPCE before (a) and after 50 (b), 100 (c) and 250 (d) potential pulse cycles between -0.2 V (4 s) and +0.8 V (0.2 s) in a solution of 0.2 M phosphate buffer (pH 6.0) containing 2.0 mM C4. Scan rate 100 mV/s.

Control experiments were conducted with the same C4 solution, and no monolayer formation was detected in the absence of an electrochemical method (at open circuit).

Figure 3.5 shows a plot of number of pulses (to get complete coverage) versus pulse potentials for SPCEs modified with C4. As can be seen in Figure 3.5, the number

of pulses decreased as pulse potentials increased from +0.5 to +0.8 V, and then became constant. A potential (+0.5 to +0.7V) lower than +0.8 V may not provide enough energy for significant Bunte salts oxidation. Therefore, many more pulses were needed at these lower potentials to get complete coverage. At even lower potentials (+0.3 to +0.4 V), the monolayer only approached but did not reach completion. Potentials higher than +0.9 V resulted in oxidation of the gold, with concomitant disordering of the monolayer. The same results were obtained from C6 and C8. C10-COOH could not form a complete monolayer even after 600 cycles at a pulse potential of +0.8 V, which may result from the incorporation of the bulky –COOH groups and the concomitant less ordered monolayers

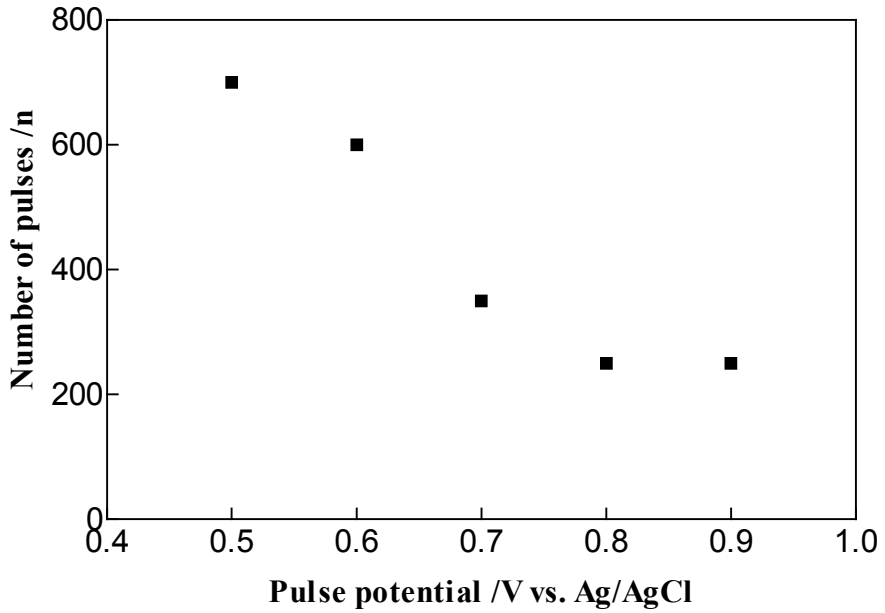

Figure 3.5 Number of pulses for formation of complete monolayers at different pulse potentials. The assembly solution: 2.0 mM C4 in 0.2 mM phosphate buffer (pH 6.0). Initial potential -0.2 V vs. Ag/AgCl held for 4s and pulse potential held for 0.2 s.

Table 3.2 Summary of potential pulse method for ECAM Formation. *

Modified Electrodes	Current Magnitude** (μA)		Current Ratio (Final/Initial)	$Fe(CN)_6^{3-}$ reduction current (μA)***
	Initial	Final		
Bare gold	57 ± 6	58 ± 8	1.02	1.8 ± 0.2
C4	56 ± 7	37 ± 5	0.66	0.02 ± 0.01
C6	55 ± 7	34 ± 5	0.62	0.010 ± 0.005
C8	55 ± 5	33 ± 4	0.60	0.005 ± 0.003
C10-COOH	58 ± 6	42 ± 6	0.72	0.40 ± 0.06

*Initial potential -0.2 V vs. Ag/AgCl (4s); pulse potential +0.8 V held for 0.2 s for 250 cycles; (n=3 for all experiments).

**Absolute magnitude (cathodic-anodic) for first and last pulse cycles.

***Data from voltammograms of 1.0 mM $K_3Fe(CN)_6$ in 0.1 M KCl; scan rate 100 mV/s; current measured at +0.18 V vs. Ag/AgCl, the cathodic peak potential at a bare gold-modified SPCE; values are background-subtracted. Background currents are obtained from 0.1 M KCl.

Table 3.2 summarizes the results obtained with C4 and other Bunte salts using the potential pulse method.

The second method employed to form monolayers was CV from -1.0 to +1.0 V at a scan rate of 10 mV/s. This is similar to the method reported by Czerwinski et al.[137] In their work, Bunte salts (hexyl thiosulfate and benzyl thiosulfate) undergo irreversible adsorption on gold and platinum disk electrodes in 0.5 M H_2SO_4 and 1 M $NaHCO_3$ solution during potential cycling in the potential region 0-1.1 V (vs. NHE). In our experiments, complete monolayers were obtained from different Bunte salts (C4, C6, and C8) after 4 cycles, in less than 15 min. Complete monolayers could not be formed from C10-COOH, even after 10 cycles, which may stem from the larger terminal group (-COOH) and the concomitant disordering of the monolayer.[105] Table 3.3 summarizes the results of these experiments.

Table 3.3 Summary of CV method for ECAM Formation. *

Modified Electrodes	$Fe(CN)_6^{3-}$ reduction current (μA)**
C4	0.02 ± 0.01
C6	0.009 ± 0.005
C8	0.004 ± 0.002
C10-COOH	0.39 ± 0.06

*-1.0 to +1.0 V vs. Ag/AgCl; scan rate 10 mV/s, 4 cycles.

** Data from voltammograms of 1.0 mM $K_3Fe(CN)_6$ in 0.1 M KCl; scan rate 100 mV/s; current measured at +0.18 V vs. Ag/AgCl, the cathodic peak potential at a bare gold-modified SPCE; values are background-subtracted. Background currents are obtained in 0.1 M KCl.

CV from -1.0 to +1.0 V at a scan rate of 10 mV/s with 4 full cycles was chosen for subsequent experiments to form monolayers.

3.3.2.2 Effect of Solvent

Ethanol: H_2O (3:1) with total concentration of 0.1 M KCl as the assembly solvent was also investigated. Complete monolayers were obtained either by potential pulse or by CV in this solvent. Figure 3.6 shows the cyclic voltammograms of 1.0 mM $K_3Fe(CN)_6$ recorded on C4-covered electrodes generated from ethanol/water (3:1, with 0.1 M KCl) and 0.2 M phosphate buffer (pH 6.0). No significant difference was observed between ethanol/water and 0.2 M phosphate buffer (pH 6.0). The aqueous phosphate buffer was chosen for further experiments.

3.3.2.3 Effect of Bunte Salt Concentration

The effect of the concentration of C6 in 0.2 M phosphate buffer (pH 6.0) on the quality of monolayers was studied using CV in 1.0 mM $K_3Fe(CN)_6$ with 0.1 M KCl at a scan rate of 100 mV/s. Monolayer-covered SPCEs were prepared using CV with 4 cycles at a scan rate of 10 mV/s in 0.2 M phosphate buffer (pH 6.0) containing C6 in the concentration range from 0.2 to 5.0 mM. For convenience, the reduction current of $Fe(CN)_6^{3-}$ at +0.18 V (cathodic peak potential at a bare gold-modified SPCE) was used for evaluation. The results are shown in Figure 3.7. It can be seen in Figure 3.7 that as C6 concentration increased from 0.2 to 2.0 mM, the reduction current decreased from about 0.46 μA to about 0.13 μA, and then became constant. The Bunte salt concentration used in further experiments was 2.0 mM.

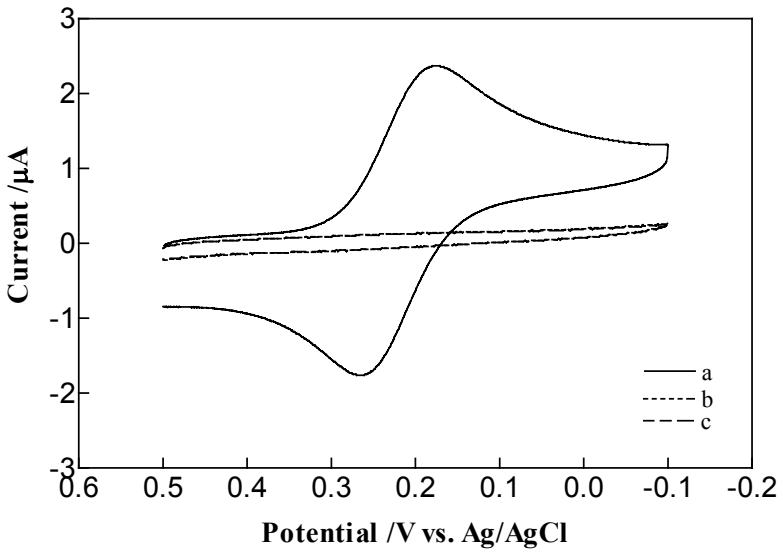

Figure 3.6 Cyclic voltammograms of 1.0 mM $K_3Fe(CN)_6$ in 0.1 M KCl recorded on C4-covered SPCEs generated from ethanol/water (3:1, with 0.1 M KCl) (b) and 0.2 M phosphate buffer (pH 6.0) (c), (a) from a bare gold SPCE. Scan rate 100 mV/s. Monolayers were formed using CV from -1.0 to +1.0 V at a scan rate of 10 mV/s with 4 cycles.

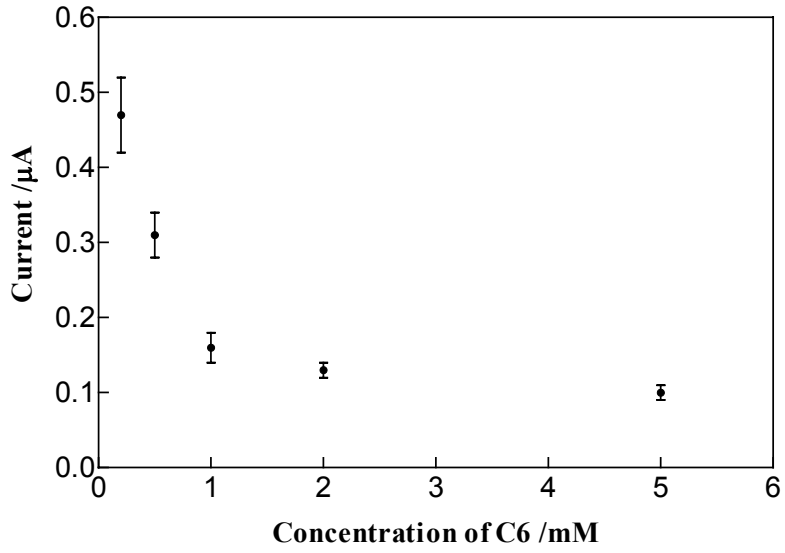

Figure 3.7 Effect of concentration of Bunte salt (C6) in the assembly solution on reduction current of $K_3Fe(CN)_6$ at +0.18 V. Data from CV of 1.0 mM $K_3Fe(CN)_6$ with 0.1 M KCl, +0.5 to -0.1 V, scan rate 100 mV/s. (n=3)

3.3.3 Electrochemical Responses of Redox Probes on Mixed Monolayers

Mixed monolayers were prepared by the CV method using a total Bunte salt concentration of 2.0 mM in 0.2 M phosphate buffer (pH 6.0). Binary salt combinations of C10-COOH with C4, C6 or C8 were used with varying molar ratios in the assembly solution. The resulting mixed monolayers were examined by CV using FCA and $K_3Fe(CN)_6$.

3.3.3.1 Electrochemical Responses of FCA on Mixed Monolayers

The cyclic voltammograms of FCA at gold-modified SPCEs with C4/C10-COOH mixed monolayers are shown in Figure 3.8. The voltammograms show a clear trend towards decreased Faradic currents for FCA as the percent C10-COOH is increased, although complete blockage is not observed with 100% C10-COOH (Figure 3.8(f)). These results suggest that FCA readily transfers electrons to the gold surface through the C4 barrier, but this process is inhibited by C10-COOH. Inhibition is likely a consequence of both the length of C10-COOH, forcing the electron-transfer reaction to occur over a greater distance, and electrostatic repulsion between the negatively charged carboxylate groups on both the FCA and the surface-bound C10-COOH (the surface-bound carboxylate groups are at least partially ionized at pH 7.0.[186]). It should be emphasized that the surface molar fractions relate to assembly solution composition and not necessarily to the final monolayer compositions.

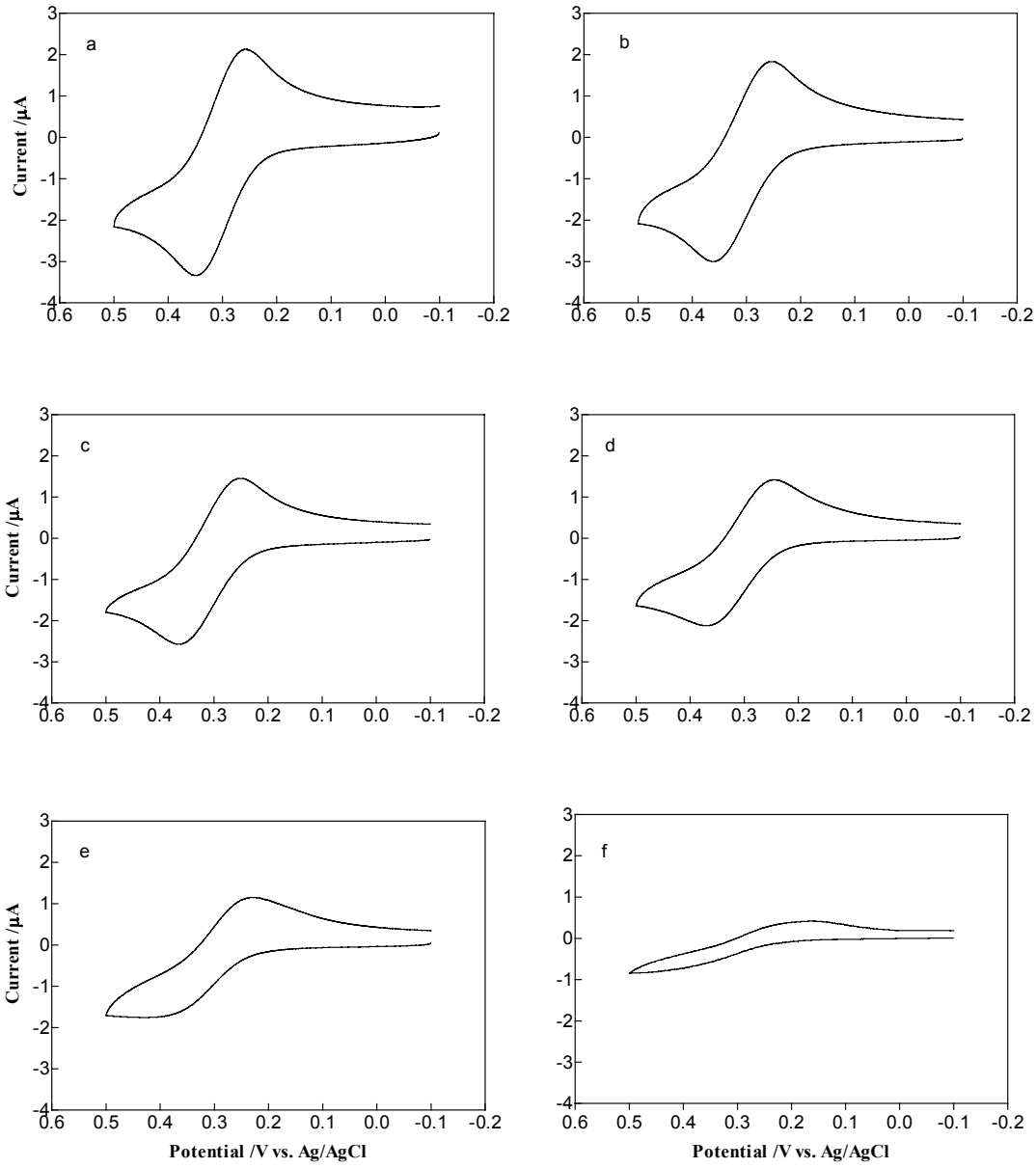

Figure 3.8 Cyclic voltammograms of 1.0 mM FCA in 0.1 M Tris buffer (pH 7.0) on (a) a bare gold-modified SPCE, and mixed monolayers (C4/C10-COOH) with (b) 90% C4, (c) 80% C4, (d) 50% C4, (e) 20% C4, and (f) 100% C10-COOH (molar percentage in the solution). Scan rate 100 mV/s.

Similar trends were observed in the systems of C6/C10-COOH and C8/C10-COOH. The resulting mixed monolayers had improved blocking effects on FCA as the content of the long chain component (C10-COOH) increases. However, with the same percentage of C10-COOH, mixed monolayers composed of different second compositions (C4, C6 or C8) had different barrier effects on FCA. Results are compared in Figure 3.9 for monolayers composed of 10% C10-COOH and 90% C4, C6 or C8.

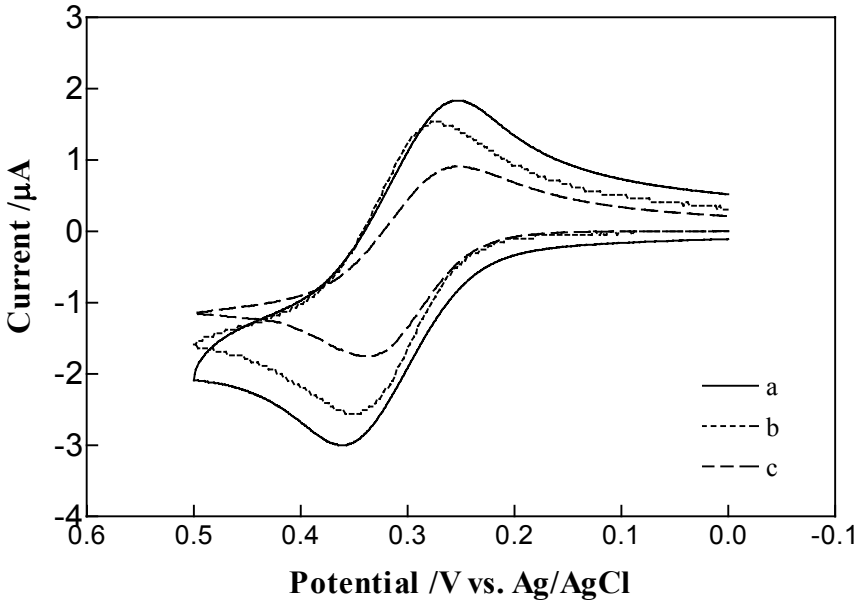

Figure 3.9 Cyclic voltammograms of 1.0 mM FCA in 0.1 M Tris buffer (pH 7.0) on mixed monolayers composed of 10% C10-COOH and 90% of (a) C4, (b) C6, and (c) C8 (molar percentage in the solution). Scan rate 100 mV/s.

Table 3.4 summarizes results obtained with FCA for all mixed monolayer systems studied.

As shown in Figure 3.9 and Table 3.4, the reaction of FCA on mixed monolayers can also be controlled by the nature of short chain components within the monolayers. While the composition of one component was fixed (for example, 10 % C10-COOH in Figure 3.9), the blocking effect increased as the chain length of the second component increased.

Table 3.4 Mixed monolayer properties (FCA used as a voltammetric probes). *

Bunte salts (CX)	Percent of Bunte salts in solution (%)		FCA anodic current (μA)**
	CX	C10-COOH	
C4	90	10	2.8 ± 0.3
	80	20	2.3 ± 0.2
	50	50	2.0 ± 0.2
	20	80	1.4 ± 0.1
	0	100	0.62 ± 0.07
C6	90	10	2.4 ± 0.3
	80	20	2.0 ± 0.2
	50	50	1.8 ± 0.2
	20	80	0.60 ± 0.07
C8	90	10	1.8 ± 0.2
	80	20	1.6 ± 0.2
	50	50	1.2 ± 0.1
	20	80	0.56 ± 0.08

*CV conditions for FCA are the same as in Figure 3.9 (n=3).

** Measured at +0.34 V vs. Ag/AgCl, the anodic peak potential at a bare gold-modified SPCE.

3.3.3.2 Electrochemical Responses of $Fe(CN)_6^{3-}$ on Mixed Monolayers

Figure 3.10 and Table 3.5 present data analogous to that shown in Figure 3.8 and

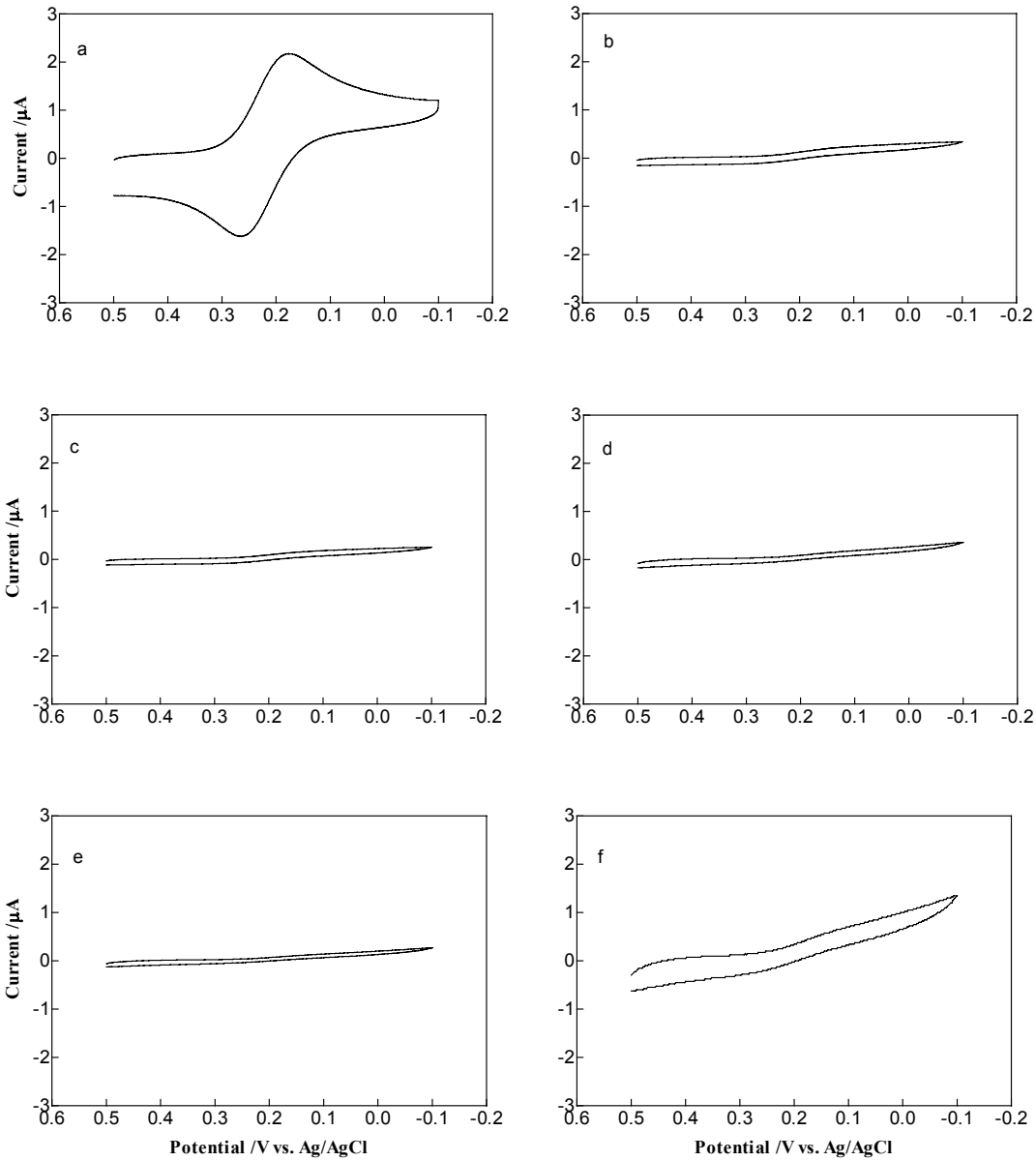

Figure 3.10 Cyclic voltammograms of 1.0 mM $K_3Fe(CN)_6$ in 0.1 M KCl on (a) a bare gold-modified SPCE, and mixed monolayers (C4/C10-COOH) with (b) 90% C4, (c) 80% C4, (d) 50% C4, (e) 20% C4, and (f) 100% C10-COOH (molar percentage in the solution). Scan rate 100 mV/s.

Table 3.4, except that the redox probe is $K_3Fe(CN)_6$. Compared to results obtained in Table 3.4, the data follows the general trend discussed for FCA, but mixed monolayers show bigger barrier effects on $K_3Fe(CN)_6$. This is likely a result of stronger electrostatic repulsion between surface-bound C10-COO^- groups and $Fe(CN)_6^{3-}$ for the mixed monolayer systems studied. Since $Fe(CN)_6^{3-}$ is more hydrophilic than FCA, it was not possible to observe a clear decrease in voltammetric signal with increasing chain length (as shown for FCA in Figure 3.9). However, both FCA and $Fe(CN)_6^{3-}$ results suggest defective monolayers when only C10-COOH is present in the assembly solution (Figure 3.8(f) and 3.10(f)); the carboxylate groups (at least partially ionized at pH 7.0[186]) are bulkier than a methyl group, and likely contribute to pinhole defects.

3.3.4 Capacitance

3.3.4.1 Single-Component Monolayers

Measurement of capacitance is another valuable method to assess the quality of molecular packing in monolayers. This method provides additional information on the degree of structural integrity of the monolayer. The capacitances of pure monolayer-covered SPCEs prepared by CV from different Bunte salts are compared in Table 3.6. Figure 3.11 shows voltammograms for a bare gold-modified and a C4-modified SPCE that were used to calculate the values shown in Table 3.6.

As compared to a bare gold-modified SPCE (Figure 3.11(a)), a monolayer-covered SPCE exhibits markedly reduced double-layer charging currents and an almost potential-independent behavior (Figure 3.11(b)), which is characteristic for thin layers with low dielectric constant blocking electron transfer to the electrode.

Table 3.5 Mixed monolayer properties ($Fe(CN)_6^{3-}$ used as a voltammetric probe).*

Bunte salts (CX)	Percent of Bunte salts in solution (%)		$Fe(CN)_6^{3-}$ reduction current (μA)**
	CX	C10-COOH	
C4	90	10	0.19 ± 0.02
	80	20	0.15 ± 0.02
	50	50	0.13 ± 0.02
	20	80	0.11 ± 0.02
	0	100	0.50 ± 0.06
C6	90	10	0.16 ± 0.02
	80	20	0.16 ± 0.02
	50	50	0.15 ± 0.02
	20	80	0.10 ± 0.01
C8	90	10	0.14 ± 0.02
	80	20	0.13 ± 0.01
	50	50	0.13 ± 0.01
	20	80	0.10 ± 0.01

*CV conditions for $Fe(CN)_6^{3-}$ are the same as in Figure 3.9 (n=3).

**Measured at +0.18 V vs. Ag/AgCl, the cathodic peak potential at a bare gold-modified SPCE.

From Table 3.6, it is obvious that the coating of a gold electrode with a monolayer causes a dramatic decrease in the electrolyte/electrode capacitance. The data can be interpreted according to the parallel plate capacitor model, in which the monolayer-coated electrode is modeled as a capacitor with the gold electrode surface and the electrolyte solution forming the two conducting plates of the capacitor.[178] In this case the capacitance can be described by the following equation:

Table 3.6 Capacitance on bare gold-modified and monolayer-covered SPCEs measured in 0.1 M KCl at +0.1 V vs. Ag/AgCl with a scan rate of 100 mV/s.

Bare gold or monolayer-covered electrode	Bare gold	C4	C6	C8	C10-COOH
C_{dl} $\mu F/cm^2$ *	140 (± 10)	24 (± 3)	15 (± 2)	8 (± 1)	46 (± 7)

* n=3; electrodes areas used in this calculation are determined by chronoamperometry.

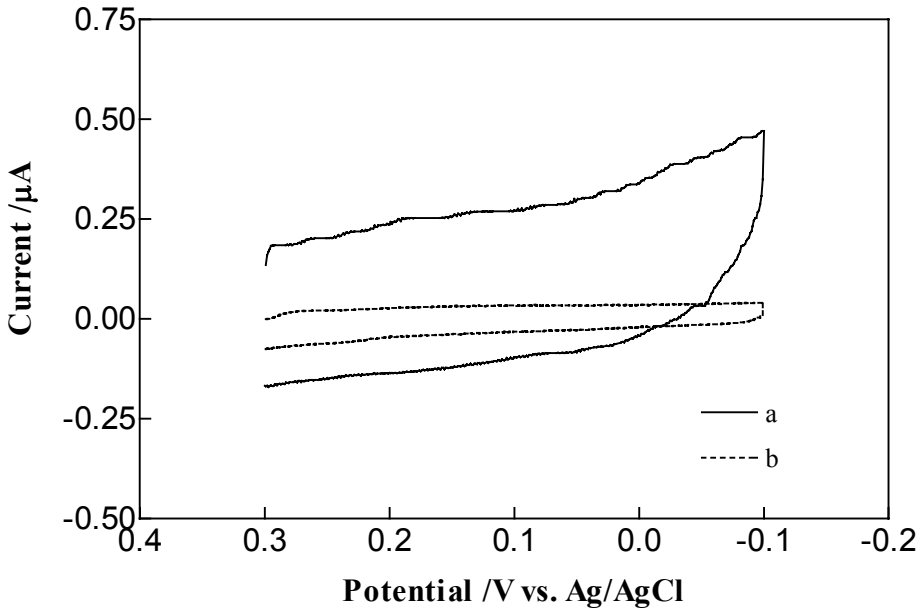

Figure 3.11 Cyclic voltammograms of 0.1 M KCl before (a) and after (b) electrochemical formation of monolayer (C4). Scan rate 100 mV/s.

$$C = \varepsilon_0 \varepsilon_r / d_{eff} \qquad (3.3)$$

where ε_r is the relative dielectric constant of the monolayer, ε_0 is the dielectric constant of vacuum (permittivity of free space), and d_{eff} is the effective thickness of the monolayer. According to this model, during the linear potential scans of a CV experiment, the charging current is independent of potential, and inversely proportional to the monolayer thickness. The experimental data are in agreement with this model, since capacitance is nearly constant with potential and the capacitance value decreased as the chain length was increased from C4 to C8.

On the other hand, the C10-COOH-based monolayer exhibited a larger capacitance. This is consistent with FCA and $Fe(CN)_6^{3-}$ results (Section 3.3.3.1 and 3.3.3.2) which suggested that the functional group (-COOH) provides electrostatic repulsion and steric hindrance resulting in a monolayer that has defects and is less compact.[105] Liquid-like packing of $HOOC(CH_2)_{10}SH$ on gold by chemisorption has been reported by Chidsey et al.[105] The incorporation of the polar carboxylic acid group to the end of polymethylene chains leads to less ordered monolayers and extensive permeation of the monolayer by water or aqueous ions due to the steric and electrostatic interactions between functional groups.[105]

Moreover, these data imply that there is no multilayer formation in any investigated system. If multilayers were formed, capacitance values lower than 1.4 $\mu F/cm^2$ should have been obtained according to the correlation between the differential capacitance and the chain length of the adsorbates.[187]

Figure 3.12 shows a plot of reciprocal capacitance of the monolayer-covered SPCEs versus the length of the hydrocarbon (i.e., the number of methylene units, n, in $CH_3(CH_2)_nS_2O_3Na$). The plot of $1/C_{dl}$ vs. n is reasonably described as a straight line with a slope of 0.02 $cm^2/\mu F$ and intercept of -0.05 $cm^2/\mu F$ (R^2=0.95). The linear dependence of $1/C_{dl}$ on n deviates lightly from that of the corresponding thiols previous reported by Widrig et al. (slope and intercept were 0.02 and 0.28 $cm^2/\mu F$, respectively).[187] The reason for this difference is not known at present. It may result from the difference of the structure or packing quality of the monolayers formed by the electrochemical method in this work, in comparison with the chemisorption method used by Widrig et al.[187]

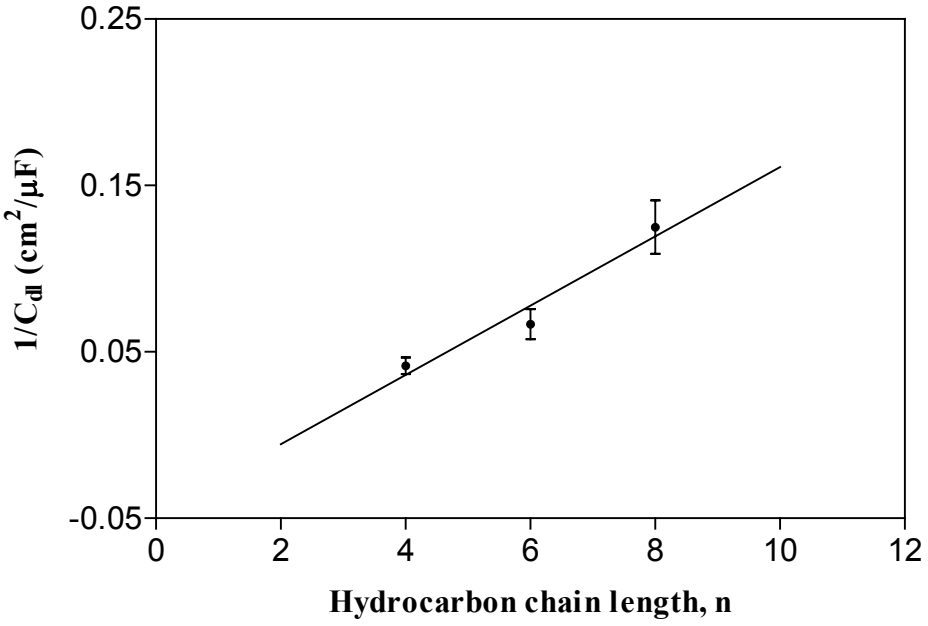

Figure 3.12 Plot of reciprocal capacitance vs. hydrocarbon chain length. Data from Table 3.6.

3.3.4.2 Binary Monolayers

The capacitances of mixed monolayer-covered electrodes prepared from C6/C10-COOH with varying molar ratio in the assembly solution are shown in Figure 3.13. It can be seen that before approaching 50% C10-COOH, with the increase of C10-COOH in the solution the capacitance decreases. These results can be interpreted using the parallel plate capacitor model (Equation 3.3). As the content of C10-COOH increases, the average d_{eff} value is expected to increase. Therefore, the monolayer capacitance decreases with an increase in C10-COOH content. Above 50% C10-COOH, the capacitance of the mixed monolayers increases with an increase in C10-COOH content. This may result from the electrostatic and steric effects introduced by the functional group (-COOH) and the concomitant disorder of the monolayers.

The measured capacitance values of mixed monolayers composed of 10% C10-COOH and 90% different second components are compared in Table 3.7.

These results are consistent with Equation 3.3, since d_{eff} is expected to increase with the average chain length present in the mixed monolayer. As shown in Table 3.7, the composition of Bunte salts in the assembly solution affects the capacitance values of the mixed monolayers, indicating that the composition or the structure of the monolayers can be controlled by the composition of the assembling solution.

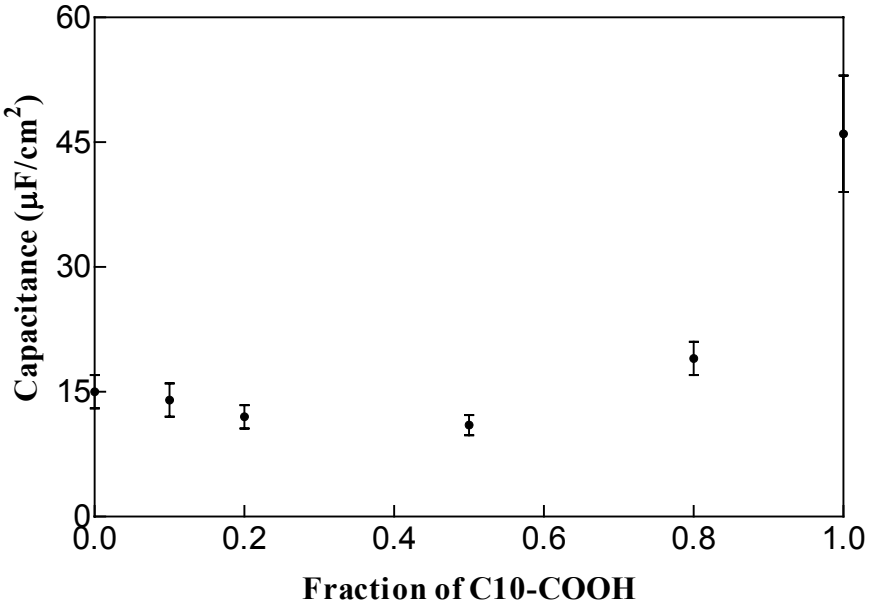

Figure 3.13 Plot of capacitance of the mixed monolayers (C6/C10-COOH) against the corresponding fraction of C10-COOH in the solution. Electrodes areas used in the calculation are determined by chronoamperometry. (n=3)

Table 3.7 Capacitance on monolayer-covered SPCEs composed of 10% C10-COOH and 90% of short chain components (C4, C6 or C8) (molar percentage in the solution) measured in 0.1 M KCl at +0.1 V vs. Ag/AgCl with a scan rate of 100 mV/s.

Monolayer-covered SPCEs	C4/C10-COOH	C6/C10-COOH	C8/C10-COOH
C_{dl} μF/cm^2 *	22 ± 3	14 ± 2	6 ± 1

*n=3; electrodes areas used in this calculation are determined by chronoamperometry.

3.3.5 Stability

The electrochemical stabilities of monolayer-modified electrodes were investigated in 0.1 M H_2SO_4 using CV in the potential range of -1.0 to +1.2 V at a scan rate of 100 mV/s. The cyclic voltammogram of a clean gold-modified SPCE exhibits the characteristic gold oxide formation at +1.0 to +1.2 V. On the return scan, an oxide stripping peak appears at around 0.70 V (Figure 3.13(a)). On the monolayer-covered electrode, the gold oxidation is not visible. Suppression of gold oxidation implies that water is effectively blocked from the gold surface. This fact points to a relatively strong bonding between the adsorbates and the gold. The monolayers were damaged when the potential exceeded the positive limit (+1.2 V), when the characteristic reduction peak of gold oxide appeared.[182] The large currents observed between -0.5 to -1.0 V are due to the reduction of water.

Storage stabilities of monolayer-modified electrodes were also investigated. Monolayer-covered electrodes were stored at 4° C in 0.2 M phosphate buffer (pH 6.0). After 24 h storage, no obvious deterioration of monolayer quality was detected (as judged by CV of 1.0 mM $K_3Fe(CN)_6$).

3.3.6 Control Experiments

Figure 3.15 and 3.16 show the cyclic voltammograms of $Fe(CN)_6^{3-}$ at a gold-modified SPCE before and after cycling in 0.3 mM $HOOC(CH_2)_{10}Br$ or NaBr. No inhibition of $Fe(CN)_6^{3-}$ reaction on electrodes after cycling in $HOOC(CH_2)_{10}Br$ or NaBr was observed. Therefore, neither $HOOC(CH_2)_{10}Br$ nor NaBr can form electrochemically monolayers on gold-modified SPCEs.

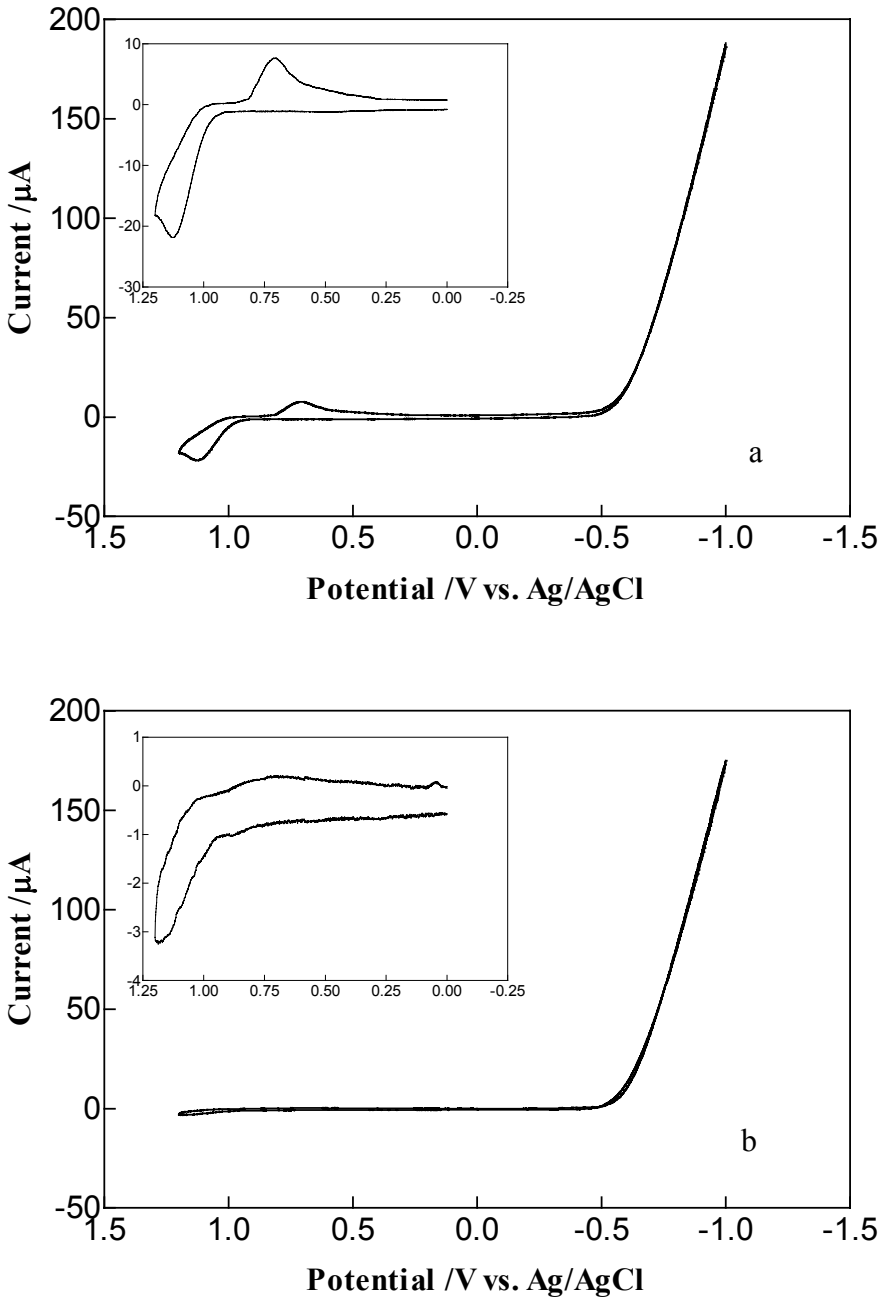

Figure 3.14 Cyclic voltammograms of 0.1 M H_2SO_4 on a gold-modified SPCE before (a), and after (b) ECAM formation of C4. Scan rate 100 mV/s. Insets show data from 0 to +1.2 V range.

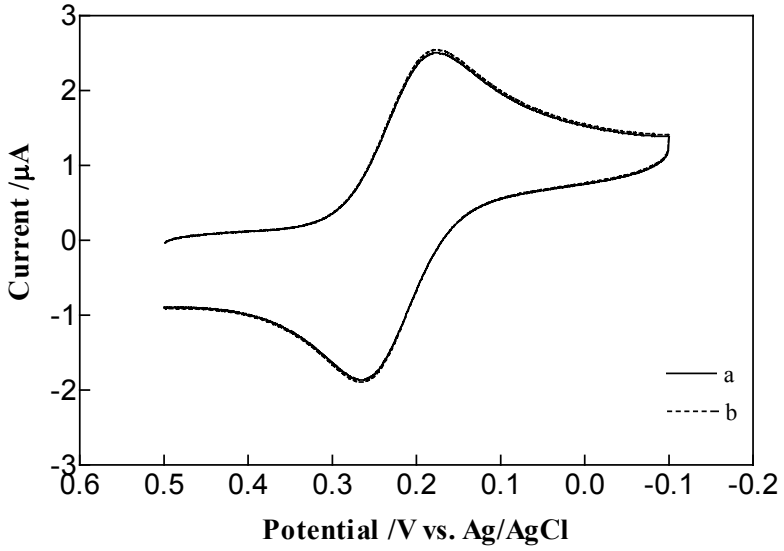

Figure 3.15 Cyclic voltammograms of 1.0 mM $K_3Fe(CN)_6$ in 0.1 M KCl recorded on a gold-modified SPCE before (a), and after (b) cycling in 0.3 mM $HOOC(CH_2)_{10}Br$ (4 cycles from -1.0 to +1.0 V, 10 mV/s). Scan rate 100 mV/s.

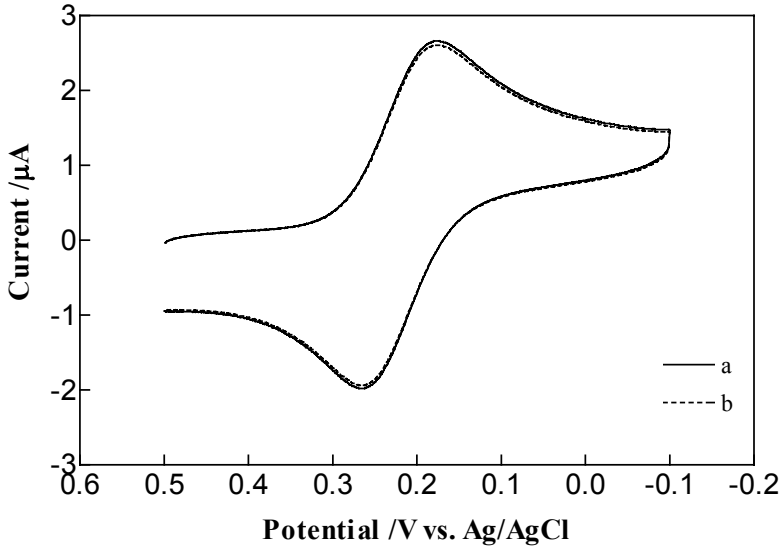

Figure 3.16 Cyclic voltammograms of 1.0 mM $K_3Fe(CN)_6$ in 0.1 M KCl recorded on a gold-modified SPCE before (a), and after (b) cycling in 0.3 mM NaBr (4 cycles from -1.0 to +1.0 V, 10 mV/s). Scan rate 100 mV/s.

Figure 3.17 shows the cyclic voltammograms of $Fe(CN)_6^{3-}$ at a bare gold-modified SPCE and a gold-modified SPCE after cycling in 2.0 mM C4 and 2.0 mM C4 with 0.3 mM $HOOC(CH_2)_{10}Br$. No obvious difference was observed between monolayer-modified electrodes either by C4 only or by C4 and $HOOC(CH_2)_{10}Br$ together. Therefore $HOOC(CH_2)_{10}Br$ does not have any influence on the formation of monolayers.

Figure 3.18 shows the cyclic voltammograms of $Fe(CN)_6^{3-}$ at a bare gold-modified SPCE and a gold-modified SPCE after cycling in 2.0 mM C4 and 2.0 mM C4 with NaBr. From Figure 3.18, it is obvious that NaBr does not have any influence on the formation of monolayers.

The capacitance values of the monolayer-modified SPCEs studied above were also determined by CV in 0.1 M KCl. The results were summarized in Table 3.8.

It can be seen from Table 3.8 that the results are in agreement with those obtained from $Fe(CN)_6^{3-}$. $HOOC(CH_2)_{10}Br$ and NaBr cannot electrochemically form monolayers and do not have any influence on the formation of monolayers.

3.4 CONCLUSIONS

Bunte salts form stable pure and binary-component monolayers on gold-modified SPCEs when assembled by electrochemical methods. The degree of the completeness of the monolayers can be controlled by pulse numbers for the potential pulse method, or by the number of cycles used in the CV method.

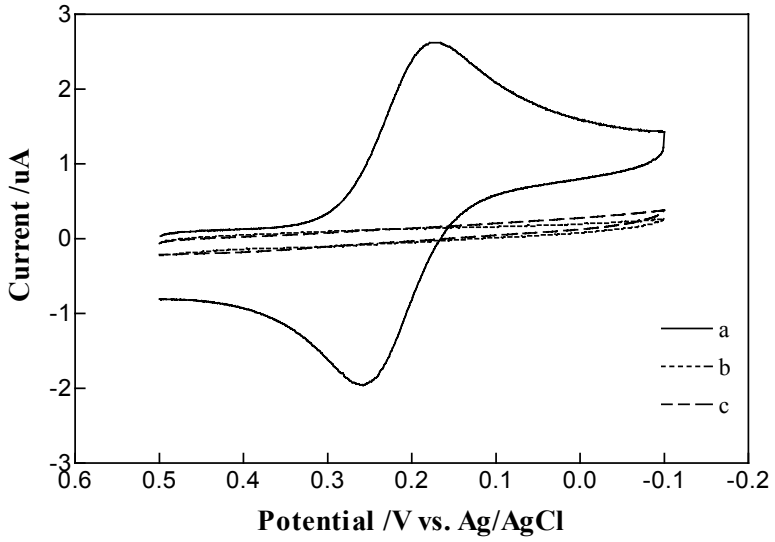

Figure 3.17 Cyclic voltammograms of 1.0 mM $K_3Fe(CN)_6$ in 0.1 M KCl recorded on a bare gold-modified SPCE (a), and gold-modified SPCEs after cycling in (b) 2.0 mM C4, (c) 2.0 mM C4 + 0.3 mM $HOOC(CH_2)_{10}Br$ (4 cycles from 1.0 to +1.0 V, 10 mV/s). Scan rate 100 mV/s.

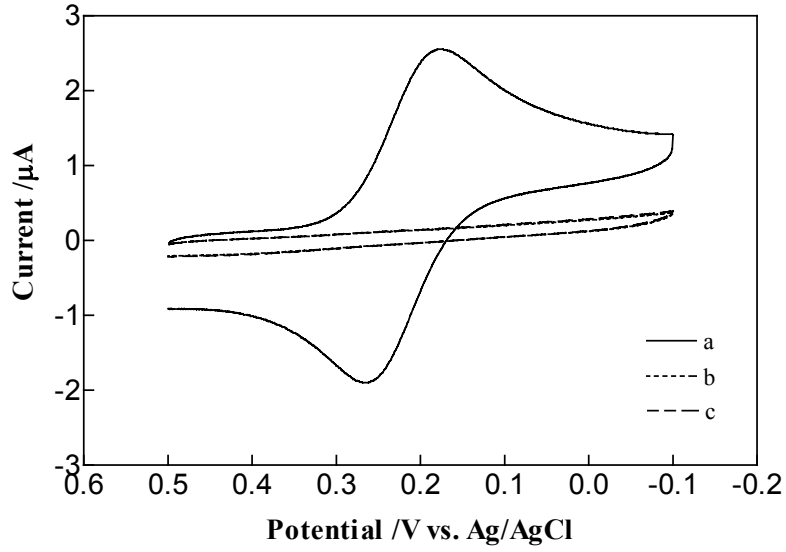

Figure 3.18 Cyclic voltammograms of 1.0 mM $K_3Fe(CN)_6$ in 0.1 M KCl recorded on (a) a bare gold-modified SPCE, and a gold-modified SPCE after cycling in (b) 2.0 mM C4, (c) 2.0 mM C4 + 0.3 mM NaBr (4 cycles from 1.0 to +1.0 V, 10 mV/s). Scan rate 100 mV/s.

Table 3.8 Capacitance on bare gold-modified and monolayer-covered SPCEs measured in 0.1 M KCl at +0.1 V vs. Ag/AgCl with a scan rate of 100 mV/s.

Bare gold or monolayer-covered SPCEs*	C_{dl} μF/cm^2 **
Bare gold-modified SPCEs	140 ± 10
0.3 mM $HOOC(CH_2)_{10}Br$	142 ± 11
0.3 mM NaBr	139 ± 10
2.0 mM C4	24 ± 3
2.0 mM C4 + 0.3 mM $HOOC(CH_2)_{10}Br$	23 ± 3
2.0 mM C4 + 0.3 mM NaBr	25 ± 4

*Monolayers were electrochemically formed from –1.0 to +1.0 V at a scan rate of 10 mV/s, 4 cycles.

**n=3; electrodes areas used in this calculation are determined by chronoamperometry.

The double layer capacitance of a pure monolayer decreases as the chain length is increased. Also, the structure of the organic monolayer clearly depends on the terminal groups, which modify the intermolecular interactions. Incorporation of the –COOH functional group disturbs the order of pure monolayers.

This research has shown that it is possible to use binary Bunte salt solutions to prepare functional composite monolayers. The composition of the monolayer is related to the ratio of the two Bunte salts in the assembling solution. The permeabilities of $K_3Fe(CN)_6$ and FCA on mixed monolayers are different. FCA penetrates the monolayers easily, but $Fe(CN)_6^{3-}$ does not. In addition, the access of FCA to the gold electrode surface can be tuned to some extent by varying the relative concentrations of

the two Bunte salts in the assembly solution, which offers the prospect of using this approach to develop highly sensitive and selective electrochemical sensors for organic and biological samples. Therefore, its potential applicability area in electrochemical analysis is believed to be wide. The following chapters discuss the applications of these modified electrodes to enzyme biosensors and immunosensors.

Chapter 4: Glucose Biosensor Based on Electrodeposition of Bunte Salts

4.1 INTRODUCTION

Biosensors are now attracting considerable attention as potential successors to a wide range of analytical techniques due to their unique properties of specificity. The immobilization of biological molecules is a crucial problem for the development of biosensors, as the immobilization procedure must maintain the activity of biological molecules in a reproducible manner. Furthermore, it is desirable that the immobilization process gives the biological molecules enhanced stability, is robust, is applicable to many different biological molecules, is chemically resistant to the reactants and products of the biochemical reaction and gives some control over the distribution and orientation of the immobilized species.

A number of techniques for immobilizing biomolecules on various matrices, such as covalent linkage, encapsulation, layer-by-layer deposition, and cross-linking, have been developed for the fabrication of biosensing devices.[188-194] Among these immobilization methods, the use of SAMs as anchor layers has been the subject of considerable research for a decade.[102, 195-197] Such organic films bring the following advantages: (i) extremely reduced thickness, (ii) surface groups optimally positioned for reaction, and (iii) control in the degree of order and density of reactive groups. SAMs have been used for the fabrication of a variety of biosensors including immunosensors[198] and enzyme biosensors.[199]

Amperometric enzyme electrodes hold a leading position among biosensor systems presently available, and have already found a large commercial market.[200, 201] In particular, glucose biosensors have attracted a great deal of interest because of the increasing incidence of diabetes.[202, 203] The enzyme, GOx, is well-known as a biological sensing material for the quantitative determination of β-D-glucose in solution because of its substrate specificity.[188, 204] GOx is a diametric protein with a molecular weight of 160 kDa and a size of ca. 8 nm × 6 nm × 5 nm.[205] The general reaction mechanism for the GOx catalyzed glucose oxidation process is described in Figure 4.1:

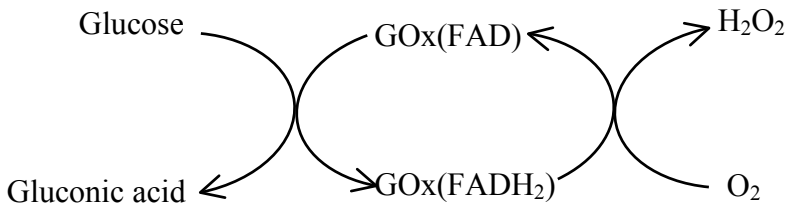

Figure 4.1 The oxidation of glucose catalyzed by GOx. GOx (FAD) and GOx ($FADH_2$) represent the oxidized and reduced forms of GOx, respectively.

First generation glucose biosensors were mostly based on direct amperometric detection of hydrogen peroxide formed as a consequence of the enzymatic reaction.[206, 207]

$$H_2O_2 \rightarrow O_2 + 2H^+ + 2e^- \qquad (4.1)$$

Even though hydrogen peroxide detection requires no additional reagents, there are some disadvantages in using an oxygen-coupled biosensor for *in vitro* monitoring of glucose in whole blood and plasma: Variations in the oxygen tension of the sample may introduce fluctuations into the electrode response. In addition, at low oxygen tension, the upper limit of linearity for the current response may be reduced. Also, the relatively high operating potentials required to oxidize hydrogen peroxide can result in interference from oxidizable constituents (ascorbic acid and uric acid) in the analyzed samples. One viable solution to these problems has been to replace the natural electron acceptor for GOx (O_2) by electroactive compounds that act as redox mediators, thus allowing work at lower potentials and reducing interference.[208] Biosensors employing mediators are so-called second generation biosensors.[209, 210] Ferrocene and its derivatives have proven to be particularly useful as mediators for amperometric enzyme electrodes.[211-220] Once ferrocene is oxidized at an electrode, the resulting ferricinium ion diffuses to the redox centre of the enzyme, where it acts as an artificial electron acceptor.

In this chapter, the application to glucose biosensors of functionalized binary monolayers, formed electrochemically from Bunte salts, is reported. The binary monolayers were mixtures of a long carboxylic acid functionalized Bunte salt (C10-COOH) with a short alkyl functionalized derivative (C4, C6, or C8). The long chain component (C10-COOH) provides binding sites for enzymes, and the short chain component (C4, C6 or C8) allows electron transfer to the underling gold layer. The immobilization of GOx molecules was achieved by covalent attachment to the carboxylic terminated monolayers with the assistance of N-ethyl-N'-(3-

imethylaminopropyl) carbodiimide (EDC) hydrochloride and n-hydroxysuccinimide (NHS). FCA was chosen as a mediator. The amperometric responses of the resulting enzyme electrodes to glucose were measured and the effects of some variables on the response were investigated.

4.2 EXPERIMENTAL SECTION

4.2.1 Materials and Instrumentation

Glucose oxidase (EC 1.1.3.4. type X-S, from *Aspergillus niger*), EDC hydrochloride, potassium phosphate and NHS were purchased from Sigma. Aldrich supplied potassium dihydrogenphosphate. D-Glucose was purchased from Sigma. A stock solution of 0.5 M glucose was prepared in 0.1 M Tris buffer (pH 7.0) at least 24 h prior to use for mutarotation to occur. The solution was stored at 4 °C. More dilute standards were prepared by appropriate dilution with 0.1 M Tris buffer (pH 7.0). Unless otherwise noted, the glucose solution was deaerated by purging with nitrogen for 30 min before use.

An EG & G Potentiostat/Galvanostat and a CHI650A Potentiostat were employed for electrochemical experiments. Bioanalytical Systems supplied Ag/AgCl (3 M NaCl) reference electrodes.

4.2.2 Methods

4.2.2.1 Preparation of Enzyme Electrodes

Binary monolayers (C4/C10-COOH, C6/C10-COOH, or C8/C10-COOH) with varying molar ratio of the two components were electrochemically formed by CV as described in Section 3.2.2.3. The terminal carboxylic groups of monolayers were activated by immersion in 0.05 M phosphate buffer (pH 5.5) containing 2 mM EDC hydrochloride and 5 mM NHS for 1 h at room temperature. In this step, EDC hydrochloride converts the carboxyl group into a reactive intermediate, which is susceptible to attack by amines on lysine residues of GOx, and amide bonds then form between the enzyme molecules and carboxyl-terminated monolayers. After the activation, the electrodes were rinsed with phosphate buffer and immediately placed in 0.05 M phosphate buffer (pH 5.5) containing 1 mg/mL GOx overnight at 4 °C. The enzyme electrodes were rinsed with water and used immediately. Figure 4.2 shows this activation reaction process.[195]

4.2.2.2 Cyclic Voltammetry

CV studies were first carried out in a conventional three-electrode configuration, with a GOx-modified SPCE (geometric area 1.0 mm^2) as the working electrode, a platinum wire as the auxiliary electrode, and Ag/AgCl (3 M NaCl) reference electrode. Later experiments used the electrochemical array (described in Chapter 2), composed of two-electrode cells, with a GOx-modified SPCE as the working electrode and a Ag/AgCl modified SPCE as the counter electrode.

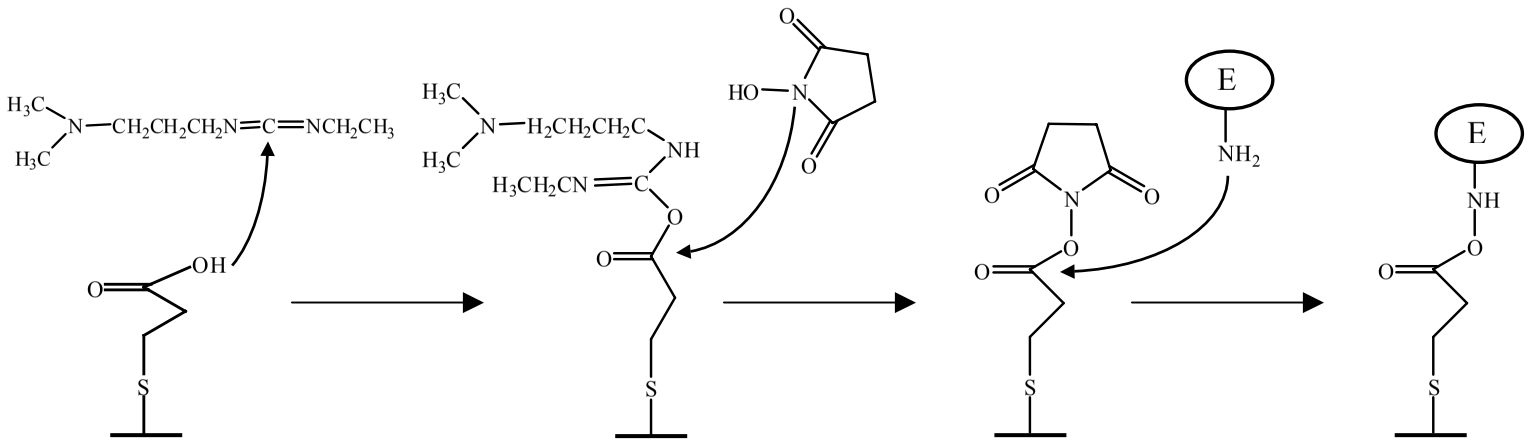

Figure 4.2 Schematic diagram showing the covalent attachment of an enzyme to a carboxyl-terminated monolayer using EDC and NHS.[195] E represents an enzyme.

4.2.2.3 Amperometric Measurement

The activity of immobilized GOx was tested by measuring the current response to glucose. In order to simplify the factors that affect the results, initial studies were carried out in a conventional three-electrode system consisting of a GOx-modified working electrode (geometric area 1.0 mm^2), an auxiliary electrode of platinum wire and a reference electrode of Ag/AgCl (3 M NaCl). The amperometric measurements at a constant potential were carried out in the solution of 0.1 M Tris buffer (pH 7.0) containing FCA and glucose without stirring. Background current was obtained from 0.1 M Tris buffer (pH 7.0) containing FCA. Steady-state currents from different concentrations of glucose were background subtracted and were then used to create calibration curves.

The electrochemical array was also evaluated for the detection of glucose. Glucose solution was introduced into the microchannel at one end using a syringe.

All experiments were performed at room temperature (20 ± 2 °C).

4.3 RESULTS AND DISCUSSION

4.3.1 Fabrication of GOx-Modified SPCEs

Following each step of the fabrication process, electrodes were characterized by CV using ferricyanide and FCA as redox probes. Figure 4.3 shows cyclic voltammograms of a modified SPCE at different stages in 0.1 M KCl solution containing 1.0 mM $K_3Fe(CN)_6$ at a scan rate of 100 mV/s. Mixed monolayer was electrochemically formed from the assembling solution containing 90% C4 and 10% C10-COOH. At a bare gold-

modified SPCE, the characteristic and well-behaved redox response of ferricyanide was observed (Figure 4.3(a)). The reaction of ferricyanide was blocked by the existence of the mixed monolayer on the electrode surface (Figure 4.3(b)). The response of the electrode after the activation step with EDC hydrochloride and NHS was very similar to Figure 4.3(b) (data not shown), indicating that the activation step did not destroy the monolayer. The immobilized GOx molecules seem to impose an additional barrier to $K_3Fe(CN)_6$ (Figure 4.3(c)).

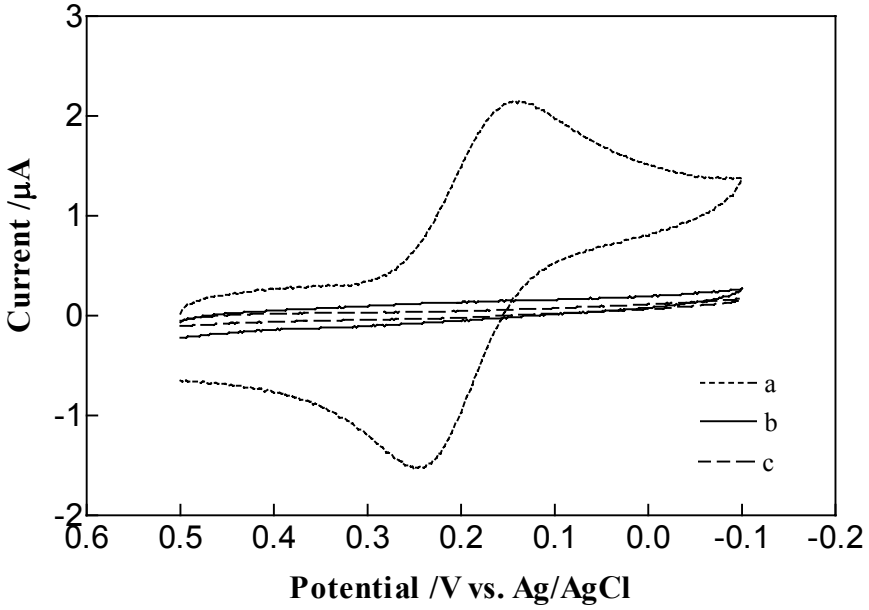

Figure 4.3 Cyclic voltammograms of 1.0 mM $K_3Fe(CN)_6$ with 0.1 M KCl on (a) a bare gold-modified SPCE, (b) after formation of a mixed monolayer (C4/C10-COOH with 10% C10-COOH in the assembling solution), and (c) after immobilization of GOx molecules. Scan rate 100 mV/s.

Figure 4.4 shows CV responses of a modified SPCE in 0.1 M Tris buffer (pH 7.0) containing 1.0 mM FCA at a scan rate of 100 mV/s. The characteristic and well-behaved redox response of FCA was observed at a bare gold-modified SPCE (Figure 4.4(a)). The monolayer had less blocking effect on FCA than on ferricyanide (Figure4.4(b) and Figure 4.3(b)). The explanation for this difference has been discussed in Chapter 3 (Section 3.3.3). The response of the electrode after the activation step with EDC and NHS did not change (data not shown). As with FCA, the immobilized GOx molecules further block the electrode surface (Figure 4.4(c)).

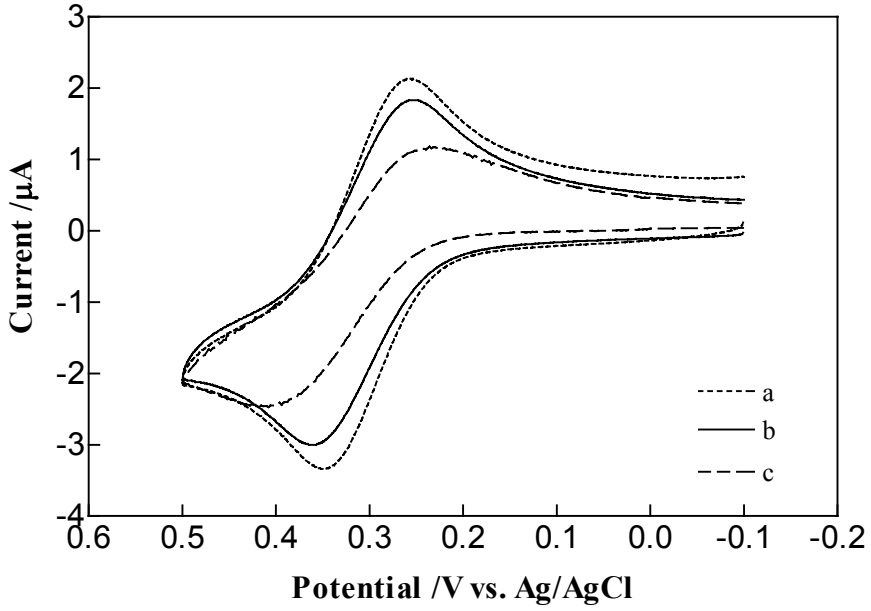

Figure 4.4 Cyclic voltammograms of 1.0 mM FCA in 0.1 M Tris buffer (pH 7.0) on (a) a bare gold-modified SPCE, (b) after formation of a mixed monolayer (C4/C10-COOH with 10% C10-COOH in the assembling solution), and (c) after immobilization of GOx molecules. Scan rate 100 mV/s.

Comparison of Figure 4.3(c) and Figure 4.4(c) shows that FCA was less affected by the presence of the monolayer/immobilized GOx layer than $K_3Fe(CN)_6$. Thus, FCA was chosen as a mediator for the glucose biosensors.

4.3.2 Electrocatalytic Oxidation of Glucose at GOx-Modified SPCEs

Figure 4.5 shows cyclic voltammograms of a GOx-modified SPCE in 0.1 M Tris buffer (pH 7.0) containing 0.2 mM FCA in the absence and presence of 10 mM glucose.

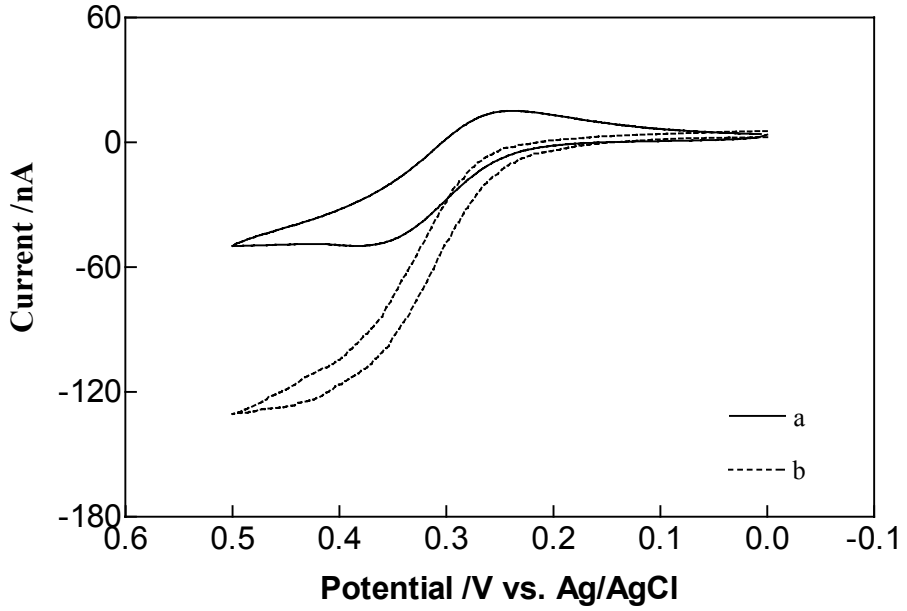

Figure 4.5 Cyclic voltammograms of a GOx-modified SPCE in 0.1 M Tris buffer (pH 7.0) containing 0.2 mM FCA before (a) and after (b) the addition of 10 mM glucose. Scan rate 2 mV/s. The GOx-modified SPCE was prepared from a mixed monolayer composed of C4/C10-COOH (10% C10-COOH in the assembling solution).

In the absence of glucose, the characteristic and well-behaved redox response of FCA was observed (Figure 4.5(a)); In the presence of glucose, an electrocatalytic anodic current was observed, indicating that GOx molecules were immobilized on the surface and maintained their biological activity. In addition, the concomitant decrease of the reductive current is indicative of the regeneration of FCA from the ferricinium ion by GOx in its reduced form. This demonstrates that FCA is a very efficient mediator between the redox centers of GOx molecules and the electrode surfaces. Figure 4.6 depicts the mediation reaction.

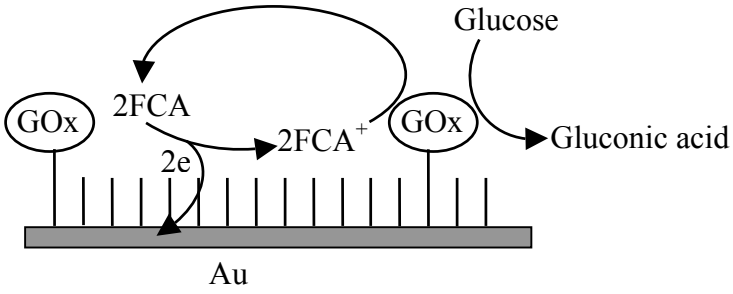

Figure 4.6 Electrical communication between the immobilized GOx molecules and the electrode surface using FCA as a mediator. FCA^+ represents the oxidized form of the mediator.

Control experiments reveal that in the absence of immobilized GOx, no electrocatalytic anodic currents were detected in the presence of glucose, and no significant oxidative current was observed in the solutions without FCA. These results confirm that the current is related to the enzymatic oxidation of glucose, and FCA facilitates electron transfer between the immobilized GOx molecules and the electrodes.

4.3.3 Optimization

In order to maximize the sensitivity of the glucose biosensor, the effects of applied potential, the concentration of the mediator, and the composition of the mixed monolayer, which provides the platform for the immobilization of GOx, were investigated.

4.3.3.1 Effect of Applied Potential

A glucose-dependent current is only realized when the electrode is poised sufficiently positive to generate the ferricinium ion from FCA. The effect of the applied potential on the biosensor response was studied over the potential the range of +0.25 to +0.5 V. The experiments were performed in 0.1 M Tris buffer (pH 7.0) containing 10 mM glucose and 0.2 mM FCA. As shown in Figure 4.7, the response of the biosensor rapidly increased as the potential increased from +0.25 to +0.45 V as the kinetics of FCA oxidation become diffusion-limited at more positive potential. When the potential was further increased to +0.5 V, the response increased slightly. Although higher applied potential results in a larger biosensor response, a potential of +0.45 V was selected as an optimum potential for all subsequent experiments because the higher applied potential may result in increased interference from the oxidation of other electroactive species that may be present in a sample, such as ascorbic acid and uric acid.

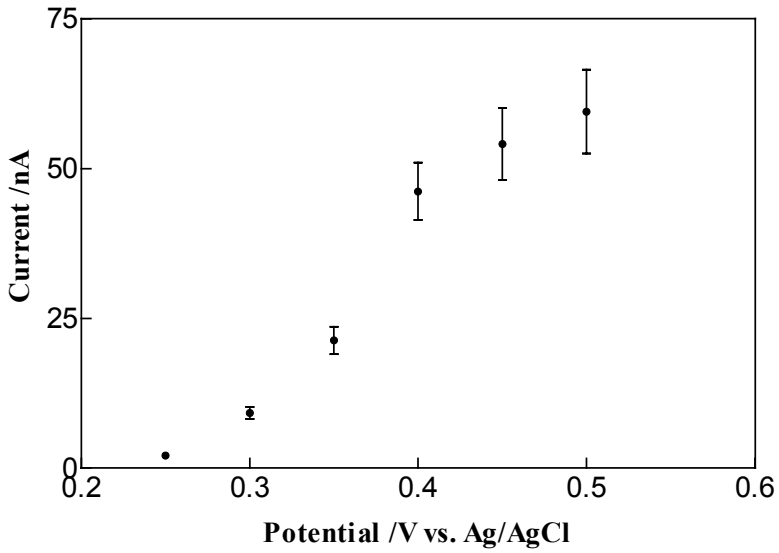

Figure 4.7 Effect of applied potential on the amperometric response of GOx-modified SPCEs. Current was measured in 0.1 M Tris buffer (pH 7.0) containing 10 mM glucose and 0.2 mM FCA. GOx-modified SPCEs were prepared under the same conditions as described in Figure 4.5. (n=3)

4.3.3.2 Effect of Mediator Concentration

The effect of mediator concentration on the biosensor response was examined with 10 mM glucose in 0.1 M Tris buffer (pH 7.0). As shown in Figure 4.8, the current increased sharply with an increase in the concentration of FCA from 0.05 to 0.2 mM, and then leveled off. Such behaviour is typical of mediator-based sensors.[221] At low mediator concentration, the current response is limited by enzyme-mediator kinetics. When the mediator concentration is high, the current response is limited by enzyme-substrate kinetics. Although higher mediator concentration results in a larger biosensor response, a concentration of 0.2 mM was selected for all further experiments because the higher concentration results in an increased background current.

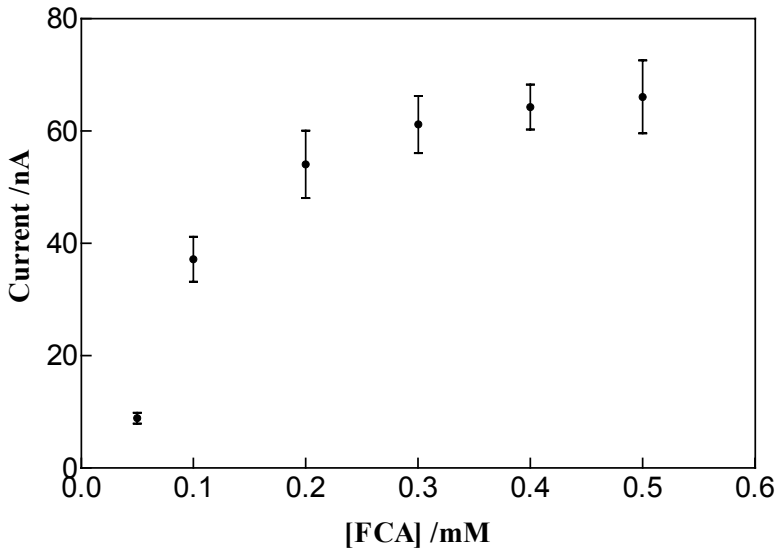

Figure 4.8 Effect of the concentration of FCA on the amperometric response of GOx-modified SPCEs. Current was measured in 0.1 M Tris buffer (pH 7.0) containing 10 mM glucose. Applied potential was +0.45 V. GOx-modified SPCEs were prepared under the same conditions as described in Figure 4.5. (n=3)

4.3.3.3 Effect of the Composition of Binary Monolayers

Binary monolayers composed of C4 and C10-COOH with varying molar ratio in the assembling solution were employed to study the effect of the monolayer composition on the response of the GOx-modified SPCEs. Calibration curves were created for these GOx-modified SPCEs. The sensitivity of the GOx-modified SPCEs to glucose (determined by linear regression over 0-10 mM glucose range) was used for evaluation. The results are presented in Figure 4.9.

Similar results were obtained with binary monolayers prepared with C6/C10-COOH (Figure 4.10) and C8/C10-COOH (Figure 4.11).

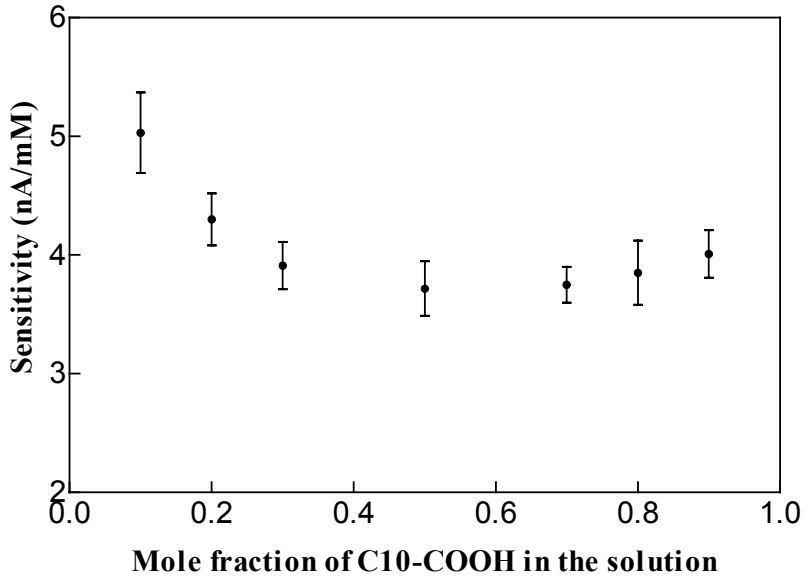

Figure 4.9 Effect of the composition of binary monolayers (C4/C10-COOH) on the amperometric response of GOx-modified SPCEs. Amperometric measurements were carried out in 0.1 M Tris buffer (pH 7.0) containing 0.2 mM FCA, with an applied potential of +0.45 V.

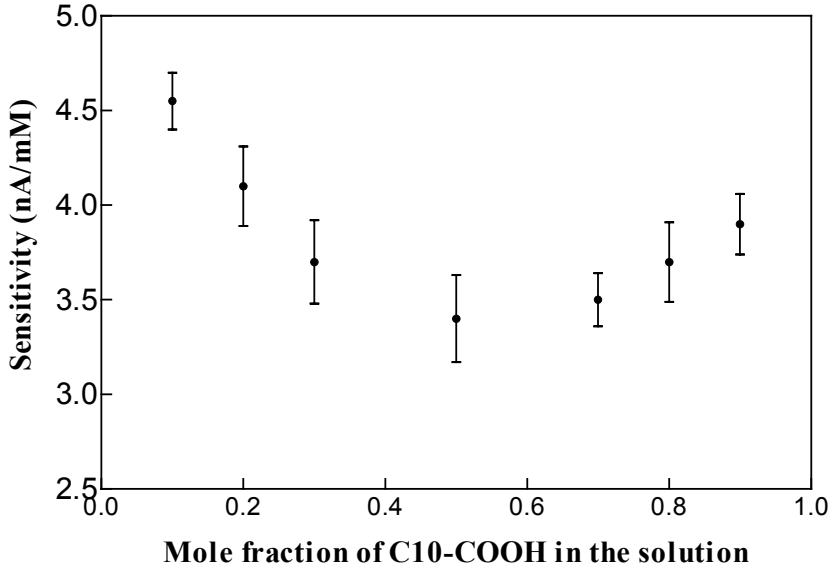

Figure 4.10 Effect of the composition of binary monolayers (C6/C10-COOH) on the amperometric response of GOx-modified SPCEs. Amperometric measurements were carried out in 0.1 M Tris buffer (pH 7.0) containing 0.2 mM FCA, with an applied potential of +0.45 V.

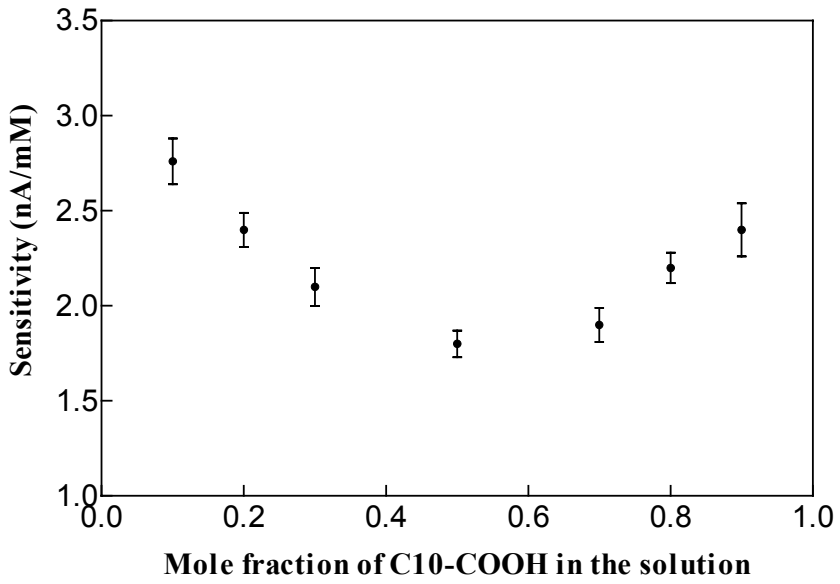

Figure 4.11 Effect of the composition of binary monolayers (C8/C10-COOH) on the amperometric response of GOx-modified SPCEs. Amperometric measurements were carried out in 0.1 M Tris buffer (pH 7.0) containing 0.2 mM FCA, with an applied potential of +0.45 V.

The results shown in Figures 4.9-4.11 were unexpected. Increasing the mole fraction of C10-COOH in the assembly solution was expected to increase the loading of C10-COOH on the electrode surface, and this should result in a higher density of GOx immobilization sites on the surface. At some critical value, the density of –COOH groups on the surface will equal the density of GOx molecules in a perfectly-formed, complete monolayer of GOx. Based on the known dimensions of GOx (its hydrodynamic radius is 5.24×10^{-7} cm based on its diffusion coefficient of 4.1×10^{-7} cm^2/s[222] and Stokes Law[8]), each GOx molecule should occupy an area of about (πr^2) on the electrode surface. If one C10-COOH group were present in this area, the mole percent of C10-COOH in the monolayer would be 0.26% using a total alkanethiol

density of 4.5×10^{14} molecules/cm^2.[223] Although this simple calculation explains the maxima in biosensor response that occur at very low C10-COOH values (Figure 4.9-4.11), it does not explain the minima that occur around 50% C10-COOH. Possibly, the increase in C10-COOH from very low values causes multiple bonding to occur between each GOx molecule and the monolayer, resulting in distortion of the GOx tertiary structure, causing loss of activity. Further increases in C10-COOH, at and above about 50%, could allow hydrogen bonding to occur between adjacent C10-COOH molecules, lowering the reactivity of these groups on the surface. It has been shown that alkanethiol monolayers formed from species containing a terminal –COOH group show much different acid-base properties in comparison with the same species present in dilute solution (pK_a values are 3.68 and 4.52 for mercaptoacetate in aqueous solution and on the surface of a monolayer-modified electrode, respectively[186]).

4.3.4 Calibration Curve

Figure 4.12 shows the amperometric responses of a GOx-modified SPCE to glucose. It can be seen that an increase in glucose concentration is accompanied by an increase in anodic current obtained at a constant potential of +0.45 V. The steady-state current can be obtained within 2 min. The background-subtracted currents at different concentrations of glucose at 2 min were used to create calibration curves. GOx-modified SPCEs prepared from different mixed monolayers were investigated. Results are shown in Figure 4.13 and Table 4.1.

As shown in Figure 4.13 and Table 4.1, the GOx-modified SPCEs prepared from mixed monolayers composed of C4/C10-COOH and C6/C10-COOH gave similar

responses, and the sensitivity values are larger than those obtained with glucose biosensors based on gold nanotube arrays (4.0 nA mM^{-1} mm^{-2})[224] and SAMs of alkanethiols (4.1 nA mM^{-1} mm^{-2}).[225] The GOx-modified SPCE obtained from the monolayer of C8/C10-COOH showed lower sensitivity. The linear responses obtained from all three types of GOx-modified SPCEs cover the clinical region for a range of 3.5-6.5 mM glucose.[226]

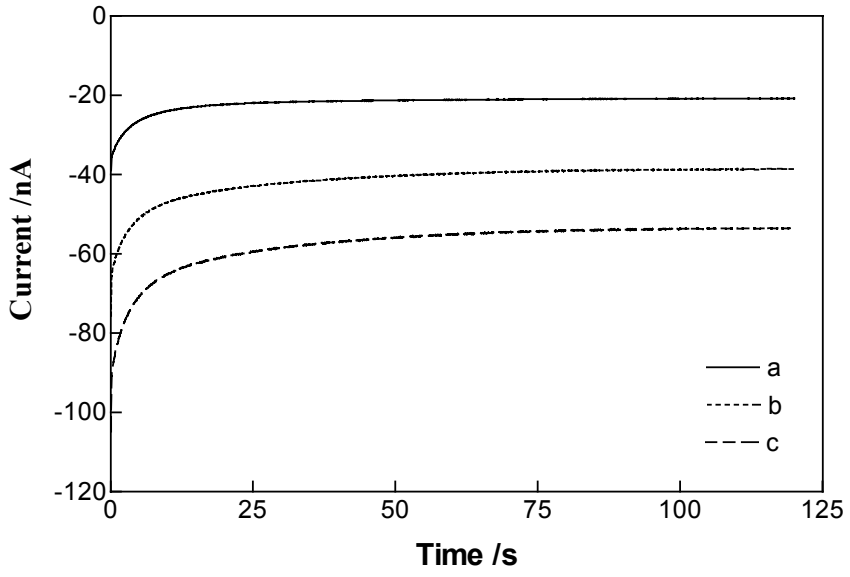

Figure 4.12 Amperometric response of a GOx-modified SPCE prepared from a mixed monolayer composed of C4/C10-COOH (10% C10-COOH in the assembling solution) in 0.1 M Tris buffer (pH 7.0) containing 0.2 mM FCA in the absence of glucose (a), and in the presence of 2.5 mM (b) and 5.0 mM (c) glucose. Applied potential was set at +0.45 V vs. Ag/AgCl.

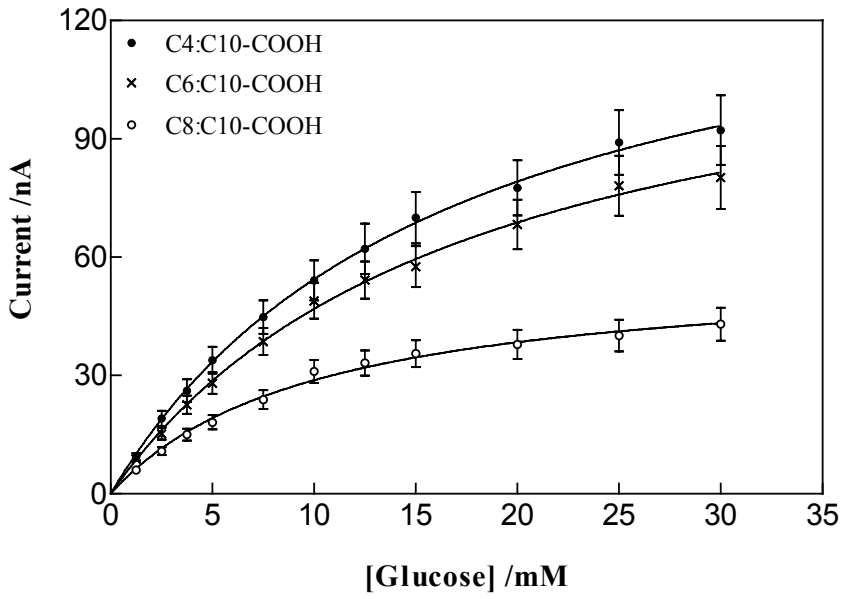

Figure 4.13 Calibration curves for the GOx-modified SPCEs prepared from different mixed monolayers (10% C10-COOH in the solution). (n=3)

Table 4.1 Data obtained from calibration curves (Figure 4.13) for the three types of GOx-modified SPCEs.

GOx-modified SPCEs	Sensitivity (nA mM^{-1})*	Detection limit (mM)**
C4/C10-COOH	5.0	0.5
C6/C10-COOH	4.6	0.6
C8/C10-COOH	2.8	0.8

*Evaluated over the 0-10 mM glucose range by linear regression.

**Detection limit estimated from S/N=3. Geometric area of the enzyme electrodes: 1 mm^2.

For all three types of enzyme electrodes, the amperometric responses increased as the glucose concentration was elevated, and the current approaches a saturation value at

high glucose concentrations (Figure 4.13). The saturated amperometric responses at high glucose concentrations suggest that the active sites of the enzyme units are saturated at these glucose levels. This is as expected for a system following Michaelis-Menten kinetics for an enzyme-catalyzed reaction between two substrates. The apparent Michaelis-Menten constant (K_m), which gives an indication of the enzyme-substrate kinetics for the enzyme electrodes, can be calculated from the Eadie-Hofstee plot:[4]

$$V = V_{max} - K_m(V/[S]) \qquad (4.2)$$

where V is the rate of the enzyme reaction at any concentration of glucose, V_{max} is the maximum rate of the enzyme reaction under saturated substrate condition, and S is the bulk concentration of substrate. This equation can be used with amperometric biosensor data by substituting I and I_{max} (currents) for V and V_{max}. The resulting Eadie-Hofstee plot is shown in Figure 4.14.

All of three plots for GOx-modified SPCEs show a linear relationship that conforms to the Michaelis-Menten equation. In order to obtain the most accurate values of K_m and I_{max}, nonlinear regression ($V = \frac{V_{max}[S]}{K_m + [S]}$) was used to calculate these values. K_m and I_{max} values for the three types of GOx-modified SPCEs are summarized in Table 4.2.

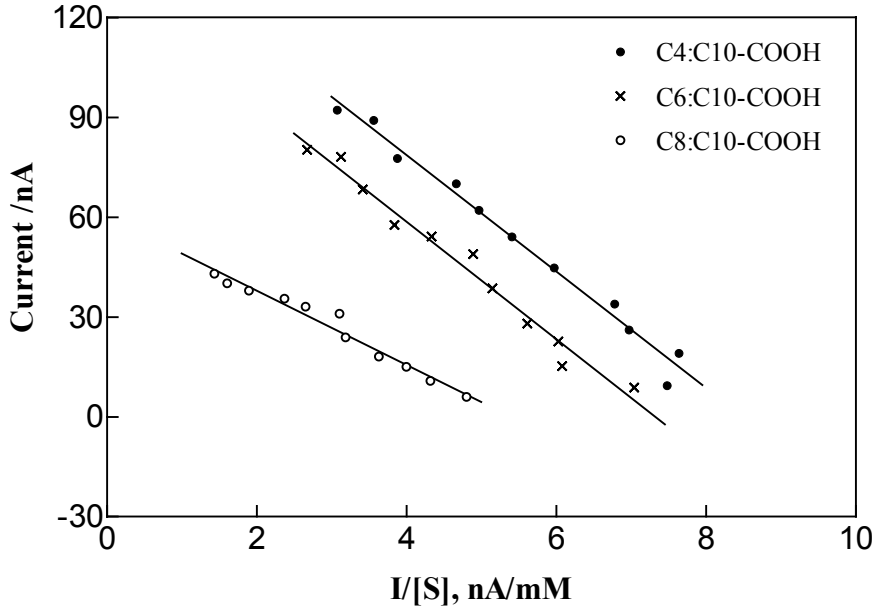

Figure 4.14 Eadie-Hofstee plots for three types of GOx-modified SPCEs. Data are from Figure 4.13.

The K_m values of all three enzyme electrodes are smaller than those obtained at enzyme electrodes by covalent immobilizing GOx on ω-carboxyl-terminated thiol-modified Pt electrode surface (21-24 mM).[227] The smaller K_m values mean that the immobilized GOx possesses a higher affinity for glucose. The K_m value for the GOx-modified SPCEs prepared from C8/C10-COOH is smaller than those from C4/C10-COOH and C6/C10-COOH, and the reason for this difference is unknown. It may result from the orientation and conformation of GOx molecules on the surface.

Table 4.2 Kinetic parameters for the three types of GOx-modified SPCEs. *

GOx-modified SPCEs	C4/C10-COOH	C6/C10-COOH	C8/C10-COOH
I_{max} (nA)**	145 ± 3	129 ± 4	58 ± 2
K_m (mM)**	16.7 ± 0.7	18 ± 1	10.1 ± 0.8
R^2 **	0.999	0.997	0.993

*Calculated from data shown in Figure 4.13 using nonlinear regression method (Prism® (3.00)).

**The results are expressed as the mean ± standard deviation.

***R-squared, a measure for goodness of fit.

I_{max} reflects the loading level of active GOx molecules on the electrode surfaces. I_{max} values for GOx-modified SPCEs prepared from C4/C10-COOH and C6/C10-COOH, 145 and 129 nA, are very close to those obtained for glucose biosensors based on a ω-carboxyl-terminated thiol SAM surface (150 nA mm^{-2}).[225] The maximum current for GOx-modified SPCEs prepared from C8/C10-COOH was only 58 nA. The possible explanation for this low I_{max} is steric hindrance, since the chain length difference for these two components (C8 and C10-COOH) is smaller than for the other two systems (C4 and C10-COOH; C6 and C10-COOH).

4.3.5 Stability

The storage stability of the proposed GOx-modified electrodes was examined by measuring currents for 5.0 mM glucose every day and keeping the electrodes at 4 °C in 0.1 M Tris buffer (pH 7.0) when not in use. The response currents were about 50% of

the original value after one week for GOx-modified SPCEs prepared from C4/C10-COOH. The GOx-modified SPCEs prepared from C6/C10-COOH and C8/C10-COOH showed similar storage stabilities; the response currents for these sensors were about 70% of the original value after one week. The proposed enzyme electrodes can therefore be used as short-term sensors. Figure 4.15 shows the response of the GOx-modified SPCE prepared from C6/C10-COOH to 5.0 mM glucose during one week of storage.

The operational stability of these enzyme electrodes was tested by determining 5.0 mM glucose continuously; the electrodes lost only 8.1 % (enzyme electrodes prepared from C4/C10-COOH) and about 5.0% (enzyme electrodes prepared from C6/C10-COOH and C8/C10COOH) of the initial response after 10 continuous tests in which 2 min measurements at +0.45 V vs. Ag/AgCl were followed by rinsing.

4.3.6 Effect of Oxygen

Another factor that must be considered for all sensors based on oxidase enzymes is the possibility of interference by oxygen. Mediator-based sensors do not require oxygen to operate, and oxygen electroactivity is suppressed at monolayer-coated electrodes and at low applied potentials H_2O_2 is not detected. However, oxygen can diminish sensor response by consuming substrate via a non-current-producing pathway, namely the enzyme-catalyzed reaction between oxygen and substrate.[228] Figure 4.16 shows glucose calibration curves for the C6/C10-COOH enzyme electrode in the absence and presence of oxygen. As shown in Figure 4.16, some interference from oxygen was observed, since a current decrease occurred in the presence of oxygen.

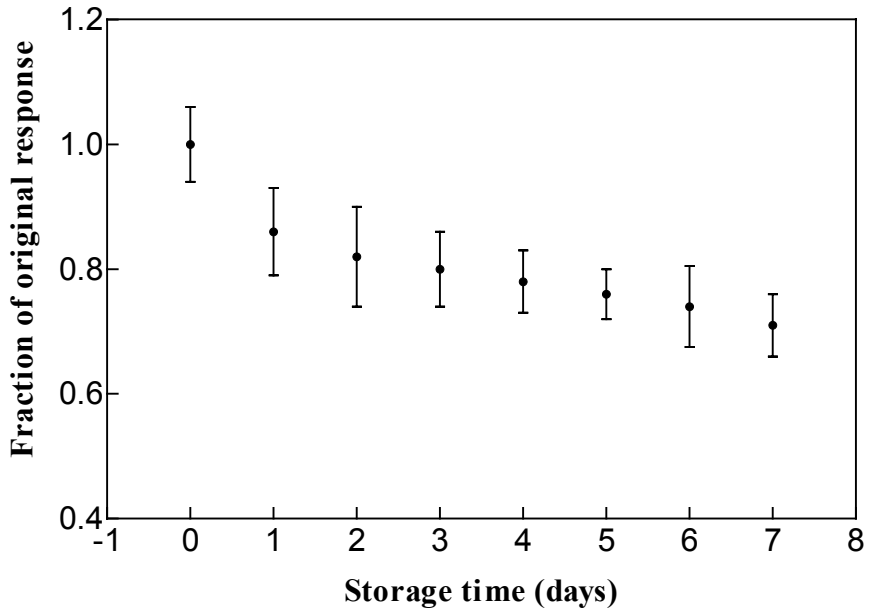

Figure 4.15 Current response of the GOx-modified SPCEs prepared from C6/COOH (10% C10-COOH in the assembling solution) to 5.0 mM glucose in 0.1 M Tris buffer (pH 7.0) containing 0.2 mM FCA as a function of the storage days. (n=3)

4.3.7 The Response of the Electrochemical Array to Glucose

Since the applied potential may have different effects on GOx-modified SPCEs used in a conventional three-electrode configuration and the proposed electrochemical array (two electrode system, described in Chapter 2), the enzyme electrodes in these two systems were investigated in 0.1 M Tris buffer (pH 7.0) containing 0.2 mM FCA using CV. Results are shown in Figure 4.17.

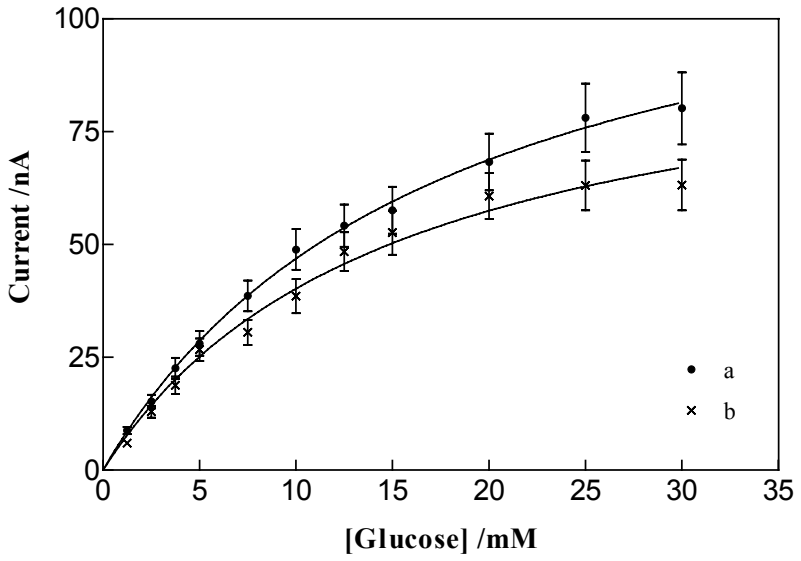

Figure 4.16 Effect of oxygen on the amperometric responses of GOx-modified SPCEs prepared from mixed monolayers of C6/C10-COOH (10% C10-COOH in the solution) (a) no O_2 present, (b) O_2 present. (n=3).

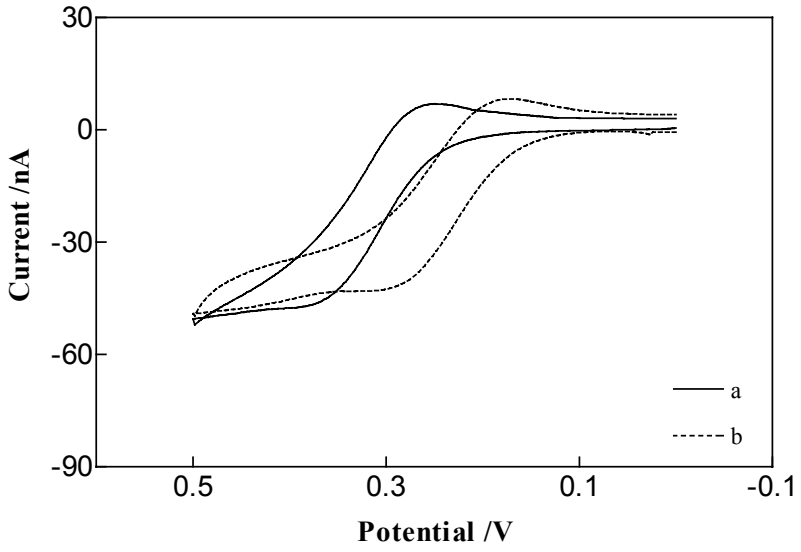

Figure 4.17 Cyclic voltammograms of 0.1 M Tris buffer (pH 7.0) containing 0.2 mM FCA on a GOx-modified SPCE used in (a) a conventional three-electrode configuration and (b) the proposed electrochemical array. Scan rate 2 mV/s. The GOx-modified SPCE was prepared from a mixed monolayer composed of C6/COOH (10% C10-COOH in the assembling solution).

As shown in Figure 4.17, the anodic peak potential in the conventional three-electrode configuration is about +0.38 V, while in the electrochemical array it is about +0.30 V. The anodic peak potential shifted negative by about 0.08 V in the array. Therefore, the applied potential for amperometric measurements in the electrochemical array was chosen as +0.37 V (+0.45 V was used with the conventional three electrode system). The difference is likely a result of the potential of the Ag/AgCl reference electrodes used in the array, since the Cl^- concentration in 0.1 M Tris buffer (pH 7.0) is about 0.09 M, compared with the value of 3 M (NaCl) in the commercial Ag/AgCl reference electrodes.

The amperometric responses of the electrochemical array to glucose at +0.37 V were used to create calibration curves and results are shown in Figure 4.18. The sensitivity obtained with the electrochemical array is 4.7 nA mM^{-1} with a detection limit of 0.8 mM (S/N=3). These values are very close to the values of 4.6 nA mM^{-1} and 0.6 mM obtained with the conventional three-electrode system (Table 4.1).

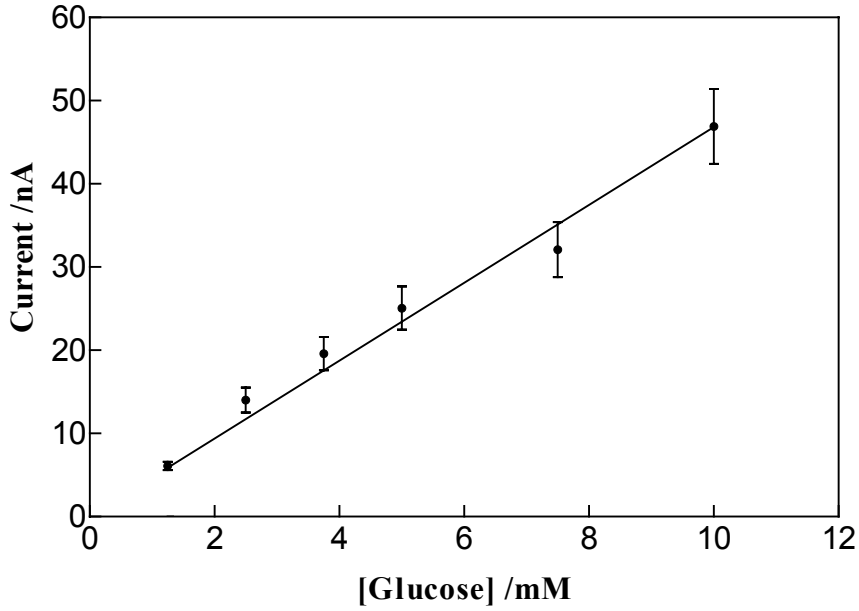

Figure 4.18 Calibration curves for the electrochemical array. The GOx-modified SPCE was prepared from a mixed monolayer composed of C6/C10-COOH (10% C10-COOH in the assembling solution). (n=4)

4.4 CONCLUSIONS

The application of functionalized binary monolayers electrochemically prepared from Bunte salts to amperometric glucose biosensors based on GOx was investigated in this chapter. These monolayers allow two-dimensional reaction matrices to be created, and this confines the biochemical reaction to the modified electrode surface. Therefore, problems associated with diffusion through a three-dimensional reaction layer, namely irreproducibility and poor response time, are overcome, provided the monolayer-enzyme layer, and other processing steps, can be prepared in a reproducible manner.

The results of our study reveal GOx (used as a model enzyme) can effectively and reproducibly be immobilized onto binary monolayers using a carbodiimide

coupling agent. The sensitivities of the resulting biosensors can be tuned by adjusting the composition of the monolayers. Optimized conditions for the fabrication and operation of the biosensor have been determined. It is anticipated that this immobilization method will be suitable for the development of other biosensors.

Chapter 5: Competitive Enzyme Immunosensor for Biotin Based on Electrodeposition of Bunte Salts

5.1 INTRODUCTION

During the past few years, immunosensors have attracted growing attention due to their main advantages over alternative methods with respect to high sensitivity, selectivity and robustness.[229] The extremely high selectivities and affinities of antibody molecules for their corresponding antigens have been widely exploited for analytical purposes in various fields (environment analysis,[230-232] clinical diagnostics[233] and the food and drink industries[234]), mainly as radio-immunoassays (RIAs) or ELISAs. However, these techniques require highly qualified personnel, long assay times, and often require sophisticated instrumentation. Thus, a wide range of immunosensors combining a classic ELISA format with amperometric, photometric, chromatographic and other detection methods has been investigated.[17, 235] Of these, optical transduction methods are the most developed in terms of commercial applications.[236] Electrochemical detection methods for immunoreactions have not yet been studied as much; however, amperometric methods appear very promising due to their main advantages of relatively high sensitivity, simplicity, low instrument cost and small instrument size.[237, 238] In addition, and distinct from optical detection requirements, the tested samples do not need to be transparent. Therefore, electrochemical detection-based immunosensors are well-suited to clinical and environmental testing where cost and instrument portability are of major concerns, and the samples are often opaque or intensely colored.

Within the existing formats of immunosensors, the heterogeneous competitive type (in which either the antigen or the antibody is immobilized onto a support) is the most common and attractive for the determination of small molecules, allowing determination of analytes in the ppb- or in some cases even in the ppt- range when enzyme labels are used. Figure 5.1(a) illustrates the principles of competitive enzyme immunosensors. Enzyme-labeled antigen competes with free antigen (the analyte) for a fixed, insufficient quantity of immobilized antibody binding sites. Unbound free antigen and enzyme-labeled antigen are then rinsed from the support. The amount of bound enzyme-labeled antigen, which is inversely related to the concentration of free antigen, is determined by the supply of suitable enzyme substrates, and results in the type of calibration curve shown in Figure 5.1(b).

The avidin-biotin system has been effectively employed as a convenient model for antibody-antigen systems to demonstrate potential immunoassay formats.[233, 239] It has also been used as a convenient immobilization system, with surface-bound avidin capturing dissolved biotinylated molecules.[233, 240] Avidin obtained from egg white has a molecular weight of 67 kDa, is a basic tetrametric glycoprotein and has four binding sites for biotin (vitamin H). Biotin is a small molecule (244.31 Da) and functions as a cofactor for many carboxylase enzymes which control the transfer reactions of carbonic acid, and it is related to the metabolism of carbon dioxide.[241] The basis for the use of the avidin-biotin system as a model for immunochemical reactions is the specificity and the exceptionally high affinity ($K_a=10^{15}$ M^{-1}) between biotin and avidin (or its bacterial analogue streptavidin from *Streptomyces avidinii*) and the consequent stability of this noncovalent interaction.[242] The interaction between avidin and biotin is so strong

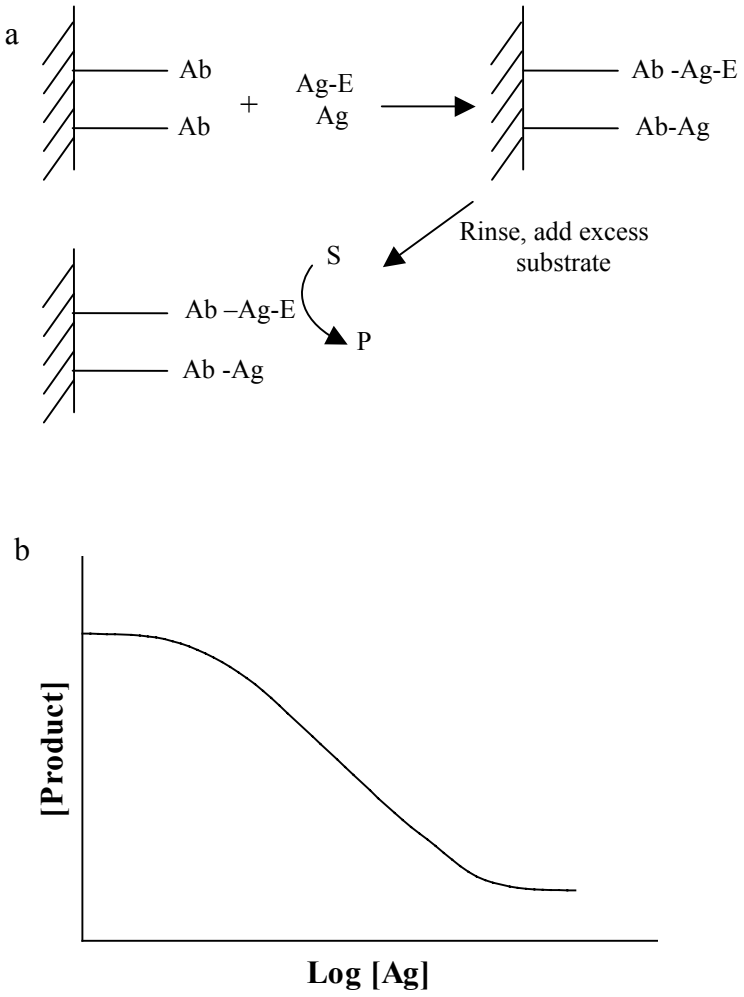

Figure 5.1 Competitive enzyme immunosensor.[4] Ab, antibody; Ag, antigen; E, enzyme; S, substrate; P: product.

that even biotin coupled to proteins is bound by avidin.[243] In addition, biotin is a small molecule and biotinylation does not usually alter the properties of the labeled molecules, e.g., enzymatic catalysis or antibody binding. Excellent sensitivity can be achieved with the avidin-biotin system because of the four biotin-binding sites of avidin and the possibility of multiple biotinyl groups on derivatized antibodies or antigens. In many cases, the signal is enhanced 10-fold or more by the system.[244, 245]

Many immunosensors based on the avidin-biotin system have been reported. A direct and indirect competitive biotin assay was reported in literature.[246] In this study, avidin was immobilized on an indium tin oxide electrode. In the competitive format, unlabeled biotin (analyte) and electroactive compound-labeled biotin (biotin was labeled with ruthenium tris(2,2'-bipyridine)) competed for limited avidin binding sites on electrodes. A detection limit of 1 ng/mL biotin was obtained, which is close to the sensitivity of some enzyme-labeled amperometric biosensors.

Wright[247] described a 'homogeneous' format enzyme channeling specific binding assay for biotin. The procedure involved the immobilization of avidin onto the surface of SPEs in which the carbon-based ink contained HRP. Competitive binding occurred between free biotin and glucose oxidase-labeled biotin for the limited number of immobilized avidin binding sites. Upon addition of glucose, the GOx label produced H_2O_2 that was detected at the underlying HRP carbon electrode. The assay showed greatest sensitivity over the biotin concentration range 0.07 to 2 μg/ mL.

A disposable competitive enzyme immunosensor based on a SPCE and the avidin-biotin system for the detection of rabbit IgG has been reported.[248] HRP and streptavidin were covalently bonded to a conducting polymer bearing carboxylic acid groups on the electrode, and biotinylated antibody was subsequently immobilized on the electrode surface using avidin-biotin coupling. This sensor was based on the competitive assay between free and labeled antigen rabbit IgG for the available binding sites of antibody anti-rabbit IgG. GOx was used as a label and in the presence of glucose, H_2O_2 formed by the enzymatic reaction was reduced by enzyme channeling via HRP bound to the electrode. The catalytic current was monitored amperometrically

at -0.35 V vs. Ag/AgCl and this method showed a linear range of rabbit IgG concentration up to 2 μg/mL with a detection limit of 0.33 μg/mL.

Like other types of biosensors, one of the most crucial steps for the successful construction of immunosensors is the appropriate and reproducible coupling of the biocomponent to the surface of the transducer. In this chapter, the application of mixed monolayers to biocomponent immobilization in a model immunosensor was investigated. The mixed monolayer was formed electrochemically from Bunte salts and was composed of a mixture of a long carboxylic acid functionalized derivative (C10-COOH) with a short methyl functionalized derivative (C6). The long chain component (C10-COOH) provides binding sites, and the short chain component allows electron transfer to the underlying gold layer. Avidin was covalently immobilized on electrodes through the carboxyl groups of the mixed monolayers using a carbodiimide coupling agent. The immunosensor was applied to the amperometric determination of biotin (model analyte) using competitive binding with lactoperoxidase-labeled biotin (B-LPOD). Benzoquinone was chosen as a mediator to shuttle electrons between the lactoperoxidase and the electrode. The experimental parameters affecting the response of the immunosensor were optimized.

5.2 EXPERIMENTAL SECTION

5.2.1 Materials and Instrumentation

Avidin (egg white), D-biotin, benzoquinone and B-LPOD (35 units/mg) were purchased from Sigma. 30% H_2O_2 was obtained from EM Science.

An EG & G Potentiostat/Galvanostat, and a CHI650A Potentiostat were employed. Bioanalytical Systems supplied Ag/AgCl (3 M NaCl) reference electrodes.

5.2.2 Methods

5.2.2.1 Preparation of Avidin-Modified Electrodes

Binary monolayers (C6/C10-COOH with 10% C10-COOH in the assembling solution) were electrochemically formed by the method described in Chapter 3. The terminal carboxylic groups of monolayers were activated by immersion in 0.05 M phosphate buffer (pH 7.0) containing 2 mM EDC hydrochloride and 5 mM NHS for 1 h at room temperature. After the activation, the electrodes were rinsed with phosphate buffer and immediately placed in 0.05 M phosphate buffer (pH 8.5) containing 1/mg mL avidin overnight at 4 °C. By this procedure, avidin was immobilized on the mixed monolayer through the formation of covalent bonds with carboxyl terminal groups of the mixed monolayer. The avidin-modified electrodes were rinsed with water and used immediately.

Control electrodes were prepared by the same procedure described above except that no activation step of –COOH with EDC hydrochloride and NHS, and 0.05 M phosphate buffer (pH 8.5) without avidin was used to incubate with activated mixed monolayer-modified electrodes at 4 °C overnight. Control experiments were performed to investigate the influence of nonspecific adsorption of B-LPOD on mixed monolayer-coated electrodes.

5.2.2.2 Cyclic Voltammetry

Modified electrodes were incubated in 0.05 M phosphate buffer (pH 7.0) containing 200 μg/mL B-LPOD for 40 min at room temperature. They were then characterized with respect to their applicability for the determination of bound B-LPOD activity by CV in 0.1 M Tris buffer (pH 7.0) containing 500 μM H_2O_2 and 0.2 mM benzoquine at a scan rate of 2 mV/s. These experiments were carried out in a conventional three-electrode configuration, with the resulting electrode (geometric area 1.0 mm^2) as the working electrode, a platinum wire as the auxiliary electrode, and Ag/AgCl (3 M NaCl) as the reference electrode.

In order to investigate the effect of applied potential on the resulting electrodes in a conventional three-electrode system and the proposed electrochemical array (two-electrode system, described in Chapter 2), CV experiments were also carried out in these two systems. An avidin-modified, monolayer-coated, gold-modified SPCE that had been incubated with B-LPOD was used as the working electrode in both systems. The home-made Ag/AgCl electrodes served as the counter electrode in the array.

5.2.2.3 Biotin Immunosensor

Biotin was determined using the competitive approach, i.e. free biotin competed with the B-LPOD for the limited avidin binding sites on the electrodes.

B-LPOD was mixed with free biotin standard solutions, and final concentration was over the range 0-200 μg/mL in 0.05 M phosphate buffer (pH 7.0). Avidin-modified electrodes were incubated in these solutions at room temperature. The unbound biotin

and B-LPOD were then removed by washing with water. The activity of the bound B-LPOD was measured using the amperometric technique with H_2O_2 as the substrate.

The experimental parameters affecting the response of the assay, such as applied potential, concentration of the mediator, concentration of H_2O_2, incubation time and B-LPOD concentration, were optimized. Optimization was carried out in a conventional three-electrode cell, with a modified SPCE (geometric area 1.0 mm^2) as the working electrode, a platinum wire as the auxiliary electrode, and Ag/AgCl (3 M NaCl) as the reference electrode.

The response of the proposed electrochemical array to biotin was also investigated.

5.3 RESULTS AND DISCUSSION

5.3.1 Electrochemical Characterization of the Immunosensor Using CV

The detection principle of the proposed assay is shown in Figure 5.2.

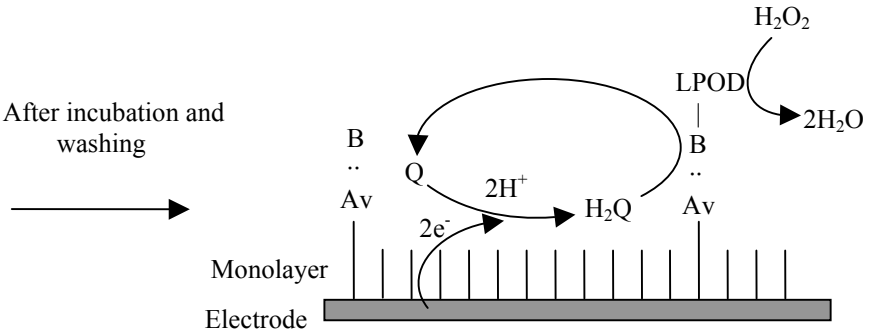

Figure 5.2 Detection principle for the proposed immunosensor for biotin: Av, avidin; B: biotin; B-LPOD, lactoperoxidase-labeled biotin; Q: benzoquinone; H_2Q: hydroquinone.

The applicability of the avidin-modified electrode to the electrochemical determination of bound B-LPOD activity is shown Figure 5.3. A large catalytic wave appeared at negative applied potentials with an obvious increase in the reduction current in the presence of benzoquinone and H_2O_2 (Figure 5.3(c)), which demonstrates that benzoquinone can shuttle electrons from the redox center of bound B-LPOD to the electrode. Therefore, benzoquinone can be used as a mediator for determination of the activity of bound B-LPOD.

Both benzoquinone and hydrogen peroxide can be reduced electrochemically. The cyclic voltammogram of the B-LPOD-modified electrode in blank 0.1 M Tris buffer pH 7.0 (data not shown) is very similar to that of the electrode in the presence of 500 μM H_2O_2 (Figure 5.3(a)). Therefore, no interference from H_2O_2 was observed within this potential range. Benzoquinone is selectively reduced even in the presence of an excess of hydrogen peroxide.

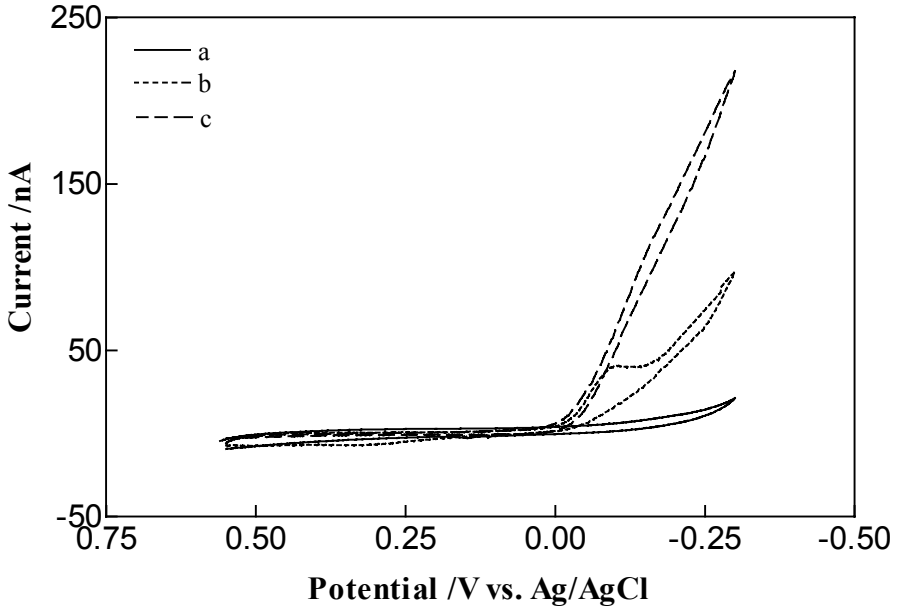

Figure 5.3 Cyclic voltammograms of avidin-modified electrodes after incubation with 200 μg/mL B-LPOD for 40 min in 0.1 M Tris buffer (pH 7.0) containing (a) 500 μM H_2O_2, (b) 0.2 mM benzoquinone, (c) 500 μM H_2O_2 and 0.2 mM benzoquinone. Scan rate 2 mV/s.

5.3.2 Amperometric Measurement of Bound B-LPOD Activity

Optimization was done with the avidin-modified electrode after incubation with 200 μg/mL B-LPOD solution for 40 min (the concentration of free biotin was set at zero in this study). The activity of the bound B-LPOD was measured using amperometry. The parameters affecting the response of the amperometric sensor (applied potential and the concentration of benzoquinone) were optimized.

5.3.2.1 Effect of Applied Potential

A hydrogen peroxide-dependent current is only realized when the electrode is poised sufficiently negative with regard to the formal potential for benzoquinone to generate

the reduced form hydroquinone, which reacts with H_2O_2 catalyzed by B-LPOD to regenerate benzoquinone as shown in Figure 5.2. The effect of the applied potential on the immunosensor response was investigated over the potential range of -0.05 to -0.3 V. The experiments were performed in 0.1 M Tris buffer (pH 7.0) containing 500 μM H_2O_2 and 0.2 mM benzoquinone. As shown in Figure 5.4, the response of the immunosensor started at -0.1 V and increased steadily as the applied potential was decreased from -0.1 to -0.3 V since benzoquinone is easily reduced at more negative potentials. Although the more negative potential results in higher immunosensor response, it may also result in increased interference from the reduction of other electroactive species in the sample. The electrode potential was selected as -0.25 V vs. Ag/AgCl for all subsequent experiments, because at this potential substantial electrocatalytic current was obtained.

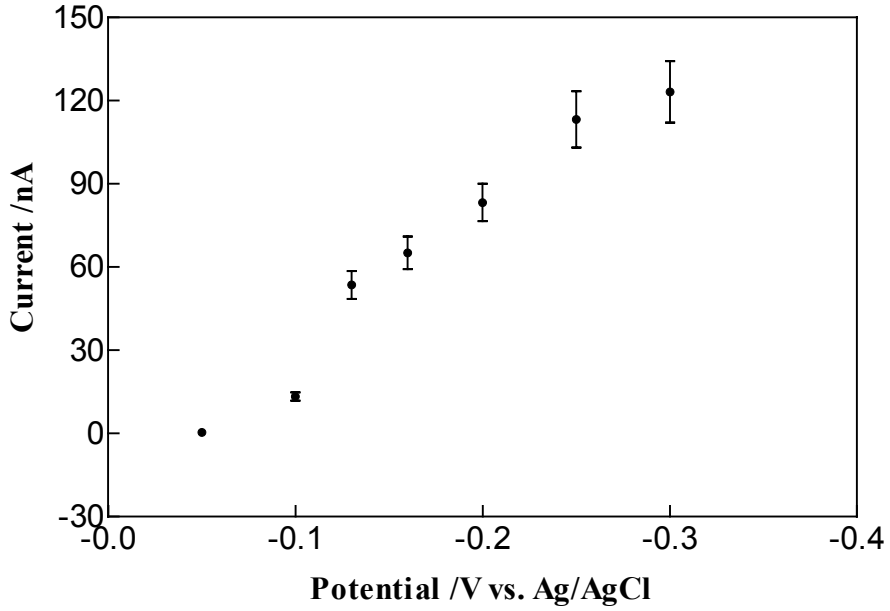

Figure 5.4 Effect of applied potential at B-LPOD-modified electrode to 500 μM H_2O_2 in 0.1 M Tris buffer (pH 7.0) containing 0.2 mM benzoquinone. (n=3)

5.3.2.2 Effect of Concentration of Mediator

The effect of benzoquinone concentration on the avidin-modified electrode response after incubation with 200 μg/mL B-LPOD for 40 min was also studied in the presence of 500 μM H_2O_2 in 0.1 M Tris buffer (pH 7.0) (Figure 5.5). The response of the B-LPOD-coated electrode increased sharply with the increase of the concentration of benzoquinone from 0.05 to 0.2 mM and then leveled off. Such behaviour is typical of a mediator-based sensor.[221] At low mediator concentration, the current response is limited by enzyme-mediator kinetics. When the mediator concentration is high, the current response is limited by enzyme-substrate kinetics. However, a higher concentration of benzoquinone produced a higher background current. Thus, the concentration of benzoquinone was fixed at 0.2 mM for all further experiments.

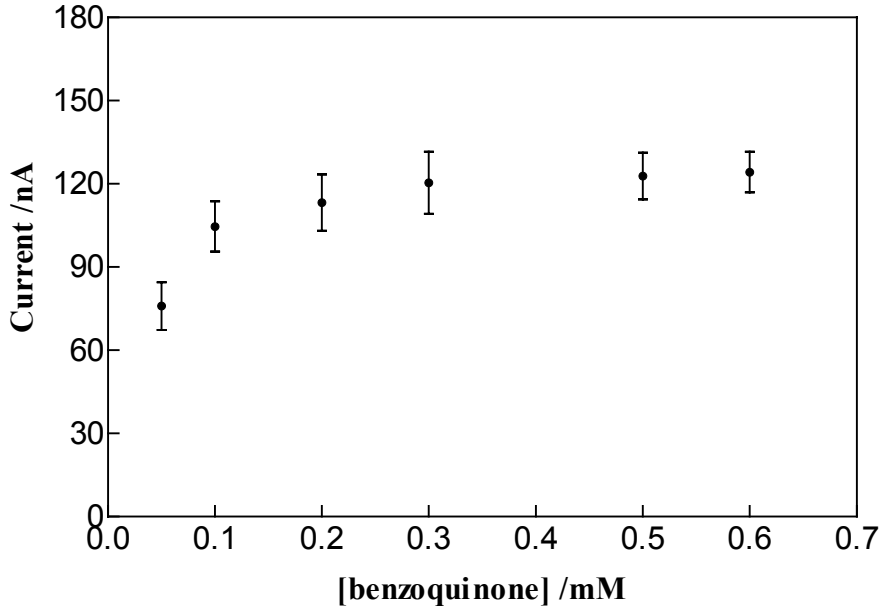

Figure 5.5 Effect of concentration of benzoquinone to 500 μM H_2O_2 in 0.1 M Tris buffer (pH 7.0). Potential was held at -0.25 V vs. Ag/AgCl (n=3)

5.3.2.3 Calibration Curve for H_2O_2

Figure 5.6 displays the amperometric current response of the immunosensor for various concentrations of H_2O_2 under the optimized experimental conditions. It can be seen that an increase in H_2O_2 concentration is accompanied by an increase in reduction currents obtained at a constant applied potential of -0.25 V. The steady-state current is obtained within 2 min. The background-subtracted currents at different concentrations of H_2O_2 at 2 min were used to create calibration curves. Background current was obtained in 0.1 M Tris buffer (pH 7.0) containing 0.2 mM benzoquinone. Figure 5.7 illustrates the calibration plot for the immunosensor as a function of H_2O_2 concentration.

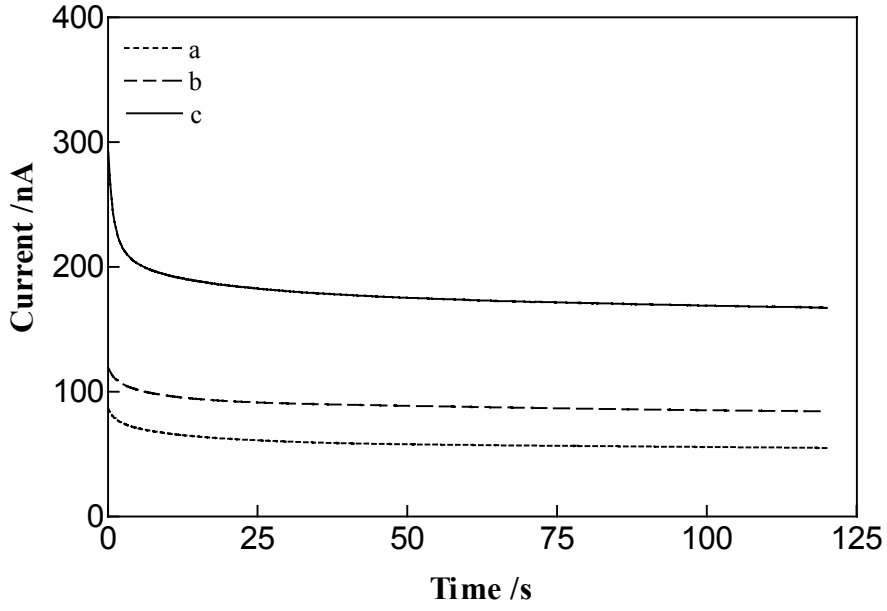

Figure 5.6 Amperometric response of the avidin-modified electrodes after incubation with 200 μg/mL B-LPOD for 40 min toward H_2O_2. (a) 0.1 M Tris buffer pH 7.0 containing 0.2 mM benzoquinone; (b) (a) + 62.5 μM H_2O_2; (c) (a) + 500 μM H_2O_2.

As can be seen in Figure 5.7, the current reaches a plateau at a H_2O_2 concentration around 750 μM. At 500 μM H_2O_2 concentration, the current is close to its maximum, suggesting saturation with H_2O_2. Therefore, the concentration of H_2O_2 was set at 500 μM for all the subsequent experiments.

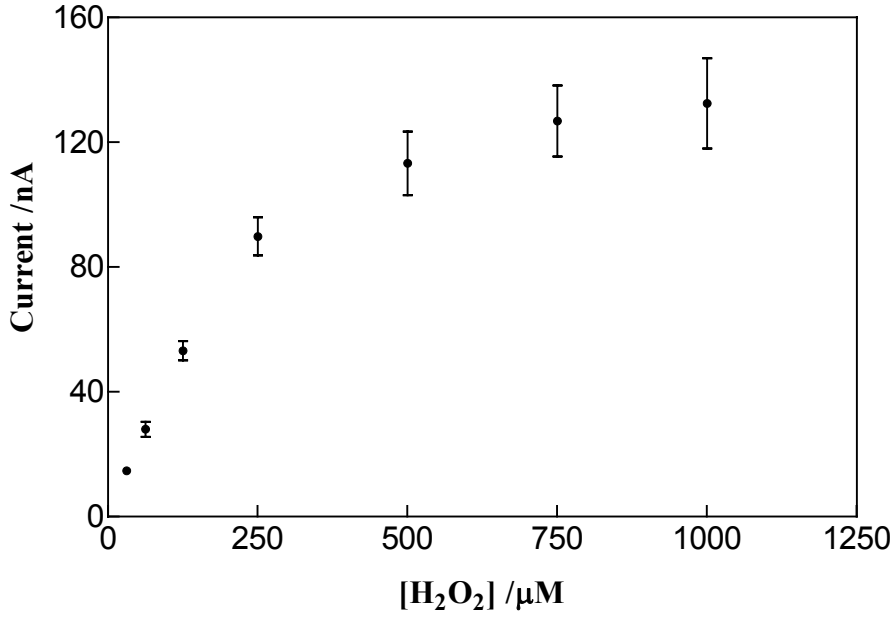

Figure 5.7 Calibration curve for the avidin-modified electrodes after incubation with 200 μg/mL B-LPOD toward H_2O_2. (n=3)

5.3.3 Biotin Immunosensor

5.3.3.1 Optimization of Analytical Conditions

The strategy for the competitive ELISA method for the determination of biotin concentration is based on competition between B-LPOD (in excess) and free biotin in solution. The activity of bound B-LPOD is assayed and correlated with biotin concentration. Accurate measurement of biotin concentration depends on the optimization of incubation time and B-LPOD concentration for the competition reaction.

The influence of incubation time (when the avidin-biotin reaction occurs) on response signal is shown in Figure 5.8. Avidin-modified electrodes were incubated with

200 μg/mL B-LPOD to study this effect. As shown in Figure 5.8, the current increased with incubation time rapidly up to 40 min and after that the variation slowed, suggesting that the reaction was complete at about 40 min. Therefore, 40 min was chosen for the subsequent study to evaluate the analytical performance of the immunosensor.

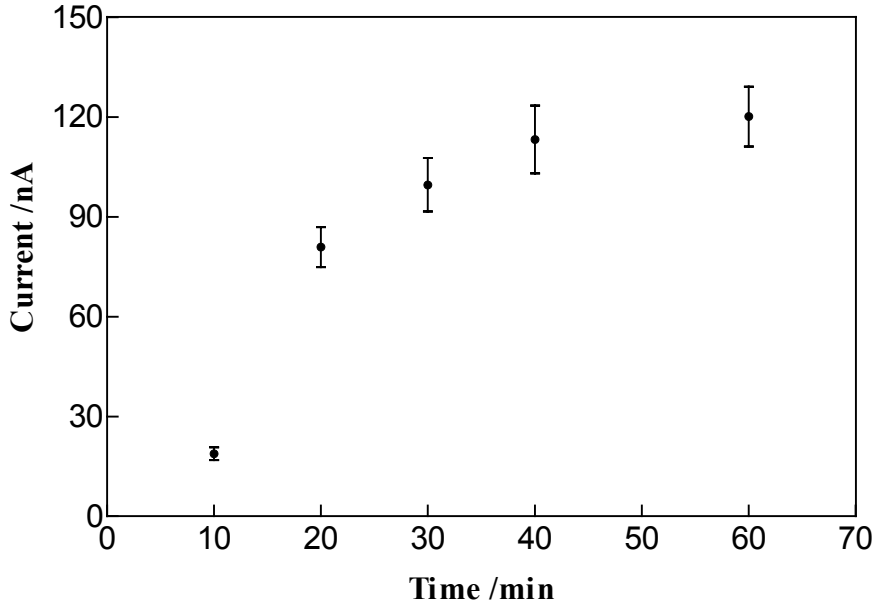

Figure 5.8 Effect of B-LPOD incubation time. Amperometric experiments were carried out in 0.1 M Tris buffer (pH 7.0) containing 0.2 mM benzoquinone and 500 μM H_2O_2. (n=3)

The concentration of B-LPOD conjugate was optimized in the absence of free biotin, because the response of the immunosensor depends on the concentration of conjugate bound to the surface of the sensor, which in turn is related to the concentration of conjugate and free biotin in the incubation solution. The results are shown in Figure 5.9. At around 75 μg/mL B-LPOD, the current reaches a plateau. At

50 μg/mL B-LPOD, the current is close to its maximum, suggesting saturation of all the available avidin binding sites. Therefore, 50 μg/mL of B-LPOD was chosen for all further competitive reactions.

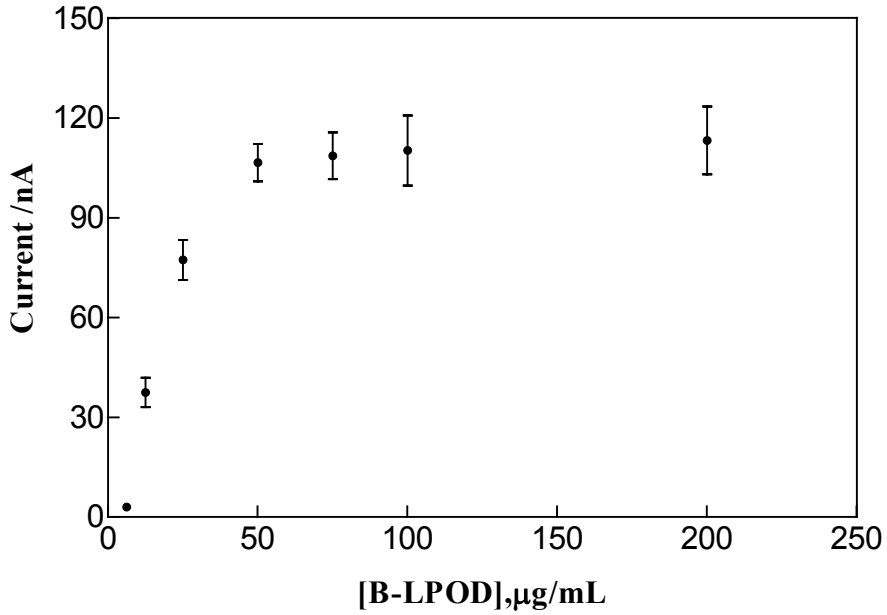

Figure 5.9 Effect of concentration of B-LPOD on the response of the immunosensor. (n=3)

5.3.3.2 Immunosensor Response to Biotin

The performance of the proposed immunsensor was evaluated for biotin quantitation. The incubation solution contained a fixed amount of B-LPOD (50 μg/mL) and various concentrations of free biotin. Results under the optimal conditions described above are shown in Figure 5.10 and Figure 5.11.

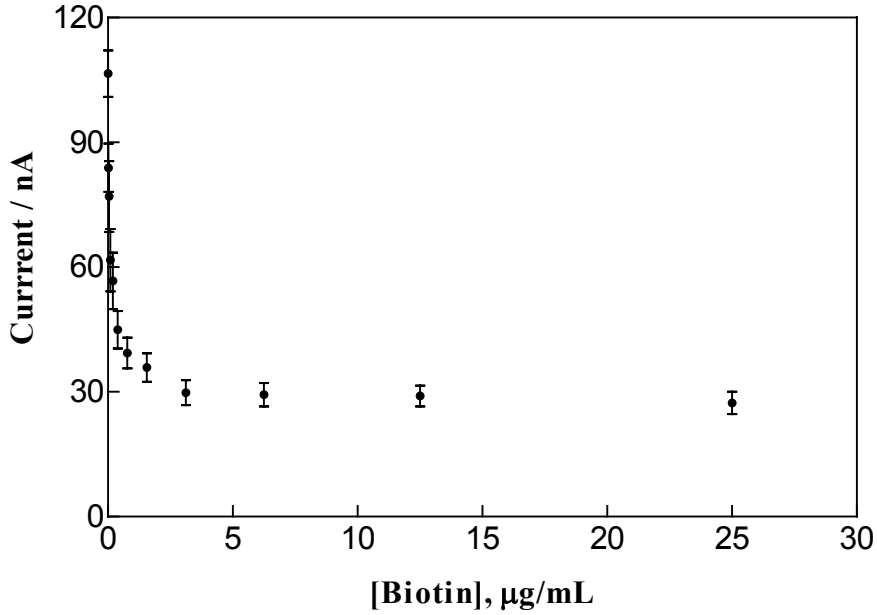

Figure 5.10 Response of the immunosensor to biotin using the optimized parameters. (n=3)

As shown in Figure 5.10, the response of the immunosensor decreases as the concentration of free biotin in solution is increased, and this is attributed to the competition between free biotin and B-LPOD for limited avidin binding sites on the electrode. The higher the concentration of free biotin present in solution, the lower is the amount of B-LPOD immobilized on the electrode surface. The maximum current represents zero concentration of free biotin.

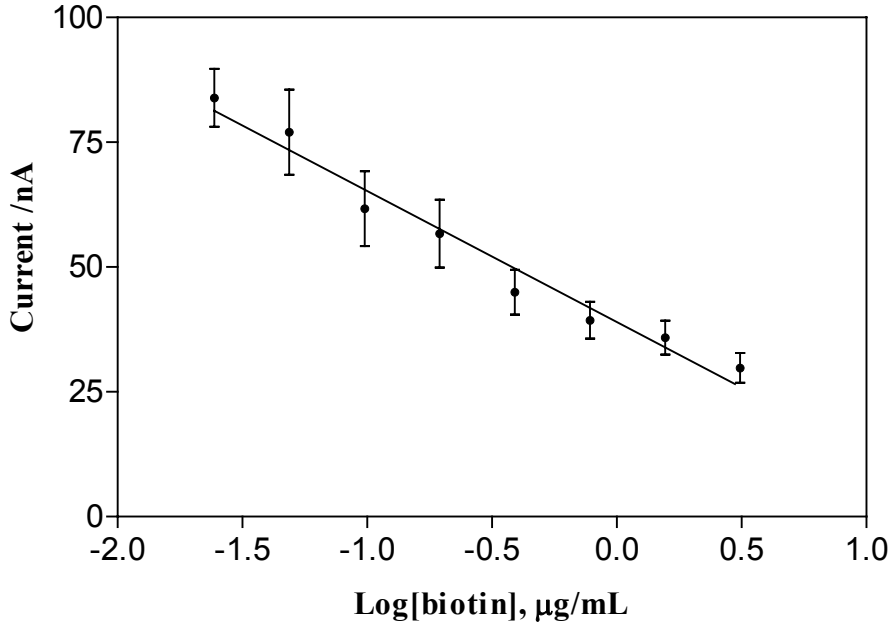

Figure 5.11 Calibration plot for the biotin sensor (data from Figure 5.10).

The immunosensor showed good linearity for biotin concentrations up to 3.125 μg/mL (R^2=0.970, Figure 5.11). The detection limit is 0.02 μg/mL (S/N=3). Each point shown in Figure 5.10 and Figure 5.11 represents the mean of three measurements using a new avidin-modified electrode, and R.S.D. was less than 12%.

5.3.3.3 Nonspecific Binding

Nonspecific binding of B-LPOD may interfere with specific competition between B-LPOD and free biotin for avidin sites on the electrode. The amperometric response of control electrodes (without immobilization of avidin), after incubation with 50 μg/mL B-LPOD for 40 min at room temperature, was measured in the presence of 500 μM H_2O_2 and 0.2 mM benzoquinone. These experiments were designed to demonstrate the maximum level of nonspecific binding of the enzyme conjugate (B-LPOD) to

monolayer-modified electrodes. The current values were about 5.6% of the signal from avidin-modified electrodes. Thus nonspecific binding of B-LPOD to the monolayer-modified electrode is low enough to be considered insignificant.

5.3.4 The Response of the Electrochemical Array to Biotin

Figure 5.12 shows cyclic voltammograms of 0.2 mM benzoquinone in a conventional three-electrode system and in the proposed electrochemical array. In both systems, the working electrode is a gold-modified SPCE (geometric area 1.0 mm^2). A platinum wire and Ag/AgCl (3 M NaCl) were used as the auxiliary electrode and reference electrode in the three-electrode system; the home-made Ag/AgCl modified SPCE served as the counter electrode in the array.

As shown in Figure 5.12, the reduction peak potential in the conventional three-electrode configuration is about -0.12 V, while in the electrochemical array it is -0.2 V. The reduction peak shifted toward negative potential by about 0.08 V in the array. Therefore, the applied potential for amperometric measurements in the electrochemical array was chosen as -0.33 V (-0.25 V was used in the conventional three-electrode system). The amperometric response of the electrochemical array to biotin at -0.33 V is shown in Figure 5.13 and Figure 5.14. The results are very similar to those obtained in the three-electrode system. The array shows good linearity with biotin concentration up to 3.125 μg/mL (R^2=0.985). The detection limit is 0.02 μg/mL (corresponding to a molar concentration of 0.08 μM, S/N=3). This detection limit can be compared to values of 0.07 and 0.33 μg/mL obtained by other groups using the avidin-biotin reaction as a model for immunosensor development.[247, 248] The detection limit in the

nano-range was obtained using alkaline phosphatase as a label and amperometric transduction (1 nM).[18]

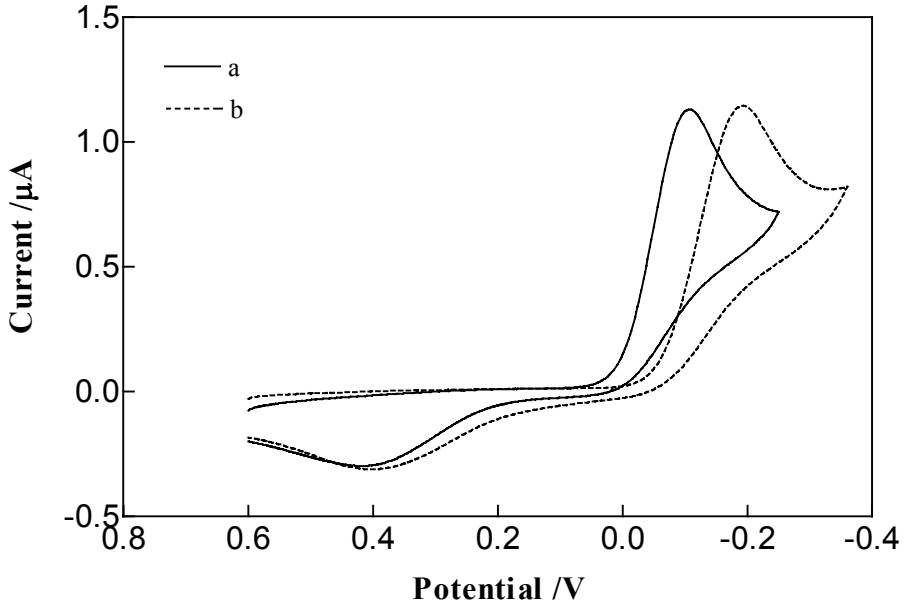

Figure 5.12 Cyclic voltammograms of 0.1 M Tris buffer (pH 7.0) containing 0.2 mM benzoquinone on a SPCE employed in (a) conventional three electrode configuration (b) the electrochemical array. Scan rate 100 mV/s.

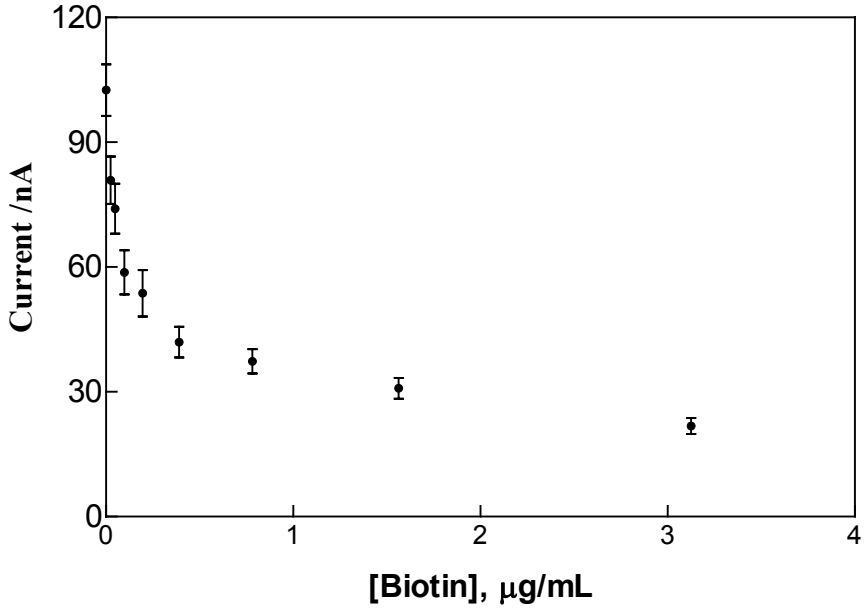

Figure 5.13 Response of the electrochemical array to biotin. (n=4)

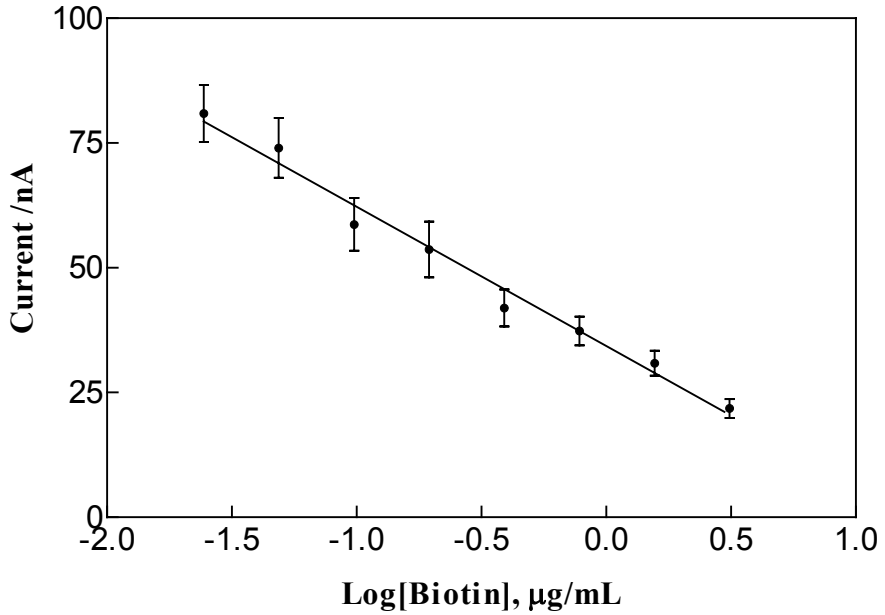

Figure 5.14 Calibration plot for biotin with the electrochemical array (data from Figure 5.13).

5.4 CONCLUSIONS

The application of the newly developed mixed-monolayer immobilization technique to a model immunosensor has been investigated in this chapter. The model immunosensor is based on the avidin-biotin system. Avidin was covalently immobilized on the surface of electrodes through the terminal carboxyl groups contained in the mixed monolayer. The model immunosensor shows good linearity for biotin up to 3.125 μg/mL (12.8 μM) with a detection limit of 0.02 μg/mL (0.08 μM, S/N=3) and R.S.D. less than 12%. This detection limit is comparable to those achieved using other reported enzyme-labeled electrochemical immunoassays.[19, 47, 249]

Chapter 6: Summary and Suggestions for Further Research

The development of screen-printing technology has enabled easy production of very flexible configurations for electrode-array devices. One of the crucial problems for the successful fabrication of biosensors is the immobilization of biomolecules. SAMs, especially functionalized monolayers, have been applied to the immobilization of biological components. Bunte salts provide a potential alternative to the use of alkanethiols for forming SAMs. Electrochemical-assembly of Bunte salts is advantageous over chemisorption of thiols in terms of selectivity, preparation procedure, formation speed and the coverage control it provides. Among these advantages, the most promising is that it allows the selective deposition of films on structures of arbitrary shape or location, such as within a fluidic microchannel.

In this work, an individually addressable electrochemical array was designed and fabricated based on screen-printing. The electrodes were screen-printed with carbon-based ink, and then were modified by gold electrodeposition or silver electrodeposition, and converted into Ag/AgCl electrodes. The home-made Ag/AgCl counter electrodes showed good storage stability. Results from SEM and XPS indicated that the surface of SPCEs was not complete covered by gold, and there were carbon particles exposed on the surface. The reproducibility of the electrochemical array was evaluated by CV, and R.S.D. values were found to be below 9.0% for electrode-to-electrode variability on the same array and different arrays. Simultaneous multichannel measurements are feasible since no chemical cross-talk was observed between adjacent sensing elements on the array.

The immobilization of biomolecules onto surfaces of electrically-conducting materials is an active area of research useful for a range of applications involving the construction of electrochemical biosensors. A general methodology that is currently being utilized for this purpose is the self-assembly of various functional groups onto specific surfaces. In this work, single- and binary-component monolayers formed electrochemically from Bunte salts were investigated. Results showed that stable single- and binary-component monolayers were formed with this method, and the degree of completeness of monolayers could be controlled by adjusting the time for oxidation of Bunte salts. The double layer capacitance for a single-component monolayer decreased as the alkyl chain length of the Bunte salt was increased. Incorporation of –COOH functional groups caused a relatively large capacitance, which was attributed to the less ordered monolayers resulting from –COOH groups.

The composition of mixed monolayers could be controlled by adjusting the composition of the assembling solution. The permeability of mixed monolayers towards $K_3Fe(CN)_6$ and FCA was different. FCA molecules were less blocked by mixed monolayers. This phenomenon may result from the difference in the nature of interactions between the probe molecules and the short chain adsorbates in the monolayers. In addition, the access of FCA to the gold electrode surface could be tuned to some extent by varying the relative concentrations of the two Bunte salts in the assembly solution, which offers the prospect of developing highly sensitive and selective electrochemical sensors for organic and biological samples.

Monolayers can be characterized by a wide variety of methods. In this project, only electrochemical methods were used. However, direct information about the

structure and composition of the monolayers is not available from electrochemical methods. I suggest that the single- and binary-component monolayers obtained from Bunte salts be further characterized by other methods, such as AFM, STM, ellipsometry, IR spectroscopy and XPS.

Electrochemical-assembly of monolayers from Bunte salts has not yet been reported for the immobilization of biomolecules. Original research reported in this thesis involved the application of this method to an enzyme biosensor and a model immunosensor.

GOx was chosen as a model enzyme since it has been well studied and is important for the detection of glucose. A functionalized binary monolayer was designed using a mixture of a long, carboxylic acid functionalized derivative (C10-COOH), and a shorter methyl functionalized derivative (C4, C6, or C8). The long chain component provides binding sites for the enzyme, and the short chain component allows electron transfer to the underlying gold layer. GOx molecules were covalently immobilized onto the carboxyl-terminated monolayers using EDC and NHS. FCA was chosen as a mediator. The resulting enzyme electrodes under optimized fabrication and operation conditions showed a linear range up to 10 mM glucose with a sensitivity of 4.6 nA mM^{-1} (in the conventional three-electrode system) and 4.7 nA mM^{-1} (in the electrochemical array). The detection limits for glucose in these two systems were 0.6 and 0.8 mM, respectively. K_m obtained under the optimized conditions was 18 mM.

In this application, the selectivity of the resulting glucose biosensor was not investigated. I suggest that this glucose biosensor be further developed to examine real

samples. The storage stability of the glucose biosensor needs to be improved if it is to be employed as a long-term sensor. Cross-linking GOx molecules immobilized on the electrode surface may improve the stability with loss of some GOx activity.

The application of the new immobilization method to a model immunosensor was also studied. A competitive enzyme immunosensor based on avidin-biotin was designed. The immobilization of avidin was achieved by covalent attachment to carboxyl-terminated mixed monolayers on the electrodes using EDC and NHS. Biotin was determined using the competitive approach, i.e. free biotin competed with the B-LPOD for limited avidin binding sites on the electrodes. The model immunosensor showed good linearity with biotin concentrations up to 3.125 μg/mL with a detection limit of 0.02 μg/mL (S/N=3) and R.S.D. less than 12%. These values are comparable to other reported enzyme-labeled electrochemical immunosensors.

The format of the model immunosensor can be employed for the detection of other analytes (antigens). Biotinylated antibody can be immobilized onto electrode surfaces using avidin-biotin coupling. Free antigen and labeled antigen would compete for the limited binding sites of avidin.

In addition, the avidin-biotin system can be employed for the immobilization of other biological components. Excellent sensitivities and low detection limits are expected because of the four biotin-binding sites of avidin. If biotinylated GOx were immobilized on avidin-modified electrodes, the resulting electrodes could be used for the detection of glucose. Since biotinylation does not usually alter the properties of biomolecules, in principle, any enzyme could be immobilized on avidin-modified

electrodes. Therefore, the immobilization method based on electrochemical-assembly of Bunte salts and avidin-biotin system is very promising.

In summary, electrochemical-assembly of Bunte salts provides a platform for immobilizing biological components. On the basis of the simplicity of the fabrication of functionalized monolayers by this method, the potential application of this method to biosensors is believed to be wide.

REFERENCES

(1) Crouch, E.; Cowell, D. C.; Hoskins, S.; Pittson, R. W.; Hart, J. P. *Anal. Biochem.* **2005**, *347*, 17-23.

(2) Montereali, M. R.; Vastarella, W.; Della Seta, L.; Pilloton, R. *Int. J. Environ. Anal. Chem.* **2005**, *85*, 795-806.

(3) De Luca, S.; Florescu, M.; Ghica, M. E.; Lupu, A.; Palleschi, G.; Brett, C. M. A.; Compagnone, D. *Talanta* **2005**, *68*, 171-178.

(4) Mikkelsen, S. R.; Corton, E. *Bioanalytical Chemistry*; John Wiley & Sons, Inc.: Hoboken, N.J., 2004, 25, 131.

(5) Clark, L. C.; Lyons, C. *Ann.NY Acad.Sci.* **1962**, *102*, 29-45.

(6) *Advances in biosensors*, first ed.; JAI: Amsterdam, 2003.

(7) Turner, A. P. F. *Biosensors & Bioelectronics* **2005**, *20*, 2387-2387.

(8) Cunningham, A. J. *Introduction to Bioanalytical Sensors*; John Wiley & Sons, Inc.: New York, 1998, 207-316.

(9) Sukeerthi, S.; Contractor, A. Q. *Indian J. Chem. Sect A-Inorg. Phys. Theor. Anal. Chem.* **1994**, *33*, 565-571.

(10) Patolsky, F.; Katz, E.; Bardea, A.; Willner, I. *Langmuir* **1999**, *15*, 3703-3706.

(11) Koncki, R.; Radomska, A.; Glab, S. *Talanta* **2000**, *52*, 13-17.

(12) Ogonczyk, D.; Tymecki, L.; Wyzkiewicz, I.; Koncki, R.; Glab, S. *Sensors and Actuators B-Chemical* **2005**, *106*, 450-454.

(13) Matthews, D. R.; Bown, E.; Watson, A.; Holman, R. R.; Steemson, J.; Hughes, S.; Scott, D. *Lancet* **1987**, *1*, 778-779.

(14) Nistor, C.; Rose, A.; Farre, M.; Stoica, L.; Wollenberger, U.; Ruzgas, T.; Pfeiffer, D.; Barcelo, D.; Gorton, L.; Emneus, J. *Anal. Chim. Acta* **2002**, *456*, 3-17.

(15) Suman, S.; Singhal, R.; Sharma, A. L.; Malthotra, B. D.; Pundir, C. S. *Sens. Actuator B-Chem.* **2005**, *107*, 768-772.

(16) Alpeeva, I. S.; Vilkanauskyte, A.; Ngounou, B.; Csoregi, E.; Sakharov, I. Y.; Gonchar, M.; Schuhmann, W. *Microchim. Acta* **2005**, *152*, 21-27.

(17) Rishpon, J.; Ivnitski, D. *Biosensors & Bioelectronics* **1997**, *12*, 195-204.

(18) Ducey, M. W.; Smith, A. M.; Guo, X. A.; Meyerhoff, M. E. *Anal. Chim. Acta* **1997**, *357*, 5-12.

(19) Benkert, A.; Scheller, F.; Schossler, W.; Hentschel, C.; Micheel, B.; Behrsing, O.; Scharte, G.; Stocklein, W.; Warsinke, A. *Anal. Chem.* **2000**, *72*, 916-921.

(20) Hart, J. P.; Wring, S. A. *Trac-Trends in Analytical Chemistry* **1997**, *16*, 89-103.

(21) Hart, J. P.; Crew, A.; Crouch, E.; Honeychurch, K. C.; Pemberton, R. M. *Analytical Letters* **2004**, *37*, 789-830.

(22) Avramescu, A.; Noguer, T.; Avramescu, M.; Marty, J. L. *Anal. Chim. Acta* **2002**, *458*, 203-213.

(23) Carsol, M. A.; Volpe, G.; Mascini, M. *Talanta* **1997**, *44*, 2151-2159.

(24) Ho, W. O.; Krause, S.; McNeil, C. J.; Pritchard, J. A.; Armstrong, R. D.; Athey, D.; Rawson, K. *Anal. Chem.* **1999**, *71*, 1940-1946.

(25) Chou, L. C. S.; Liu, C. C. *Sens. Actuator B-Chem.* **2005**, *110*, 204-208.

(26) Pemberton, R. M.; Hart, J. P.; Mottram, T. T. *Biosensors & Bioelectronics* **2001**, *16*, 715-723.

(27) Alarcon, S. H.; Micheli, L.; Palleschi, G.; Compagnone, D. *Anal. Lett.* **2004**, *37*, 1545-1558.

(28) Micheli, L.; Grecco, R.; Badea, M.; Moscone, D.; Palleschi, G. *Biosensors & Bioelectronics* **2005**, *21*, 588-596.

(29) Ruffien, A.; Dequaire, M.; Brossier, P. *Chem. Commun.* **2003**, 912-913.

(30) Nunes, G. S.; Jeanty, G.; Marty, J. L. *Anal. Chim. Acta* **2004**, *523*, 107-115.

(31) Touloupakis, E.; Giannoudi, L.; Piletsky, S. A.; Guzzella, L.; Pozzoni, F.; Giardi, M. T. *Biosensors & Bioelectronics* **2005**, *20*, 1984-1992.

(32) Ertl, P.; Wagner, M.; Corton, E.; Mikkelsen, S. R. *Biosensors & Bioelectronics* **2003**, *18*, 907-916.

(33) Bagel, O.; Limoges, B.; Schollhorn, B.; Degrand, C. *Anal. Chem.* **1997**, *69*, 4688-4694.

(34) Kulys, J. *Biosensors & Bioelectronics* **1999**, *14*, 473-479.

(35) Wang, J.; Tian, B. M.; Nascimento, V. B.; Angnes, L. *Electrochim. Acta* **1998**, *43*, 3459-3465.

(36) Dock, E.; Ruzgas, T. *Electroanalysis* **2003**, *15*, 492-498.

(37) Cui, G.; Yoo, J. H.; Lee, J. S.; Yoo, J.; Uhm, J. H.; Cha, G. S.; Nam, H. *Analyst* **2001**, *126*, 1399-1403.

(38) Wang, J.; Pedrero, M.; Sakslund, H.; Hammerich, O.; Pingarron, J. *Analyst* **1996**, *121*, 345-350.

(39) Solna, R.; Dock, E.; Christenson, A.; Winther-Nielsen, M.; Carlsson, C.; Emneus, J.; Ruzgas, T.; Skladal, P. *Anal. Chim. Acta* **2005**, *528*, 9-19.

(40) Dequaire, M.; Degrand, C.; Limoges, B. *Anal. Chem.* **2000**, *72*, 5521-5528.

(41) Albareda-Sirvent, M.; Merkoci, A.; Alegret, S. *Sens. Actuator B-Chem.* **2000**, *69*, 153-163.

(42) Vasilescu, A.; Andreescu, S.; Bala, C.; Litescu, S. C.; Noguer, T.; Marty, J. L. *Biosensors & Bioelectronics* **2003**, *18*, 781-790.

(43) Rojas, J.; Tachon, A. F.; Chevalier, D.; Noguer, T.; Marty, U.; Ghommidh, C. *Sens. Actuator B-Chem.* **2004**, *102*, 284-290.

(44) Collier, W. A.; Janssen, D.; Hart, A. L. *Biosensors & Bioelectronics* **1996**, *11*, 1041-1049.

(45) Galan-Vidal, C. A.; Munoz, J.; Dominguez, C.; Alegret, S. *Sens. Actuator B-Chem.* **1997**, *45*, 55-62.

(46) Olschewski, H.; Erlenkotter, A.; Zaborosch, C.; Chemnitius, G. C. *Enzyme Microb. Technol.* **2000**, *26*, 537-543.

(47) Hart, J. P.; Pemberton, R. M.; Luxton, R.; Wedge, R. *Biosensors & Bioelectronics* **1997**, *12*, 1113-1121.

(48) Schmidt, A.; Rohm, I.; Ruger, P.; Weise, W.; Bilitewski, U. *Fresenius J. Anal. Chem.* **1994**, *349*, 607-612.

(49) Weetall, H. H.; Hotaling, T. *Biosensors* **1987**, *3*, 57-63.

(50) Wittstock, G. *Anal. Bioanal. Chem.* **2002**, *372*, 16-17.

(51) Yu, P. G.; Wilson, G. S. *Faraday Discuss.* **2000**, 305-317.

(52) Wang, J.; Polsky, R.; Tian, B. M.; Chatrathi, M. P. *Anal. Chem.* **2000**, *72*, 5285-5289.

(53) El-Deab, M. S.; Ohsaka, T. *Electrochim. Acta* **2004**, *49*, 2189-2194.

(54) Burke, L. D.; O'Mullane, A. P. *J. Solid State Electrochem.* **2000**, *4*, 285-297.

(55) DeBono, R. F.; Loucks, G. D.; DellaManna, D.; Krull, U. J. *Can. J. Chem.-Rev. Can. Chim.* **1996**, *74*, 677-688.

(56) Jurczakowski, R.; Hitz, C.; Lasia, A. *J. Electroanal. Chem.* **2004**, *572*, 355-366.

(57) Bunde, R. L.; Jarvi, E. J.; Rosentreter, J. J. *Talanta* **1998**, *46*, 1223-1236.

(58) Sumi, T.; Wano, H.; Uosaki, K. *J. Electroanal. Chem.* **2003**, *550*, 321-325.

(59) Yang, D. F.; Morin, M. *J. Electroanal. Chem.* **1998**, *441*, 173-181.

(60) Finklea, H. O. In *Electroanalytical Chemistry: A Series of Advances, Vol 19*; Marcel Dekker: New York, 1996; Vol. 19, 109-335.

(61) Nuzzo, R. G.; Allara, D. L. *J. Am. Chem. Soc.* **1983**, *105*, 4481-4483.

(62) Ulman, A. *Chemical reviews* **1996**, *96*, 1533-1554.

(63) Gooding, J. J.; Erokhin, P.; Hibbert, D. B. *Biosensors & Bioelectronics* **2000**, *15*, 229-239.

(64) Pirrung, M. C. *Angew. Chem.-Int. Edit.* **2002**, *41*, 1276-1289.

(65) Shah, R. R.; Abbott, N. L. *Science* **2001**, *293*, 1296-1299.

(66) Huang, L.; Reekmans, G.; Saerens, D.; Friedt, J. M.; Frederix, F.; Francis, L.; Muyldermans, S.; Campitelli, A.; Van Hoof, C. *Biosensors & Bioelectronics* **2005**, *21*, 483-490.

(67) Turyan, I.; Mandler, D. *Anal. Chem.* **1997**, *69*, 894-897.

(68) Susmel, S.; Guilbault, G. G.; O'Sullivan, C. K. *Biosensors & Bioelectronics* **2003**, *18*, 881-889.

(69) Purvis, D.; Leonardova, O.; Farmakovsky, D.; Cherkasov, V. *Biosensors & Bioelectronics* **2003**, *18*, 1385-1390.

(70) Held, M.; Schuhmann, W.; Jahreis, K.; Schmidt, H. L. *Biosensors & Bioelectronics* **2002**, *17*, 1089-1094.

(71) Carpini, G.; Lucarelli, F.; Marrazza, G.; Mascini, M. *Biosensors & Bioelectronics* **2004**, *20*, 167-175.

(72) Niemeyer, C. M. *Angew. Chem.-Int. Edit.* **2001**, *40*, 4128-4158.

(73) Shipway, A. N.; Willner, I. *Chem. Commun.* **2001**, 2035-2045.

(74) Nam, J. M.; Thaxton, C. S.; Mirkin, C. A. *Science* **2003**, *301*, 1884-1886.

(75) Fritzsche, W.; Taton, T. A. *Nanotechnology* **2003**, *14*, R63-R73.

(76) Gu, H. Y.; Yu, A. M.; Chen, H. Y. *J. Electroanal. Chem.* **2001**, *516*, 119-126.

(77) Liu, S. Q.; Ju, H. X. *Anal. Biochem.* **2002**, *307*, 110-116.

(78) Liu, S. Q.; Ju, H. X. *Biosensors & Bioelectronics* **2003**, *19*, 177-183.

(79) Li, C. Z.; Liu, Y. L.; Luong, J. H. T. *Anal. Chem.* **2005**, *77*, 478-485.

(80) Zhang, S. X.; Wang, N.; Niu, Y. M.; Sun, C. Q. *Sens. Actuator B-Chem.* **2005**, *109*, 367-374.

(81) Love, J. C.; Estroff, L. A.; Kriebel, J. K.; Nuzzo, R. G.; Whitesides, G. M. *Chemical Reviews* **2005**, *105*, 1103-1169.

(82) Resch, R.; Meltzer, S.; Vallant, T.; Hoffmann, H.; Koel, B. E.; Madhukar, A.; Requicha, A. A. G.; Will, P. *Langmuir* **2001**, *17*, 5666-5670.

(83) You, T. Y.; Niwa, O.; Tomita, M.; Hirono, S. *Anal. Chem.* **2003**, *75*, 2080-2085.

(84) Sarkar, D. K.; Zhou, X. J.; Tannous, A.; Leung, K. T. *J. Phys. Chem. B* **2003**, *107*, 2879-2881.

(85) Liu, Y. L.; Male, K. B.; Bouvrette, P.; Luong, J. H. T. *Chem. Mat.* **2003**, *15*, 4172-4180.

(86) Arai, G.; Masuda, M.; Yasumori, I. *Bull. Chem. Soc. Jpn.* **1994**, *67*, 2962-2966.

(87) Arai, G.; Takahashi, S.; Yasumori, I. *J. Electroanal. Chem.* **1996**, *410*, 173-179.

(88) Wang, J.; Tian, B. *Anal. Chem.* **1993**, *65*, 1529-1532.

(89) Wang, J.; Tian, B. *Anal. Chim. Acta* **1993**, *274*, 1-6.

(90) Turner, A. P. F. *Biosensor: Fundamentals and Applications*; Oxford University Press: Oxford, 1989, 85-97.

(91) Hobara, D.; Imabayashi, S.; Kakiuchi, T. *Nano Lett.* **2002**, *2*, 1021-1025.

(92) Hobara, D.; Uno, Y.; Kakiuchi, T. *Bunseki Kagaku* **2002**, *51*, 455-460.

(93) Mrksich, M.; Whitesides, G. M. *Annu. Rev. Biophys. Biomolec. Struct.* **1996**, *25*, 55-78.

(94) Willner, I.; Rubin, S.; Cohen, Y. *J. Am. Chem. Soc.* **1993**, *115*, 4937-4938.

(95) Katz, E.; Willner, I. *J. Electroanal. Chem.* **1996**, *418*, 67-72.

(96) Kajiya, Y.; Okamoto, T.; Yoneyama, H. *Chemistry Letters* **1993**, 2107-2110.

(97) Willner, I.; Liondagan, M.; Marxtibbon, S.; Katz, E. *J. Am. Chem. Soc.* **1995**, *117*, 6581-6592.

(98) Imamura, M.; Haruyama, T.; Kobatake, E.; Ikariyama, Y.; Aizawa, M. *Sens. Actuator B-Chem.* **1995**, *24*, 113-116.

(99) Creager, S. E.; Olsen, K. G. *Anal. Chim. Acta* **1995**, *307*, 277-289.

(100) Dong, X. D.; Lu, J. T.; Cha, C. S. *Bioelectrochem. Bioenerg.* **1995**, *36*, 73-76.

(101) Sawaguchi, T. *Bioelectrochem. Bioenerg.* **1992**, *29*, 127-133.

(102) Willner, I.; Katz, E.; Riklin, A.; Kasher, R. *J. Am. Chem. Soc.* **1992**, *114*, 10965-10966.

(103) Collison, M., Bowden, E.F., and Tarlov, M.J. *Langmuir* **1992**, *8*, 1247-1250.

(104) Dong, S. J.; Li, J. H. *Bioelectrochem. Bioenerg.* **1997**, *42*, 7-13.

(105) Chidsey, C. E. D.; Loiacono, D. N. *Langmuir* **1990**, *6*, 682-691.

(106) Wink, T.; vanZuilen, S. J.; Bult, A.; vanBennekom, W. P. *Analyst* **1997**, *122*, R43-R50.

(107) Guiomar, A. J.; Guthrie, J. T.; Evans, S. D. *Langmuir* **1999**, *15*, 1198-1207.

(108) Chidsey, C. E. D. *Science* **1991**, *251*, 919-922.

(109) Chidsey, C. E. D.; Bertozzi, C. R.; Putvinski, T. M.; Mujsce, A. M. *J. Am. Chem. Soc.* **1990**, *112*, 4301-4306.

(110) Mittlerneher, S.; Spinke, J.; Liley, M.; Nelles, G.; Weisser, M.; Back, R.; Wenz, G.; Knoll, W. *Biosensors & Bioelectronics* **1995**, *10*, 903-916.

(111) Bain, C. D.; Whitesides, G. M. *J. Am. Chem. Soc.* **1988**, *110*, 6560-6561.

(112) Bain, C. D.; Evall, J.; Whitesides, G. M. *J. Am. Chem. Soc.* **1989**, *111*, 7155-7164.

(113) Folkers, J. P.; Laibinis, P. E.; Whitesides, G. M. *Langmuir* **1992**, *8*, 1330-1341.

(114) Hobara, D.; Sasaki, T.; Imabayashi, S.; Kakiuchi, T. *Langmuir* **1999**, *15*, 5073-5078.

(115) Smith, R. K.; Reed, S. M.; Lewis, P. A.; Monnell, J. D.; Clegg, R. S.; Kelly, K. F.; Bumm, L. A.; Hutchison, J. E.; Weiss, P. S. *J. Phys. Chem. B* **2001**, *105*, 1119-1122.

(116) Folkers, J. P.; Laibinis, P. E.; Whitesides, G. M. *J. Adhes. Sci. Technol.* **1992**, *6*, 1397-1410.

(117) Folkers, J. P.; Laibinis, P. E.; Whitesides, G. M.; Deutch, J. *J. Phys. Chem.* **1994**, *98*, 563-571.

(118) Hobara, D.; Kakiuchi, T. *Electrochemistry Communications* **2001**, *3*, 154-157.

(119) Stranick, S. J.; Parikh, A. N.; Tao, Y. T.; Allara, D. L.; Weiss, P. S. *J. Phys. Chem.* **1994**, *98*, 7636-7646.

(120) Bain, C. D.; Whitesides, G. M. *Langmuir* **1989**, *5*, 1370-1378.

(121) Lewis, P. A.; Smith, R. K.; Kelly, K. F.; Bumm, L. A.; Reed, S. M.; Clegg, R. S.; Gunderson, J. D.; Hutchison, J. E.; Weiss, P. S. *J. Phys. Chem. B* **2001**, *105*, 10630-10636.

(122) Bumm, L. A.; Arnold, J. J.; Charles, L. F.; Dunbar, T. D.; Allara, D. L.; Weiss, P. S. *J. Am. Chem. Soc.* **1999**, *121*, 8017-8021.

(123) Lukkari, J.; Meretoja, M.; Kartio, I.; Laajalehto, K.; Rajamaki, M.; Lindstrom, M.; Kankare, J. *Langmuir* **1999**, *15*, 3529-3537.

(124) Hsueh, C. C.; Lee, M. T.; Freund, M. S.; Ferguson, G. S. *Angew. Chem.-Int. Edit.* **2000**, *39*, 1228-1230.

(125) Lusk, A. T.; Jennings, G. K. *Langmuir* **2001**, *17*, 7830-7836.

(126) Nann, T.; Urban, G. A. *J. Electroanal. Chem.* **2001**, *505*, 125-132.

(127) Distler, H. *Angew. Chem.-Int. Edit.* **1967**, *6*, 544-553.

(128) Jung, C.; Dannenberger, O.; Xu, Y.; Buck, M.; Grunze, M. *Langmuir* **1998**, *14*, 1103-1107.

(129) Shon, Y. S.; Gross, S. M.; Dawson, B.; Porter, M.; Murray, R. W. *Langmuir* **2000**, *16*, 6555-6561.

(130) Shon, Y. S.; Cutler, E. *Langmuir* **2004**, *20*, 6626-6630.

(131) Laiho, T.; Lukkari, J.; Meretoja, M.; Laajalehto, K.; Kankare, J.; Leiro, J. A. *Surf. Sci.* **2005**, *584*, 83-89.

(132) Weisshaar, D. E.; Lamp, B. D.; Porter, M. D. *J. Am. Chem. Soc.* **1992**, *114*, 5860-5862.

(133) Tender, L. M.; Worley, R. L.; Fan, H. Y.; Lopez, G. P. *Langmuir* **1996**, *12*, 5515-5518.

(134) Riepl, M.; Mirsky, V. M.; Wolfbeis, O. S. *Mikrochim. Acta* **1999**, *131*, 29-34.

(135) Ron, H.; Rubinstein, I. *J. Am. Chem. Soc.* **1998**, *120*, 13444-13452.

(136) Rohwerder, M.; de Weldige, K.; Stratmann, M. *J. Solid State Electrochem.* **1998**, *2*, 88-93.

(137) Czerwinski, A.; Orzeszko, A.; Kazimierczuk, Z.; Marassi, R.; Zamponi, S. *Anal. Lett.* **1997**, *30*, 2391-2408.

(138) Schmidt, J. C. *Field Anal. Chem. Technol.* **1998**, *2*, 351-361.

(139) Knecht, B. G.; Strasser, A.; Dietrich, R.; Martlbauer, E.; Niessner, R.; Weller, M. G. *Anal. Chem.* **2004**, *76*, 646-654.

(140) Ngundi, M. M.; Shriver-Lake, L. C.; Moore, M. H.; Lassman, M. E.; Ligler, F. S.; Taitt, C. R. *Anal. Chem.* **2005**, *77*, 148-154.

(141) Jawaheer, S.; White, S. F.; Rughooputh, S.; Cullen, D. C. *Biosensors & Bioelectronics* **2003**, *18*, 1429-1437.

(142) Sapelnikova, S.; Dock, E.; Solna, R.; Skladal, P.; Ruzgas, T.; Emneus, J. *Anal. Bioanal. Chem.* **2003**, *376*, 1098-1103.

(143) Rowe, C. A.; Tender, L. M.; Feldstein, M. J.; Golden, J. P.; Scruggs, S. B.; MacCraith, B. D.; Cras, J. J.; Ligler, F. S. *Anal. Chem.* **1999**, *71*, 3846-3852.

(144) Rowe, C. A.; Scruggs, S. B.; Feldstein, M. J.; Golden, J. P.; Ligler, F. S. *Anal. Chem.* **1999**, *71*, 433-439.

(145) Bard, A. J.; Faulkner, L. R. *Electrochemical Methods*; Wiley: New York, 2001, 176,233.

(146) Suzuki, M.; Akaguma, H. *Sens. Actuator B-Chem.* **2000**, *64*, 136-141.

(147) Niwa, O. *Electroanalysis* **1995**, *7*, 606-613.

(148) Wang, J.; Freiha, B. A. *Journal of Chromatography* **1984**, *298*, 79-87.

(149) Evans, U.; Colavita, P. E.; Doescher, M. S.; Schiza, M.; Myrick, M. L. *Nano Lett.* **2002**, *2*, 641-645.

(150) Simm, A. O.; Ward-Jones, S.; Banks, C. E.; Compton, R. G. *Anal. Sci.* **2005**, *21*, 667-671.

(151) Fletcher, S.; Horne, M. D. *Electrochemistry Communications* **1999**, *1*, 502-512.

(152) Caudill, W. L.; Howell, J. O.; Wightman, R. M. *Anal. Chem.* **1982**, *54*, 2532-2535.

(153) Desmond, D.; Lane, B.; Alderman, J.; Glennon, J. D.; Diamond, D.; Arrigan, D. W. M. *Sens. Actuator B-Chem.* **1997**, *44*, 389-396.

(154) Mroz, A.; Borchardt, M.; Diekmann, C.; Cammann, K.; Knoll, M.; Dumschat, C. *Analyst* **1998**, *123*, 1373-1376.

(155) Suzuki, H.; Hirakawa, T.; Sasaki, S.; Karube, I. *Sens. Actuator B-Chem.* **1998**, *46*, 146-154.

(156) Tymecki, L.; Zwierkowska, Z.; Koncki, R. *Anal. Chim. Acta* **2004**, *526*, 3-11.

(157) Sapelnikova, S.; Dock, E.; Ruzgas, T.; Emneus, J. *Talanta* **2003**, *61*, 473-483.

(158) Osborne, P. G.; Niwa, O.; Yamamoto, K. *Anal. Chem.* **1998**, *70*, 1701-1706.

(159) Mann, T. M.Sc., University of Waterloo, Waterloo, 2004.

(160) Hager, G. M.Sc., University of Waterloo, Waterloo, 2001.

(161) McDonald, J. C.; Duffy, D. C.; Anderson, J. R.; Chiu, D. T.; Wu, H. K.; Schueller, O. J. A.; Whitesides, G. M. *Electrophoresis* **2000**, *21*, 27-40.

(162) PalomarPardave, M.; Ramirez, M. T.; Gonzalez, I.; Serruya, A.; Scharifker, B. R. *Journal of the Electrochemical Society* **1996**, *143*, 1551-1558.

(163) *Biosensors: A practical approach*; IRL Press at Oxford University Press: Oxford, England, 1990, 28-29.

(164) Harris, D. C. *Quantitative chemical analysis*, Fifth ed.; W.H.Freeman: New York, 2000, AP27-38.

(165) Cassidy, J.; Ghoroghchian, J.; Sarfarazi, F.; Smith, J. J.; Pons, S. *Electrochim. Acta* **1986**, *31*, 629-636.

(166) Scharifker, B. R. *J. Electroanal. Chem.* **1988**, *240*, 61-76.

(167) Bain, C. D.; Whitesides, G. M. *Science* **1988**, *240*, 62-63.

(168) Bain, C. D.; Troughton, E. B.; Tao, Y. T.; Evall, J.; Whitesides, G. M.; Nuzzo, R. G. *J. Am. Chem. Soc.* **1989**, *111*, 321-335.

(169) Milligan, B.; Swan, J. M. *Journal of the Chemical Society* **1962**, 2172-2177.

(170) Lee, M. T.; Hsueh, C. C.; Freund, M. S.; Ferguson, G. S. *Langmuir* **2003**, *19*, 5246-5253.

(171) Ulman, A. *An Introduction to Ultrathin Organic Films: From Langmuir-Blodgett to Self-Assembly*; Academic Press: New York, 1991, 288-289.

(172) Bunte, H. *Chem.Ber.* **1874**, *7*, 646-648.

(173) Westlake, H. E.; Dougherty, G. *J. Am. Chem. Soc.* **1942**, *64*, 149-150.

(174) Weiss, U.; Sokol, S. *J. Am. Chem. Soc.* **1950**, *72*, 1687-1689.

(175) Kice, J. L. *J. Org. Chem.* **1963**, *28*, 957-961.

(176) Orzeszko, A. *J. Polym. Mater.* **1994**, *11*, 69-71.

(177) Zhao, X. M.; Wilbur, J. L.; Whitesides, G. M. *Langmuir* **1996**, *12*, 3257-3264.

(178) Porter, M. D.; Bright, T. B.; Allara, D. L.; Chidsey, C. E. D. *J. Am. Chem. Soc.* **1987**, *109*, 3559-3568.

(179) Bard, A. J.; Faulkner, L. R. *Electrochemical Methods, Fundamentals and Applications*; John Wiley & Sons: New York, 1980, 233.

(180) Adams, R. N. *Electrochemistry at Solid Electrodes*; Marcel Dekker Inc.: New York, 1969, 50-58.

(181) Sawyer, D. T.; Roberts Jr, J. L. *Experimental Electrochemistry for Chemists*; Wiley: New York, 1974, 74-75.

(182) Oesch, U.; Janata, J. *Electrochim. Acta* **1983**, *28*, 1237-1246.

(183) Conway, B. E.; Currie, J. C. *Journal of the Electrochemical Society* **1978**, *125*, 257-264.

(184) Angell, D. H.; Dickinso.T *J. Electroanal. Chem.* **1972**, *35*, 55-72.

(185) Gennett, T.; Weaver, M. J. *Anal. Chem.* **1984**, *56*, 1444-1448.

(186) Molinero, V.; Calvo, E. J. *J. Electroanal. Chem.* **1998**, *445*, 17-25.

(187) Widrig, C. A.; Chung, C.; Porter, M. D. *J. Electroanal. Chem.* **1991**, *310*, 335-359.

(188) Liu, X.; Neoh, K. G.; Cen, L.; Kang, E. T. *Biosensors & Bioelectronics* **2004**, *19*, 823-834.

(189) Cen, L.; Neoh, K. G.; Kang, E. T. *Biosensors & Bioelectronics* **2003**, *18*, 363-374.

(190) Deshpande, M. V.; Amalnerkar, D. P. *Progress in Polymer Science* **1993**, *18*, 623-649.

(191) Ogawa, K.; Nakajima-Kambe, T.; Nakahara, T.; Kokufuta, E. *Biomacromolecules* **2002**, *3*, 625-631.

(192) Shi, L. X.; Lu, Y. X.; Sun, J.; Zhang, J.; Sun, C. Q.; Liu, J. Q.; Shen, J. C. *Biomacromolecules* **2003**, *4*, 1161-1167.

(193) Tiller, J. C.; Rieseler, R.; Berlin, P.; Klemm, D. *Biomacromolecules* **2002**, *3*, 1021-1029.

(194) Gulla, K. C.; Gouda, M. D.; Thakur, M. S.; Karanth, N. G. *Biosensors & Bioelectronics* **2004**, *19*, 621-625.

(195) Gooding, J. J.; Hibbert, D. B. *Trac-Trends Anal. Chem.* **1999**, *18*, 525-533.

(196) Katz, E.; Riklin, A.; Willner, I. *J. Electroanal. Chem.* **1993**, *354*, 129-144.

(197) Chaki, N. K.; Vijayamohanan, K. *Biosensors & Bioelectronics* **2002**, *17*, 1-12.

(198) Adanyi, N.; Varadi, M.; Kim, N.; Szendro, I. *Curr. Appl. Phys.* **2006**, *6*, 279-286.

(199) Mena, M. L.; Carralero, V.; Gonzalez-Cortes, A.; Yanez-Sedeno, P.; Pingarron, J. M. *Electroanalysis* **2005**, *17*, 2147-2155.

(200) Rechnitz, G. A. *Anal. Chim. Acta* **1986**, *180*, 281-287.

(201) Frew, J. E.; Hill, H. A. O. *Anal. Chem.* **1987**, *59*, A933-944.

(202) Chinnayelka, S.; McShane, M. J. *Biomacromolecules* **2004**, *5*, 1657-1661.

(203) Malhotra, B. D.; Chaubey, A. *Sens. Actuator B-Chem.* **2003**, *91*, 117-127.

(204) Suzuki, H.; Kumagai, A.; Ogawa, K.; Kokufuta, E. *Biomacromolecules* **2004**, *5*, 486-491.

(205) Hecht, H. J.; Kalisz, H. M.; Hendle, J.; Schmid, R. D.; Schomburg, D. *J. Mol. Biol.* **1993**, *229*, 153-172.

(206) Reach, G.; Wilson, G. S. *Anal. Chem.* **1992**, *64*, A381-A386.

(207) Wang, J.; Liu, J.; Chen, L.; Lu, F. *Anal. Chem.* **1994**, *66*, 3600-3603.

(208) Cass, A. E. G.; Davis, G.; Francis, G. D.; Hill, H. A. O.; Aston, W. J.; Higgins, I. J.; Plotkin, E. V.; Scott, L. D. L.; Turner, A. P. F. *Anal. Chem.* **1984**, *56*, 667-671.

(209) Fei, J. J.; Wu, Y. H.; Ji, X. B.; Wang, J.; Hu, S. S.; Gao, Z. Q. *Anal. Sci.* **2003**, *19*, 1259-1263.

(210) Serban, S.; El Murr, N. *Anal. Lett.* **2003**, *36*, 1739-1753.

(211) Li, J.; Chia, L. S.; Goh, N. K.; Tan, S. N.; Ge, H. *Sens. Actuator B-Chem.* **1997**, *40*, 135-141.

(212) Nakabayashi, Y.; Wakuda, M.; Imai, H. *Anal. Sci.* **1998**, *14*, 1069-1076.

(213) Bu, H. Z.; Mikkelsen, S. R.; English, A. M. *Anal. Chem.* **1998**, *70*, 4320-4325.

(214) Miao, Y.; Chia, L. S.; Goh, N. K.; Tan, S. N. *Electroanalysis* **2001**, *13*, 347-349.

(215) Fiorito, P. A.; de Torresi, S. I. C. *J. Braz. Chem. Soc.* **2001**, *12*, 729-733.

(216) Vidal, J. C.; Garcia, E.; Castillo, J. R. *Anal. Sci.* **2002**, *18*, 537-542.

(217) Tkac, J.; Vostiar, I.; Gemeiner, P.; Sturdik, E. *Bioelectrochemistry* **2002**, *55*, 149-151.

(218) Razumiene, J.; Gureviciene, V.; Vilkanauskyte, A.; Marcinkeviciene, L.; Bachmatova, I.; Meskys, R.; Laurinavicius, V. *Sens. Actuator B-Chem.* **2003**, *95*, 378-383.

(219) Yang, X. H.; Hua, L.; Gong, H. Q.; Tan, S. N. *Anal. Chim. Acta* **2003**, *478*, 67-75.

(220) Kase, Y.; Muguruma, H. *Anal. Sci.* **2004**, *20*, 1143-1146.

(221) Oungpipat, W.; Alexander, P. W.; Southwellkeely, P. *Anal. Chim. Acta* **1995**, *309*, 35-45.

(222) Degani, Y.; Heller, A. *J. Am. Chem. Soc.* **1988**, *110*, 2615-2620.

(223) Dubois, L. H.; Nuzzo, R. G. *Annu. Rev. Phys. Chem.* **1992**, *43*, 437-463.

(224) Delvaux, M.; Demoustier-Champagne, S. *Biosensors & Bioelectronics* **2003**, *18*, 943-951.

(225) Gooding, J. J.; Pugliano, L.; Hibbert, D. B.; Erokhin, P. *Electrochemistry Communications* **2000**, *2*, 217-221.

(226) Heider, G. H.; Sasso, S. V.; Huang, K. M.; Yacynych, A. M.; Wieck, H. J. *Anal. Chem.* **1990**, *62*, 1106-1110.

(227) Dong, X. D.; Lu, J. T.; Cha, C. S. *Bioelectrochem. Bioenerg.* **1997**, *42*, 63-69.

(228) Gregg, B. A.; Heller, A. *J. Phys. Chem.* **1991**, *95*, 5976-5980.

(229) Hock, B. *Anal. Chim. Acta* **1997**, *347*, 177-186.

(230) Suri, C. R.; Raje, M.; Varshney, G. C. *Crit. Rev. Biotechnol.* **2002**, *22*, 15-32.

(231) Mallat, E.; Barcelo, D.; Barzen, C.; Gauglitz, G.; Abuknesha, R. *Trac-Trends Anal. Chem.* **2001**, *20*, 124-132.

(232) Van Emon, J. M.; Gerlach, C. L.; Bowman, K. *J. Chromatogr. B* **1998**, *715*, 211-228.

(233) Luppa, P. B.; Sokoll, L. J.; Chan, D. W. *Clin. Chim. Acta* **2001**, *314*, 1-26.

(234) Mello, L. D.; Kubota, L. T. *Food Chem.* **2002**, *77*, 237-256.

(235) Kalab, T.; Skladal, P. *Electroanalysis* **1997**, *9*, 293-297.

(236) Byfield, M. P.; Abuknesha, R. A. *Biosensors & Bioelectronics* **1994**, *9*, 373-400.

(237) Skladal, P. *Electroanalysis* **1997**, *9*, 737-745.

(238) Madou, M.; Tierney, M. J. *Appl. Biochem. Biotechnol.* **1993**, *41*, 109-128.

(239) Ho, W. O.; Athey, D.; McNeil, C. J.; Hager, H. J.; Evans, G. P.; Mullen, W. H. *J. Electroanal. Chem.* **1993**, *351*, 185-197.

(240) Song, J. M.; Vo-Dinh, T. *Anal. Chim. Acta* **2004**, *507*, 115-121.

(241) Guchhait, R. B.; Polakis, S. E.; Dimroth, P.; Stoll, E.; Moss, J.; Lane, M. D. *J. Biol. Chem.* **1974**, *249*, 6633-6645.

(242) Diamandis, E. P.; Christopoulos, T. K. *Clin. Chem.* **1991**, *37*, 625-636.

(243) Bayer, E. A.; Wilchek, M. *Method Enzymol.* **1990**, *184*, 174-187.

(244) Wilchek, M.; Bayer, E. A. *Method Enzymol.* **1990**, *184*, 14-45.

(245) Ternynck, T.; Avrameas, S. *Method Enzymol.* **1990**, *184*, 469-481.

(246) Guo, L. H.; Yang, X. Q. *Analyst* **2005**, *130*, 1027-1031.

(247) Wright, J. D.; Rawson, K. M.; Ho, W. O.; Athey, D.; McNeil, C. J. *Biosensors & Bioelectronics* **1995**, *10*, 495-500.

(248) Darain, F.; Park, S. U.; Shim, Y. B. *Biosensors & Bioelectronics* **2003**, *18*, 773-780.

(249) Wehmeyer, K. R.; Halsall, H. B.; Heineman, W. R.; Volle, C. P.; Chen, I. W. *Anal. Chem.* **1986**, *58*, 135-139.